EDUCACIÓN
SECRETARÍA DE EDUCACIÓN PÚBLICA

Instituto Tecnológico de La Laguna

TECNOLÓGICO NACIONAL DE MÉXICO

DIVISIÓN DE ESTUDIOS DE POSGRADO E INVESTIGACIÓN

“Diagnóstico y Control Tolerante a Fallas en Vehículos Aéreos No-Tripulados”

POR

ING. Romeo Falcón Prado

T E S I S

PRESENTADO COMO REQUISITO PARCIAL PARA OBTENER EL GRADO DE DOCTOR EN CIENCIAS EN INGENIERÍA ELÉCTRICA

DIRECTOR DE TESIS

Dr. Héctor Ríos Barajas

CODIRECTOR DE TESIS

Dr. Alejandro Enrique Dzul López

ISSN: 0188-9060

RIITEC: (05)-TDCIE-2022

Torreón, Coahuila. México

Agosto, 2022

Instituto Tecnológico de La Laguna

Torreón, Coah., 22/Agosto/2022
Dependencia: DEPI/CPCIE
Oficio: DEPI/CDCIE/064/2022
Asunto: Autorización de impresión de tesis.

M.C. ROMEO FALCÓN PRADO
C. CANDIDATO AL GRADO DE DOCTOR EN CIENCIAS EN INGENIERÍA ELÉCTRICA.
PRESENTE

Después de haber sometido a revisión su trabajo de tesis titulado:

"Diagnóstico y Control Tolerante a Fallas en Vehículos Aéreos No-Tripulados"

Habiendo cumplido con todas las indicaciones que el jurado revisor de tesis hizo, se le comunica que se le concede la autorización con número de registro **RIITEC: (05)-TDCIE-2022**, para que proceda a la impresión del mismo.

A T E N T A M E N T E
Educación Tecnológica Agente de Innovación

EDUCACIÓN | TECNOLÓGICO NACIONAL DE MÉXICO
SECRETARÍA DE EDUCACIÓN PÚBLICA
INSTITUTO TECNOLOGICO DE LA LAGUNA
DIVISIÓN DE ESTUDIOS DE POSGRADO E INVESTIGACIÓN

DR. JOSÉ IRVING HERNÁNDEZ JACQUEZ
Jefe de la División de Estudios de Posgrado e Investigación
del Instituto Tecnológico de la Laguna

Instituto Tecnológico de La Laguna

Torreón Coah., 22/Agosto/2022

DR. JOSÉ IRVING HERNÁNDEZ JACQUEZ
JEFE DE LA DIVISIÓN DE ESTUDIOS DE POSGRADO E INVESTIGACIÓN

Por medio de la presente, hacemos de su conocimiento que después de haber sometido a revisión el trabajo de tesis titulado:

"Diagnóstico y Control Tolerante a Fallas en Vehículos Aéreos No Tripulados "

Desarrollado por el **C. M.C. Romeo Falcón Prado** , con número de control **D1813010** y habiendo cumplido con todas las correcciones que se le indicaron, estamos de acuerdo que se le conceda la autorización de la fecha de examen de grado para que proceda a la impresión de la misma.

ATENTAMENTE
EDUCACIÓN TECNOLÓGICA FUENTE DE INNOVACIÓN

Dr. Héctor Ríos Barajas
Asesor/Director de Tesis

Dr. Alejandro Enrique Dzul López
Coasesor/Co Director de Tesis

Dr. Víctor Adrián Santibáñez Dávila
Comité Tutorial

Dr. Miguel Ángel Llama Leal
Comité Tutorial

Dra. Dolores Alejandra Ferreira de Loza
Comité Tutorial Externo

The realization of this project has been possible thanks to the following tutorial committee:

Advisor: Dr. Héctor Ríos Barajas
Co–advisor: Dr. Alejandro Enrique Dzul López
Tutorial Committee: Dra. Dolores Alejandra Ferreira de Loza
Tutorial Committee: Dr. Víctor Adrian Santibáñez Dávila
Tutorial Committee: Dr. Miguel Ángel Llama Leal

Dedicated to my parents, Teresa and Ricardo, for their love and support, every goal achieved is thanks to them. To my brothers, Ricardo and Lucía, who have been by my side supporting me.

ABSTRACT

This thesis presents the design of fault diagnosis and fault–tolerant control methods for the trajectory tracking problem in quad–rotors. The problem considers external disturbances, and two different actuator faulty scenarios: multiple losses of rotor effectiveness or a complete rotor failure. To deal with the fault–tolerant problem, the design of robust flight controllers is required in order to counteract the effect of external disturbances affecting the quad–rotor. For this purpose, Continuous Sliding-Mode Control strategies and an Attractive Ellipsoid–Based robust control method are designed to deal with the effect of external disturbances achieving the trajectory tracking. For the fault diagnosis strategy a finite–time sliding–mode observer is proposed to estimate the whole system state and provide a set of residuals. These residuals allow us to detect, isolate and identify multiple actuator faults despite the presence of uniformly bounded and Lipschitz disturbances. Using the proposed fault diagnosis, an actuator fault accommodation controller is developed to solve the trajectory tracking problem in quad–rotors under the effects of multiple losses of rotor effectiveness and external disturbances. The fault accommodation partially compensates the actuator faults allowing the use of a baseline robust–nominal controller that deals with external disturbances. Additionally, in order to deal with the rotor failure scenario, an active fault–tolerant control is proposed. First, the rotor failure is isolated using the proposed fault diagnosis, and then, a combination of a finite–time sliding–mode observer, PID controllers, and continuous high–order sliding–modes controllers is proposed. Such a strategy allows the yaw angular velocity to remain bounded and the position tracking to be achieved even in the presence of some external disturbances. Numerical simulations and experimental results on the Quanser's QBall2 show the performance of the proposed strategies.

ACKNOWLEDGEMENTS

To my parents, Teresa and Ricardo, for their love, patience and support in every step of my life. To my brothers, Ricardo and Lucía, who have been by my side supporting me. My heart and my gratitude to you forever.

To Dr. Héctor Ríos for giving me the opportunity to work with him, for his guidance and advice during my Ph.D. studies. Your lessons and experiences have made me disciplined, professional and strong, preparing me for the challenges to come. To Dr. Alejandro Dzul for his kindness and empathy that have made me a better person.

To my friends and lab partners Edgar Martínez, Pablo Rochel, Jorge Chin, Ignacio Aguilera, Roberto Franco, Eduardo de la Cruz, Ariana Gutierrez for his unconditional support, friendship and experiences.

To the Instituto Tecnológico de la Laguna and the Tecnológico Nacional de México for its facilities. To the CONACYT for the financial support provided during the Ph.D. project, under the CVU 785635.

ACRONYMS

AEM	Attractive Ellipsoid Method
CTC	Continuous Twisting Controller
DAQ	Data Acquisition Card
FAC	Fault Accommodation Controller
FD	Fault Diagnosis
FTC	Fault–Tolerant Control
FT–ISS	Finite–Time Input–to–State Stable
FT–SMO	Finite–Time Sliding–Mode Observer
GSTA	Generalized Super–Twisting Algorithm
GSTO	Generalized Super–Twisting Observers
GUES	Globally Uniformly Exponentially Stable
GUFTS	Globally Uniformly Finite–Time Stable
GUS	Globally Uniformly Stable
HOSMC	High–Order Sliding–Modes Controllers
ISS	Input–to–State Stable
LMI	Linear Matrix Inequality
LOE	Loss Of Effectiveness
NTSMC	Nonsingular Terminal Sliding–Mode Control
PID	Proportional–Integral–Derivative
SISO	Single–Input Single–Output
SMC	Sliding–Mode Control
SMO	Sliding–Mode Observer
STA	Super–Twisting Algorithm
STSMC	Singular Terminal Sliding–Mode Control
UAV	Unmanned Aerial Vehicles
UES	Uniformly Exponentially Stable
UFTS	Uniformly Finite–Time Stable
US	Uniformly Stable

CONTENTS

1 INTRODUCTION

Summary. *This chapter introduces the motivation of the work and the considered problem statements as well as the goals. Afterwards, we provide the state of the art related to the problem statements. Then, the main contribution of the thesis is presented in addition to the scientific production. Finally, we provide the structure of the rest of the document.*

1.1 MOTIVATION

Among the Unmanned Aerial Vehicles (UAVs), the quad–rotor remains as the most used vehicle due to flight flexibility to perform vertical take–off and landing tasks, simplicity of operation and low cost. Consequently, they are used by a wide variety of applications, *e.g.*, agriculture (see Fig 1a), civil events (see Fig 1b), military applications (see Fig 1c), security, industrial supervision, *etc*. (see, for instance, [1]). The growing demand for safety, reliability and acceptable performance level for these tasks is a priority, being a topic of interest in the field of robust control design for these vehicles (see, for instance, [2] and [3]).

However, the design of autonomous flight control systems for quad–rotors is not an easy task in general. The complexity in the controller design for these systems arises from a combination of its under–actuated nature, coupling between translational and rotational dynamics, which are nonlinear, and of course due to the effects of disturbances associated with the environment and payload mass variations. Several control methods have been proposed for the stabilization of quad–rotors; for instance, adaptive control (*e.g.*, [4] and [5]), backstepping control (*e.g.*, [6] and [7]), nested saturation control [8], $\mathcal{H}_\infty$ control [9], immersion and invariance methodology [10], Proportional–Integral–Derivative (PID) controllers [11], feedback linearization (*e.g.*, [12] and [13]), *etc*. Among all these control techniques, the sliding–mode control (SMC) theory (see, *e.g.*, [14] and [15]) has demonstrated to be one of the most useful strategies due to its accuracy and robustness properties as well as finite–time convergence. However, in practical applications, the standard SMC techniques have presented the so–called chattering effect (see, *e.g.*, [16] and [17]), one of the main drawbacks of this control technique.

On the other hand, the *Continuous*–SMC techniques mitigate the chattering problem since the applied control signal is continuous [18]. Nevertheless, such an advantage is compromised by the class of disturbances that these controllers counteract, *i.e.*, Lipschitz continuous. The Super–Twisting algorithm (STA) [19] is a pioneer in these types of controllers, while more recent strategies include the Continuous Twisting Controller (CTC) [20], Continuous Singular Terminal Sliding–Mode Control (STSMC) [21] and Continuous Nonsingular Terminal Sliding–Mode Control (NTSMC) [22].

However, most of these techniques are effective when the system works under rotor nominal conditions. In the presence of actuators faults, the performance level may considerably be degraded when the control commands are operating in a faulty scenario. Moreover, a rotor failure can provoke a dangerous midair collision or hit the ground, being dangerous in the surrounding environment. Such was the case of an accident

(a) Quad–rotors in agriculture

(b) Quad–rotors in civil events

(c) Quad–rotors in military applications

(d) Quad–rotor crashing due to actuator failure

Figure 1: Quad–rotors in practical environments

caused by the sudden rotor failure of a quad–rotor during the Ski World Cup 2016 held in Italy. In this civil event, one competitor nearly suffered serious injuries, or even the death, when a news quad–rotor crashed near him, sending blades, gears and machinery all over the place (see Fig 1d). Therefore, in order to increase safety and robustness, the design of a Fault Diagnosis (FD) method, in order to detect, isolate and identify the magnitude of multiple faults, and the design of a Fault–Tolerant Control (FTC), must be taken into account in order to guarantee system stability and acceptable performance in presence of actuator faults, or even under a rotor failure. Making use of an FTC, it is possible to cope with the faulty quad–rotor and accomplish the tracking task, or, if it is necessary, to carry out landing actions.

1.2 PROBLEM STATEMENTS

The simplified quad–rotor dynamics (see Fig. 2, and for modeling details, see [23]), is given by

$$\dot{\xi}_1 = \xi_2, \tag{1a}$$
$$\dot{\xi}_2 = g_\xi(\eta_1)u_m - G - \Lambda_\xi \xi_2 + d_\xi, \tag{1b}$$
$$\dot{\eta}_1 = \eta_2, \tag{1c}$$
$$\dot{\eta}_2 = J\tau + \Xi w_\eta(\eta_2) - \Lambda_\eta \eta_2 + d_\eta, \tag{1d}$$

where $\xi_1 := (x, y, z)^T \in \mathbb{R}^3$, $\xi_2 := (\dot{x}, \dot{y}, \dot{z})^T \in \mathbb{R}^3$, $\eta_1 := (\phi, \theta, \psi)^T \in \mathbb{R}^3$, $\eta_2 := (\dot{\phi}, \dot{\theta}, \dot{\psi})^T \in \mathbb{R}^3$, $d_\xi := (d_x, d_y, d_z)^T \in \mathbb{R}^3$ and $d_\eta := (d_\phi, d_\theta, d_\psi)^T \in \mathbb{R}^3$. The variables x, $y \in \mathbb{R}$ are the coordinates in the horizontal plane, $z \in \mathbb{R}$ is the vertical position, while ϕ, θ and $\psi \in \mathbb{R}$ are the roll angle around the X–axis, the pitch an-

gle around the Y–axis, and the yaw angle around the Z–axis, respectively. The terms $G := (0,0,g)^T \in \mathbb{R}^3$, $J := \text{diag}(J_x^{-1}, J_y^{-1}, J_z^{-1}) \in \mathbb{R}^{3\times3}$ and $\tau := (\tau_\phi, \tau_\theta, \tau_\psi)^T \in \mathbb{R}^3$ are the gravity vector, the inertial matrix and the angular moment vector, with g as the gravitational acceleration, J_x, J_y and J_z as the moments of inertia along X, Y and Z–axis, while τ_ϕ, τ_θ and $\tau_\psi \in \mathbb{R}$ represent the roll, pitch and yaw angular moments, respectively. The term $u_m := u_z/m$, with $u_z \in \mathbb{R}$ representing the main thrust and $m \in \mathbb{R}_+$ the mass of the quad–rotor. The matrices $\Lambda_\xi := \text{diag}(a_x, a_y, a_z) \in \mathbb{R}^{3\times3}$, $\Lambda_\eta := \text{diag}(a_\phi/J_x, a_\theta/J_y, a_\psi/J_z) \in \mathbb{R}^{3\times3}$ and $\Xi := \text{diag}(b_\phi, b_\theta, b_\psi) \in \mathbb{R}^{3\times3}$ are given by the aerodynamic damping coefficients a_x, a_y and a_z, the rotational resistance moment coefficients a_ϕ, a_θ and a_ψ, and the inertial coefficients $b_\phi := (J_y - J_z)/J_x$, $b_\theta := (J_z - J_x)/J_y$ and $b_\psi := (J_x - J_y)/J_z$. The functions $g_\xi : \mathbb{R}^3 \to \mathbb{R}^3$ and $w_\eta : \mathbb{R}^3 \to \mathbb{R}^3$ are given as: $g_\xi(\eta_1) := (c\phi s\theta c\psi + s\phi s\psi, c\phi s\theta s\psi - s\phi c\psi, c\phi c\theta)^T$ and $w_\eta(\eta_2) := (\dot\theta\dot\psi, \dot\phi\dot\psi, \dot\phi\dot\theta)^T$, respectively. The terms d_x, d_y, d_z, d_ϕ, d_θ and $d_\psi \in \mathbb{R}$ represent disturbances given by uncertainties and external perturbations, *e.g.*, some unmodeled dynamics and wind gusts. Take into account that the notation $s\star := \sin(\star)$ and $c\star := \cos(\star)$ is considered.

In this thesis, the "+" configuration of the quad–rotor is considered. Then, the relation between the control inputs u_z, τ_ϕ, τ_θ, τ_ψ and the thrusts T_i, generated by the i–th rotor, is given by

$$\underbrace{\begin{bmatrix} u_z \\ \tau_\phi \\ \tau_\theta \\ \tau_\psi \end{bmatrix}}_{u} = \underbrace{\begin{bmatrix} 1 & 1 & 1 & 1 \\ 0 & 0 & L & -L \\ L & -L & 0 & 0 \\ K_\tau & K_\tau & -K_\tau & -K_\tau \end{bmatrix}}_{M} \underbrace{\begin{bmatrix} T_1 \\ T_2 \\ T_3 \\ T_4 \end{bmatrix}}_{T}, \tag{2}$$

where u is the control input vector, T is the thrust vector and M is the full rank matrix that relates the control signals to the thrusts. The constant L represents the distance between the motors and the center of mass of the quad–rotor, while K_τ represents the thrust coefficient.

As in [24], [25] and [26], actuator faults are represented by a partial Loss Of Effectiveness (LOE) in the rotors. For instance, a propeller structural damage or an unexpected change in the rotor physical parameters, would result in an LOE on the thrust generated by the respective rotor.

Therefore, in presence of faults, the current command thrust $\bar T$ is given as

$$\bar T(t) = (I_4 - \Gamma(t))\, T(t) = T(t) - f(t), \tag{3}$$

where $\Gamma(t) := \text{diag}(\gamma_1(t), \gamma_2(t), \gamma_3(t), \gamma_4(t)) \in \mathbb{R}^{4\times4}$ is the LOE matrix and $f(t) = \Gamma(t)T(t) := (f_1(t), f_2(t), f_3(t), f_4(t))^T \in \mathbb{R}^4$ is the fault vector. The term $\gamma_i(t) \in (0,1)$

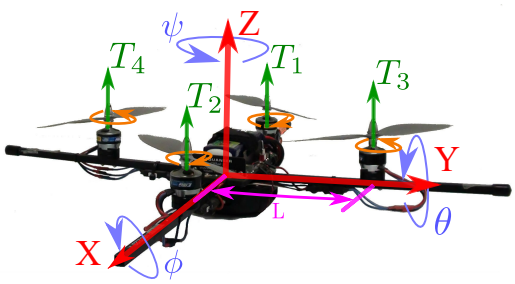

Figure 2: Schematic representation of the quad–rotor

represents the case of an LOE fault in the i–th rotor. The case of $\gamma_i(t) = 0$ represents a healthy rotor, while $\gamma_i(t) = 1$ means that the i–th actuator is fully damaged. Note that the current command thrust $\bar{T}$ is not measured and therefore is unknown.

The goals of this work are listed below:

1. To design robust control strategies to robustly track a desired trajectory for the coordinates x, y, z and the angle ψ, despite some uncertainties and external perturbations.

2. To design an FD method to detect (discern if there are faults or not), isolate (if there are faults, determine which rotors are faulty) and identify the magnitude of each LOE.

3. To design an actuator Fault Accommodation Controller (FAC) to achieve the tracking of a desired trajectory under the influence of possible multiple LOEs.

4. To design an active FTC to achieve the tracking of a desired trajectory under the influence of a rotor failure.

It is assumed that only the positions and angles of the vehicle are measurable.

1.3 STATE OF THE ART

The design of robust controllers applied to quad–rotors is a well treated topic in the literature. A wide variety of strategies have been reported. For instance, in [10] an asymptotic tracking controller is proposed using an immersion and invariance–based adaptive control. A robust cascade controller is presented in [27] based on a robust compensation–based hierarchical control for quad–rotors under external perturbations and multiple delays. In [28], a hierarchical controller for UAVs is proposed based on singular perturbation theory. Different observer–based controllers are designed in [29], [30], [31] and [32] for the trajectory tracking problem of quad–rotors. In [33] a nonlinear ellipsoid based attitude control is proposed for aggressive trajectories in a quad–rotor. However, as mention in Section 1.1, the SMC theory highlights due to its accuracy and robustness properties as well as finite–time convergence.

In the context of SMC theory, in [34] an STA based control is proposed for robust tracking attitude in a quad–rotor under the presence of external perturbations. In [35], a discontinuous model–free–based terminal SMC is presented to control the attitude and position of a quad–rotor despite some uncertainties in a finite time. In the same vein, [36] presents the design of a controller based on the block control technique combined with the STA for the trajectory tracking problem. In [37], a second–order SMC approach is proposed to solve the tracking problem for a quad–rotor. In [38], a chattering–free SMC approach is provided for a real–time application on a quad–rotor to control the attitude. A model–free based terminal SMC is proposed in [35] to control the attitude and position of a quad–rotor under external perturbations. In [39], an integral backstepping combined with the SMC is applied in a quad–rotor to accomplish trajectory tracking. An adaptive fuzzy integral SMC is proposed in [40] for the robust stabilization of a quad–rotor. In [41] an SMC driven by a Sliding–Mode Observer (SMO) is proposed for a quad–rotor under the presence of unknown disturbances. In the same context, in [42] and [43] a high–order SMO has been applied to robustify a flight controller for a quad–rotor. In [2], a robust tracking output–based control strategy with a SMO is proposed for

a quad–rotor under the influence of disturbances, and validated through experimental results.

The work presented in [2] is of great interest since a series of *Continuous*–SMCs (TC, STSMC, NTSMC), together with an Finite–Time Sliding–Mode Observer (FT–SMO), are proposed to the robust trajectory tracking problem in a quad–rotor. Nevertheless, real–time experimental results are only presented for the STSMC. In [44] the previous work is extended, where all these controllers are implemented experimentally, showing a comparative study of their performances.

In all the above strategies, it is ensured that the quad–rotor fulfills the task as long as it works under rotor nominal conditions. In the presence of actuators faults, the performance level may considerably be degraded when the control commands are operating in a faulty scenario. Therefore, in order to increase safety and robustness, an FTC must be designed in order to guarantee system stability and acceptable performance in presence of actuator faults, or even under a rotor failure. The FTC techniques can be classified as two types: passive and active [45].

In the passive techniques, the control law is not changed when a fault occurs and, similar to the robust control approach, the faults can be considered as disturbances. Such approaches have the advantage of not changing the control law in faulty situations but the fault tolerance deteriorates [45]. In the literature there are several works related to passive FTCs applied to quad–rotors. For instance, in [4], a model reference adaptive controller is designed to deal with actuator faults and external perturbations. In [46], an adaptive FTC, based on radial basis function neural networks, is proposed to deal with actuator faults and external perturbations. A passive FTC is proposed in [47] based on the inherent robustness of SMCs. In [48], an adaptive SMC is used to estimate an upper bound of the actuator fault and compensate it. In [49], an adaptive SMC allocation scheme is proposed for accommodating simultaneous actuator faults. However, in the previous works, the faults are not detected and are suitable for goals associated with low performance levels. In this sense, the faults may exceed the FTC capability causing a dangerous collision.

On the other hand, in active FTCs, the FD, *i.e.*, detection, isolation and identification of the faults, plays a major role. In this sense, making use of an FD, the control law can be modified in order to cope with the faulty quad–rotor and accomplish the trajectory tracking task, or, if it is necessary, to carry out landing actions. There are also several works related to active FTCs applied to quad–rotors. For instance, in [50], an adaptive finite–time extended state observer is designed to compensate external perturbations and accommodating actuator faults. In [51], a robust adaptive fault estimation observer is proposed for the design of an active FTC. In the same vein, in [52], an active FTC, based on an adaptive sliding–mode control and recurrent neural networks, is designed only for the rotational subsystem of a quad–rotor considering faults and model uncertainties. An active FTC, based on a nonlinear adaptive FD, is employed for a fault accommodation technique in [24]. In the previous works, the active FTC allows much more demanding objectives in presence of faults. However, knowledge of the fault effect is essential, and it depends mainly on the FD.

Regarding the FD problem in quad–rotors, there are several works reported in the literature. In [53], a torque model, with an FD method, is proposed for the Z–axis accelerometer and the magnetic sensor. An approach for sensor fault reconstruction in presence of external perturbations is designed in [54]. In [55], an FD based on a polyno-

mial observer is proposed for actuator faults without considering disturbances. In the same context, [56] deals with the design of a model–based FD, which can be used to detect sensor and actuator faults, based on a set of residuals. In [57], a residual is generated by the parity space method for actuator faults, and the recursive least squares algorithm is used to identify the fault. In [58], an FD method, based on a two–stage Kalman filter, is designed for actuator faults. In [25], an FD scheme, based on an adaptive augmented state Kalman filter, is designed for actuators faults and external perturbations in the attitude subsystem. In [26], an adaptive Thau observer is developed to build a set of residuals to identify actuators faults. In [59], an adaptive observer–based fault identification scheme is presented for actuator faults without considering external perturbations in the analysis. Nevertheless, in the previous works, the disturbances can affect the performance level since most of the proposed methodologies do not deal with faults and disturbances simultaneously.

In the previous context, SMOs are frequently adopted to deal with disturbance/fault estimation because of their robustness and finite–time convergence. For instance, in [60], an actuator fault reconstruction method is developed for a quad–rotor using an SMO. In [61], a residual–based FD approach is proposed for a 3–degrees of freedom helicopter by using SMOs. In [62], an FD scheme is developed based on a bank of SMOs, which identifies certain types of disturbances and faults. In [63], an FTC driven by SMOs is proposed to deal with disturbances and sudden actuator faults in a quad–rotor. However, in the previous works, the SMOs identify the total uncertainty without distinguishing between faults and disturbances. The problem of distinguishing the fault effect from the disturbances is complex because both of them act in the same input channels, and hence, it is not possible to decouple the faults from disturbances, and deal with the FD. It is worth mentioning that very few works, related to the development of FD methodologies for the quad–rotor, have been reported in the literature addressing the problem of distinguishing between faults and disturbances (see, for instance, [25]).

In the context of rotor failures, in [64], after the complete loss of an actuator, a transformation of the quad–rotor system into a tri–rotor system is proposed. In this approach, disturbances are not considered in the analysis and it is essential to redistribute the quad–rotor weight in order to shift its gravity center toward the rear rotor. Following a similar idea, in [65], a strategy to transform the quad–rotor system into a bi–rotor system is considered neglecting the effect of disturbances. Such an approach turns off the propeller that is aligned on the same axis of the faulty rotor, losing the pitch or roll angle, depending on the pair of rotors that stopped working, as well as the yaw angle. In [66], an FTC, based on periodic solutions, is proposed for a quad–rotor to maintain a regulation task after the loss of one, two or three propellers. However, disturbances are not taken into account, the stability analysis is not addressed and only regulation tasks are considered. In [67], once the yaw rate is stabilized, a cyclic reference is provided for the roll and pitch command angles in order to achieve a regulation goal, but disturbances are not considered. In [68], a multi–loop hybrid nonlinear controller is designed for the quad–rotor system with a single failure. Such a scheme is validated through experimental tests for high–speed tasks in the failure scenario, but it lacks a formal closed–loop stability proof. In [69], an FTC is proposed for a quad–rotor considering a rotor failure and disturbances. The proposed strategy is based on a NTSMC, exploiting its robustness properties, but the yaw dynamics is totally ignored and cannot guarantee

the generation of positive thrusts. In the aforementioned works, the effect of a rotor failure on the angular moments is not considered but there exists.

1.4 CONTRIBUTION

To sum up, the literature shows the following gaps in the considered problem statements:

1. Trajectory tracking control design:
   - Several works do not consider the disturbed case.
   - Most of the works assume that the whole state is measurable.
   - Only the attitude subsystem is addressed.
   - Experimental implementation remains as a challenging problem.
2. FD design:
   - Most of the works do not consider the disturbed case.
   - Distinguishing between faults and disturbances remains as an open problem.
   - Experimental implementation remains as a challenging problem.
3. FTC design under:
   (a) Multiple losses of rotor effectiveness:
   - Most of the works do not consider the disturbed case.
   - Only the attitude subsystem and hover tasks are addressed.
   - Many works do not deal with the problem of multiple actuator faults.
   - The magnitude of each fault is not identified.
   - Experimental implementation remains as a challenging problem.

   (b) A rotor failure:
   - Most of the works do not consider the disturbed case.
   - Only hover tasks are addressed.
   - Not a single work considers the restriction of the signs in the pitching and rolling moments.
   - Not a single work formally analyzes the behavior of the yaw dynamics.

Motivated by the aforementioned gaps, this thesis contributes with:

1. The design of robust trajectory tracking control strategies given by:
   - Continuous High–Order Sliding–Mode Controllers (HOSMCs) and PID controllers, together with an FT–SMO;
   - An Attractive Ellipsoid Method (AEM) controller, together with Generalized Super–Twisting observers (GSTOs).

   The proposed strategies have the following features:
   - Disturbances acting on the whole quad–rotor dynamics are considered.

- Only the position and angles are measurable.
- Experimental results show the performance of such strategies

2. An FD strategy, based on an FT–SMO, is proposed to detect, isolate and identify faults. The proposed strategy possesses the following features:
   - Multiple actuators faults are considered.
   - The presence of disturbances is considered.
   - Experimental results show the performance of the proposed FD strategy.
3. The design of FTCs to deal with:
   (a) Multiple losses of rotor effectiveness, where:
   - An FAC strategy partially compensate multiple actuator faults.
   - The presence of disturbances is considered.
   - The trajectory tracking task is considered.
   - Experimental results show the performance of the proposed FTC.

   (b) A rotor failure, where:
   - The presence of disturbances is considered.
   - The trajectory tracking task is considered.
   - The physical restrictions are not violated.
   - The yaw dynamics behavior is analyzed.
   - Numerical results show the performance of the proposed FTC.

A schematic diagram of the above–mentioned main contributions about the FD and FTC in quad–rotors is depicted in Fig. 3.

1.5 PUBLISHED RESULTS

The content of this thesis has been partially published as follows:

- Chapter 2 – Robust Control Strategies
  1. IEEE Transactions on Industrial Electronics 2019 [2].
  2. Control Engineering Practice 2019 [44].
  3. IEEE Transactions on Industrial Electronics 2020 [3].
  4. International Workshop on Variable Structure Systems 2018 [72].
  5. Congreso Mexicano de Robótica 2018 [73].
  6. Congreso Nacional de Control Automático 2019 [74]
  7. Congreso Nacional de Control Automático 2022 [75]

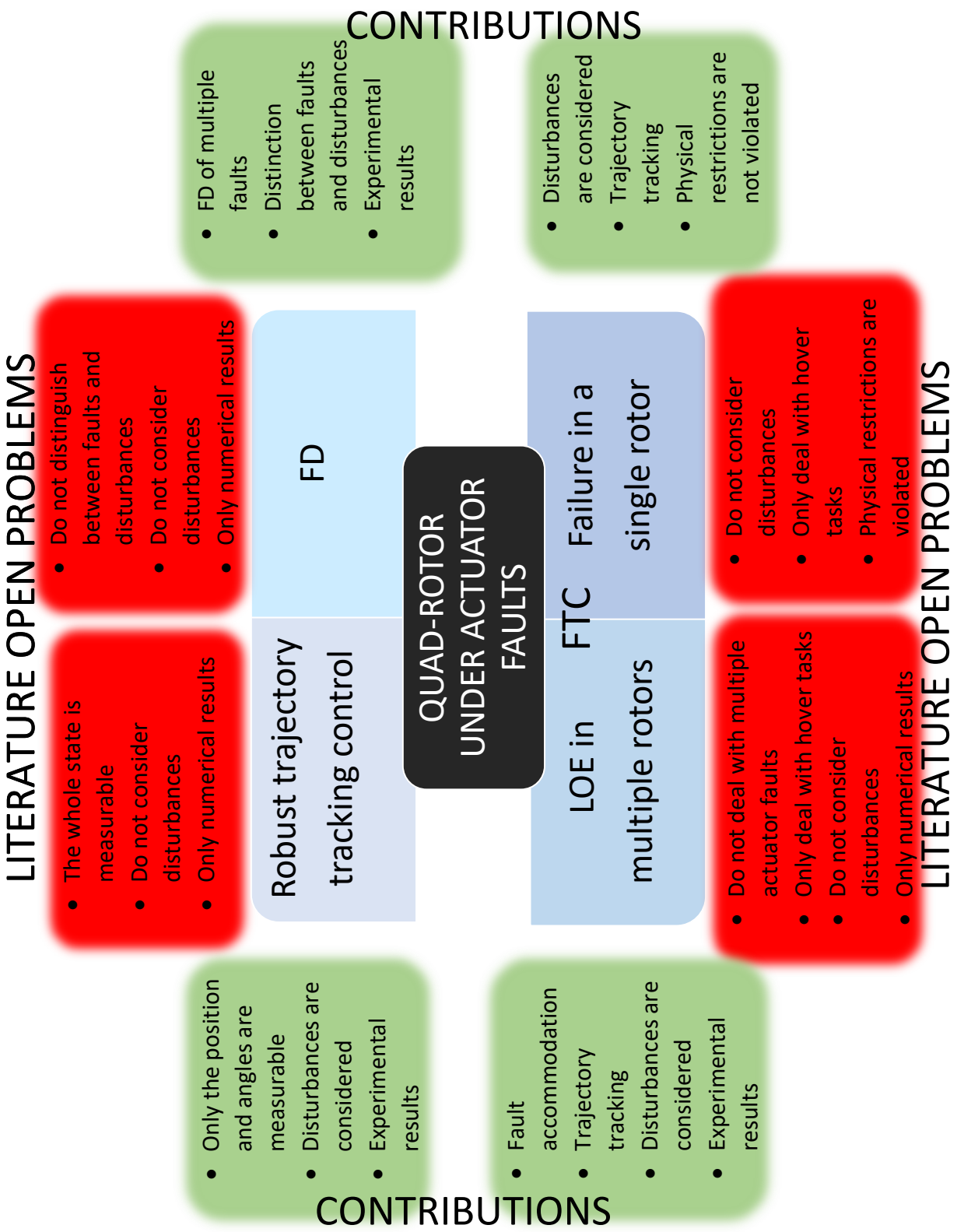

Figure 3: Schematic diagram of the academic contribution about the FTC in quad–rotors

- Chapter 3 – Fault Diagnosis Strategy
  1. IEEE/ASME Transactions on Mechatronics 2022 [77].
  2. Congreso Nacional de Control Automático 2019 [76].
- Chapter 4 – Active Fault Accommodation Control Design
  1. Congreso Nacional de Control Automático 2021 [78].
  2. Conference on Decision and Control 2021 [79].
- Chapter 5 – Fault Tolerant Control for a Rotor Failure
  1. International Journal of Robust and Nonlinear Control 2022 [82].
  2. Congreso Argentino de Control Automático 2020 [80]
  3. Congreso Mexicano de Robótica 2021 [81].

The Appendix C presents a detailed list of the publications made throughout the doctoral studies.

1.6 THESIS STRUCTURE

This thesis is organized as follows. Chapter 2 presents different robust control strategies to deal with the effect of disturbances. The proposed FD method is described in Chapter 3. The active FAC is designed in Chapter 4. An active FTC is proposed to deal with the rotor failure scenario in Chapter 5. Some concluding remarks are given in Chapter 6. Finally, the proofs of some of the proposed results are given in the Appendix A, some details of the experimental platform are given in the Appendix B, and a list of the publications made throughout the PhD studies is given in the Appendix C.

2 ROBUST CONTROL STRATEGIES

Summary. *This chapter introduces the notation and some preliminaries concepts considered in this work. Then, the problem statement of this chapter is formally established. Afterward, different HOSMCs and PID controllers, together with an FT–SMO, as well as an AEM–based controller, together with GSTOs for a quad–rotor under the influence of disturbances are proposed. Experimental results of both strategies are shown.*

2.1 PRELIMINARIES

2.1.1 *Notation*

$0_n \in \mathbb{R}^{n\times n}$ and $I_n \in \mathbb{R}^{n\times n}$ denote the zero and identity matrices of dimension n, respectively; $\wedge$ denotes the logical operator AND; denote $\mathbb{R}_+ := \{x \in \mathbb{R} : x \geqslant 0\}$; for a Lebesgue measurable function $d : \mathbb{R}_+ \to \mathbb{R}^m$, define the norm $\|d\|_{[t_0,t_1)} = \operatorname{esssup}_{t\in[t_0,t_1)}\|d(t)\|$, then $\|d\|_f = \|d\|_{[t_f,+\infty)}$ and $\|d\|_\infty = \|d\|_{[0,+\infty)}$; the set of $d(t)$ with the property $\|d\|_\infty < +\infty$ is denoted as $\mathcal{L}_\infty$; and $\mathcal{L}_D = \{d \in \mathcal{L}_\infty : \|d\|_\infty \leqslant D\}$, for any $D > 0$. A sequence of integers $1, \ldots, n$ is denoted as $\overline{1,n}$. The function $\lceil s \rfloor^\beta := |s|^\beta \operatorname{sign}(s)$, for any $s \in \mathbb{R}$ and $\beta \in \mathbb{R}_{\geqslant 0}$, and $\lceil \mathbf{s} \rfloor^\beta := (\lceil s_1 \rfloor^\beta, \ldots, \lceil s_n \rfloor^\beta)^T$, for any $\mathbf{s} \in \mathbb{R}^n$.

2.1.2 *Stability Concepts*

A continuous function $\alpha : \mathbb{R}_+ \to \mathbb{R}_+$ belongs to class $\mathcal{K}$ if it is strictly increasing and $\alpha(0) = 0$; it belongs to class $\mathcal{K}_\infty$ if it is also unbounded. A continuous function $\beta : \mathbb{R}_+ \times \mathbb{R}_+ \to \mathbb{R}_+$ belongs to class $\mathcal{KL}$ if for each fixed s, $\beta(\cdot, s) \in \mathcal{K}$, and $\beta(r, \cdot)$ is strictly decreasing to zero for any fixed $r \in \mathbb{R}_+$. The function β belongs to class $\mathcal{KL}_T$ if for each fixed s, $\beta(\cdot, s) \in \mathcal{K}$, and for each fixed r, there exists $0 < T(r) < \infty$ such that $\beta(r, s)$ is decreasing to zero with respect to $s < T(r)$, and $\beta(r, s) = 0$ for all $s \geqslant T(r)$.

Consider a time–dependent differential equation [83]:

$$\frac{dx(t)}{dt} = f(t, x(t)),\ t \geqslant t_0,\ t_0 \in \mathbb{R}, \tag{4}$$

where $x(t) \in \mathbb{R}^n$ is the state vector; $f : \mathbb{R} \times \mathbb{R}^n \to \mathbb{R}^n$ is a continuous function with respect to x and piece–wise continuous with respect to t, and $f(t, 0) = 0$ for all $t \in \mathbb{R}$. The solution of the system (4), for an initial condition $x_0 \in \mathbb{R}^n$ at time instant $t_0 \in \mathbb{R}$, is denoted as $x(t, t_0, x_0)$ and defined on some finite time interval $[t_0, t_0 + T)$ such that $0 \leqslant T < \infty$. Let Ω be open neighborhood of the origin in $\mathbb{R}^n$, $0 \in \Omega$.

Definition 1 *(see* [83] *and* [84]*): At the steady state $x = 0$, the system (4) is said to have the following properties*

a) *Uniformly Stable (*US*) if for any $\epsilon > 0$ there is $\delta(\epsilon)$ such that for any $x_0 \in \Omega$, if $\|x_0\| \leqslant \delta(\epsilon)$ then $\|x(t, t_0, x_0)\| \leqslant \epsilon$ for all $t \geqslant t_0$, for any $t_0 \in \mathbb{R}$;*

b) *Uniformly Exponentially Stable (*UES*) if it is* US *and exponentially converging from* Ω*, i.e. for any* $x_0 \in \Omega$ *there exist* $k, \gamma > 0$ *such that* $\|x(t, t_0, x_0)\| \leqslant k\|x_0\|e^{-\gamma(t-t_0)}$ *for all* $t \geqslant t_0$*, for any* $t_0 \in \mathbb{R}$*;*

c) *Uniformly Finite–Time Stable (*UFTS*) if it is* US *and finite–time converging from* Ω*, i.e. for any* $x_0 \in \Omega$ *there exists* $0 \leqslant T_{x_0} < +\infty$ *seuch that* $x(t, t_0, x_0) = 0$ *for all* $t \geqslant t_0 + T_{x_0}$*, for any* $t_0 \in \mathbb{R}$*. The function* $T_0(x_0) = \inf\{T_{x_0} \geqslant 0 : x(t, t_0, x_0) = 0 \ \forall t \geqslant t_0 + T_{x_0}\}$ *is called the settling-time of the system* (4)*.*

If $\Omega = \mathbb{R}^n$*, then* $x = 0$ *is said to be globally* US *(*GUS*),* UES *(*GUES*), or* UFTS *(*GUFTS*), respectively.*

Definition 2 [85]. *System* (4) *is called Input–to–State Stable (*ISS*) if for any input* $u \in \mathcal{L}_\infty$ *there exist functions* $\beta \in \mathcal{KL}$ *and* $\gamma \in \mathcal{K}$ *such that*

$$\|x(t, t_0, x_0, u)\| \leqslant \beta(\|x_0\|, t) + \gamma(\|u\|_\infty), \ \forall t \geqslant 0.$$

Moreover, if the function $\beta \in \mathcal{KL}_T$*, system* (4) *is said to be Finite–Time Input–to–State Stable (*FT–ISS*).*

2.2 PROBLEM STATEMENT

Let us recall the quad–rotor dynamics:

$$\dot{\xi}_1 = \xi_2, \tag{5a}$$
$$\dot{\xi}_2 = g_\xi(\eta_1)u_m - G - \Lambda_\xi \xi_2 + d_\xi, \tag{5b}$$
$$\dot{\eta}_1 = \eta_2, \tag{5c}$$
$$\dot{\eta}_2 = J\tau + \Xi w_\eta(\eta_2) - \Lambda_\eta \eta_2 + d_\eta, \tag{5d}$$

where $\xi_1 := (x, y, z)^T \in \mathbb{R}^3$, $\xi_2 := (\dot{x}, \dot{y}, \dot{z})^T \in \mathbb{R}^3$, $\eta_1 := (\phi, \theta, \psi)^T \in \mathbb{R}^3$ and $\eta_2 := (\dot{\phi}, \dot{\theta}, \dot{\psi})^T \in \mathbb{R}^3$ represent the quad–rotor positions, linear velocities, angles and angular velocities , respectively. The term $u_m := u_z/m$, with $u_z \in \mathbb{R}$ representing the main thrust and $m \in \mathbb{R}_+$ the mass of the quad–rotor. $\tau := (\tau_\phi, \tau_\theta, \tau_\psi)^T \in \mathbb{R}^3$ represents the angular moment vector with τ_ϕ, τ_θ and $\tau_\psi \in \mathbb{R}$ as the roll, pitch and yaw angular moments, respectively. $d_\xi := (d_x, d_y, d_z)^T \in \mathbb{R}^3$ and $d_\eta := (d_\phi, d_\theta, d_\psi)^T \in \mathbb{R}^3$ represent disturbances given by uncertainties and external perturbations, *e.g.*, some unmodeled dynamics and wind gusts.

The goal in this chapter is to design robust control strategies to robustly track a desired trajectory for the coordinates x, y, z and the angle ψ, despite some uncertainties and external perturbations. It is assumed that only the positions and angles of the vehicle are measurable.

Before proceeding, the following assumptions are introduced.

Assumption 1 *The desired trajectories* $x_d(t)$, $y_d(t)$, $z_d(t)$ *and* $\psi_d(t)$ *are bounded and continuously differentiable.*

Assumption 2 *The disturbances are uniformly bounded and Lipschitz, i.e.,* $d_x \in \mathcal{L}_{D_1}$, $d_y \in \mathcal{L}_{D_2}$, $d_z \in \mathcal{L}_{D_3}$, $d_\phi \in \mathcal{L}_{D_4}$, $d_\theta \in \mathcal{L}_{D_5}$, $d_\psi \in \mathcal{L}_{D_6}$, $\dot{d}_x \in \mathcal{L}_{\bar{D}_1}$, $\dot{d}_y \in \mathcal{L}_{\bar{D}_2}$, $\dot{d}_z \in \mathcal{L}_{\bar{D}_3}$, $\dot{d}_\phi \in \mathcal{L}_{\bar{D}_4}$, $\dot{d}_\theta \in \mathcal{L}_{\bar{D}_5}$, $\dot{d}_\psi \in \mathcal{L}_{\bar{D}_6}$*; with known positive constants* D_j *and* $\bar{D}_j$*, with* $j = \overline{1,6}$*.*

Assumptions 1 and 2 characterize the class of desired trajectories and disturbances that the proposed controllers will be able to deal with. It is worth mentioning that external perturbations, as wind gusts, are generally modeled as sinusoidal signals, which are clearly bounded and Lipschitz [86]. However, since the quad–rotor does not perform aggressive maneuvers, then the load disturbances can be classified into this class of perturbations.

In the following, the design of multiple robust tracking output–control strategies for a quad–rotor is addressed.

2.3 CONTINUOUS SLIDING–MODE CONTROL STRATEGIES

The robust tracking controllers designed in this Section are composed on a combination between PID controllers and cascaded HOSMCs, together with an FT–SMO. Firstly, the design of the FT–SMO is presented.

2.3.1 *Finite–Time Sliding Mode-Observer*

Let us introduce the following constraint.

Assumption 3 *The term $w_\eta(\eta_2)$ is Lipschitz, i.e., $\|w_\eta(\eta_2) - w_\eta(\hat{\eta}_2)\|_\infty \leqslant L_\vartheta \|\eta_2 - \hat{\eta}_2\|_\infty$, for any $\eta_2, \hat{\eta}_2 \in \mathbb{R}^4$.*

Note that the previous constraint is satisfied as long as the quad–rotor does not perform aggressive maneuvers, *i.e.*, any trajectory for which the roll and pitch angles exceed $\pm\pi/2$ [rad], and whose angular velocities growth faster than a linear rate.

In this sense, Assumption 3 implies that the pitch and roll angles must hold $|\phi| < \pi/2$ and $|\theta| < \pi/2$, respectively; and this could be possible if the desired trajectories are Lipschitz; therefore, such a constraint is satisfied.

The FT–SMO has the following structure [18]

$$\dot{\hat{\xi}}_1 = \hat{\xi}_2 + \hat{K}_1 \varphi_1(\hat{e}_\xi), \tag{6a}$$

$$\dot{\hat{\xi}}_2 = g_\xi(\eta_1) u_m - G - \Lambda_\xi \xi_2 + \hat{\xi}_3 + \hat{K}_2 \varphi_2(\hat{e}_\xi), \tag{6b}$$

$$\dot{\hat{\xi}}_3 = \hat{K}_3 \varphi_3(\hat{e}_\xi), \tag{6c}$$

$$\dot{\hat{\eta}}_1 = \hat{\eta}_2 + \hat{K}_4 \varphi_1(\hat{e}_\eta), \tag{6d}$$

$$\dot{\hat{\eta}}_2 = J\tau + \Xi w_\eta(\eta_2) - \Lambda_\eta \eta_2 + \hat{\eta}_3 + \hat{K}_5 \varphi_2(\hat{e}_\eta), \tag{6e}$$

$$\dot{\hat{\eta}}_3 = \hat{K}_6 \varphi_3(\hat{e}_\eta), \tag{6f}$$

where $\hat{e}_\xi := \xi_1 - \hat{\xi}_1 \in \mathbb{R}^3$ and $\hat{e}_\eta := \eta_1 - \hat{\eta}_1 \in \mathbb{R}^3$ are the output errors, respectively; the nonlinear output injections φ_1, φ_2, $\varphi_3 : \mathbb{R}^3 \to \mathbb{R}^3$ are given as $\varphi_1(\mathbf{s}) := \lceil \mathbf{s} \rfloor^{\frac{2}{3}}$, $\varphi_2(\mathbf{s}) := \lceil \mathbf{s} \rfloor^{\frac{1}{3}}$ and $\varphi_3(\mathbf{s}) := \lceil \mathbf{s} \rfloor^0$, for any $\mathbf{s} \in \mathbb{R}^3$, with some design diagonal gain matrices $\hat{K}_j = \mathrm{diag}(\hat{k}_{j1}, \hat{k}_{j2}, \hat{k}_{j3}) \in \mathbb{R}^{3\times 3}$ with $j = \overline{1,6}$.

Define the state estimation error as $\hat{e}_r := (\hat{e}_\xi, \hat{\varepsilon}_\xi, \hat{e}_\eta, \hat{\varepsilon}_\eta, \hat{e}_\xi, \hat{e}_\eta)^T \in \mathbb{R}^{18}$, where $\hat{\varepsilon}_\xi := \xi_2 - \hat{\xi}_2 \in \mathbb{R}^3$ and $\hat{\varepsilon}_\eta := \eta_2 - \hat{\eta}_2 \in \mathbb{R}^3$ are the linear and angular velocity estimation errors, respectively, while $\hat{e}_\xi := d_\xi(t) - \hat{\xi}_3$ and $\hat{e}_\eta := d_\eta(t) - \hat{\eta}_3$ are the estimation

errors of the disturbances. In this sense, the total uncertainty affecting the estimation error between system (1) and the FT–SMO (6) is given by

$$\Delta = \begin{pmatrix} \Delta_\xi \\ \Delta_\eta \end{pmatrix} := \begin{pmatrix} d_\xi - \Lambda_\xi \hat{\varepsilon}_\xi \\ d_\eta - \Lambda_\eta \hat{\varepsilon}_\eta + \Xi(w_\eta(\eta_2) - w_\eta(\hat{\eta}_2)) \end{pmatrix}.$$

Due to Assumptions 2 and 3, such disturbances, velocities and nonlinear terms are bounded and Lipschitz, *i.e.*, $\Delta \in \mathcal{L}_\delta$ and $\dot{\Delta} \in \mathcal{L}_{\bar{\delta}}$, with known positive constants δ and $\bar{\delta}$.

The following theorem describes the finite–time convergence properties of the FT–SMO.

Theorem 1 [2], [87]. *Let the observer* (6) *be applied to system* (5)*, and Assumptions 2 and 3 be satisfied. Suppose that the observer parameters are selected as* $\hat{K}_1 = \hat{K}_4 = 2\bar{\delta}^{\frac{1}{3}} I_3$, $\hat{K}_2 = \hat{K}_5 = 1.5\bar{\delta}^{\frac{1}{2}} I_3$ *and* $\hat{K}_3 = \hat{K}_6 = 1.1\bar{\delta} I_3$*; then, at the steady state* $\hat{e}_r = 0$*, the state estimation error dynamics is* UFTS.

Under Assumptions 2, and 3, the state estimation error dynamics is decoupled into six independent Single–Input Single–Output (SISO) systems, where each error dynamics is in the same form given by [18]. The design parameter $\bar{\delta}$, for the gain matrices $\hat{K}_j$, $j = \overline{1,6}$, ensures the finite–time convergence to zero for the six SISO state estimation error dynamics.

Hence, the corresponding error dynamics can be written as follows

$$\begin{aligned} \dot{\hat{e}}_\xi &= \hat{\varepsilon}_\xi - \hat{K}_1 \varphi_1(\hat{e}_\xi), \quad \dot{\hat{e}}_\eta = \hat{\varepsilon}_\eta - \hat{K}_4 \varphi_1(\hat{e}_\eta), \\ \dot{\hat{\varepsilon}}_\xi &= \hat{e}_\xi - \hat{K}_2 \varphi_2(\hat{e}_\xi), \quad \dot{\hat{\varepsilon}}_\eta = \hat{e}_\eta - \hat{K}_5 \varphi_2(\hat{e}_\eta), \\ \dot{\hat{e}}_\xi &= \dot{d_\xi} - \hat{K}_3 \varphi_3(\hat{e}_\xi), \quad \dot{\hat{e}}_\eta = \dot{d_\eta} - \hat{K}_6 \varphi_3(\hat{e}_\eta). \end{aligned}$$

According to Theorem 1, such an error dynamics is UFTS, which implies that $\hat{\xi}_1(t) = \xi_1(t)$, $\hat{\xi}_2(t) = (\dot{\hat{x}}, \dot{\hat{y}}, \dot{\hat{z}})^T = \xi_2(t)$, $\hat{\xi}_3(t) = d_\xi(t)$ and $\hat{\eta}_1(t) = \eta_1(t)$, $\hat{\eta}_2(t) = (\dot{\hat{\phi}}, \dot{\hat{\theta}}, \dot{\hat{\psi}})^T = \eta_2(t)$, $\hat{\eta}_3(t) = d_\eta(t)$, for all $t \geqslant \mathcal{T}_0 > 0$. Hence, if Assumption 2 holds, then the FT–SMO given by (6) provides the following disturbance identifications for all $t \geqslant \mathcal{T}_0$

$$\hat{\xi}_3(t) = (\hat{\xi}_x(t), \hat{\xi}_y(t), \hat{\xi}_z(t))^T = (d_x(t), d_y(t), d_z(t))^T, \tag{7a}$$

$$\hat{\eta}_3(t) = (\hat{\eta}_x(t), \hat{\eta}_y(t), \hat{\eta}_z(t))^T = (d_\phi(t), d_\theta(t), d_\psi(t))^T. \tag{7b}$$

Note that such identification terms can be used to robustify any type of control strategy, including a simple linear strategy.

2.3.2 *Control Design*

The proposed strategy is based on two cascading loops. The internal loop controls the attitude of the vehicle, while the external loop contains the controllers of the translational coordinates. In this way, the external loop generates a desired roll and pitch angles, that the internal loop will use in the attitude control.

Let us define the tracking errors as

$$\begin{aligned} e_\xi &= (e_x, e_y, e_z)^T := \xi_1 - \xi_d, \quad e_\eta = \left(e_\phi, e_\theta, e_\psi\right)^T := \eta_1 - \eta_d, \\ \varepsilon_\xi &= (\varepsilon_x, \varepsilon_y, \varepsilon_z)^T := \hat{\xi}_2 - \dot{\xi}_d, \quad \varepsilon_\eta = \left(\varepsilon_\phi, \varepsilon_\theta, \varepsilon_\psi\right)^T := \hat{\eta}_2 - \dot{\eta}_d, \end{aligned}$$

where $\xi_d := (x_d, y_d, z_d)^T \in \mathbb{R}^3$ and $\eta_d := (\phi_\star, \theta_\star, \psi_d)^T \in \mathbb{R}^3$ are the desired trajectories, with $\phi_\star$ and $\theta_\star$ being reference signals to be designed. Then, the tracking error dynamics is given as follows:

$$\dot{e}_\xi = \varepsilon_\xi, \tag{8a}$$
$$\dot{\varepsilon}_\xi = g_\xi(\eta_1)u_m - G - \Lambda_\xi \xi_2 + d_\xi - \ddot{\xi}_d, \tag{8b}$$
$$\dot{e}_\eta = \varepsilon_\eta, \tag{8c}$$
$$\dot{\varepsilon}_\eta = J\tau + \Xi w_\eta(\eta_2) - \Lambda_\eta \eta_2 + d_\eta - \ddot{\eta}_d. \tag{8d}$$

Note that due to the underactuated nature of the quad–rotor, one cannot control all the positions and angles independently. Hence, the references signals $\phi_\star$ and $\theta_\star$ as well as the control input u_m and τ must be properly designed in order to achieve a desired position ξ_d and a desired angle ψ_d . To do this, a virtual control $\nu := (\nu_x, \nu_y, \nu_z)^T \in \mathbb{R}^3$ is introduced in the position error dynamics, *i.e.*,

$$\dot{e}_\xi = \varepsilon_\xi, \tag{9a}$$
$$\dot{\varepsilon}_\xi = \nu + w_\xi(\eta_1, u_z, \nu) + g_\xi(\eta_1)u_m - G - \Lambda_\xi \xi_2 + d_\xi - \ddot{\xi}_d, \tag{9b}$$
$$\dot{e}_\eta = \varepsilon_\eta, \tag{9c}$$
$$\dot{\varepsilon}_\eta = J\tau + \Xi w_\eta(\eta_2) - \Lambda_\eta \eta_2 + d_\eta - \ddot{\eta}_d. \tag{9d}$$

where the disturbance term $w_\xi \in \mathbb{R}^3$ is given as $w_\xi(\eta_1, u_z, \nu) := u_m g_\xi(\eta_1) - G - \nu$. Thus, the virtual control ν may be chosen as follows [2]:

$$\phi_\star = \arcsin[u_m^{-1}(\nu_x \sin(\psi_d) - \nu_y \cos(\psi_d))], \tag{10a}$$
$$\theta_\star = \arctan[(\nu_z + g)^{-1}(\nu_x \cos(\psi_d) + \nu_y \sin(\psi_d))], \tag{10b}$$
$$u_m = \sqrt{\nu_x^2 + \nu_y^2 + (\nu_z + g)^2}, \tag{10c}$$

where the virtual control ν, and the angular moment vector τ take the following form

$$\nu = \bar{\nu} + \Lambda_\xi \xi_2 + \ddot{\xi}_d - \hat{\xi}_3, \tag{11a}$$
$$\tau = J^{-1}(\bar{\tau} - \Xi w_\eta(\eta_2) + \Lambda_\eta \eta_2 + \ddot{\eta}_d - \hat{\eta}_3). \tag{11b}$$

The virtual controller $\bar{\nu}$ is designed as a PID controller, *i.e.*,

$$\bar{\nu} = K_{i\xi}\bar{e}_\xi + K_{p\xi}e_\xi + K_{d\xi}\varepsilon_\xi, \tag{12}$$

where $K_{i\xi} = \mathrm{diag}(k_{x1}, k_{y1}, k_{z1}) \in \mathbb{R}^{3\times3}$, $K_{p\xi} = \mathrm{diag}(k_{x2}, k_{y2}, k_{z2}) \in \mathbb{R}^{3\times3}$, $K_{d\xi} = \mathrm{diag}(k_{x3}, k_{y3}, k_{z3}) \in \mathbb{R}^{3\times3}$ and $\bar{e}_\xi := (\bar{e}_x, \bar{e}_y, \bar{e}_z)^T \in \mathbb{R}^3$, with $\bar{e}_p := \int_0^t e_p(\tau)d\tau$, $p = x, y, z$; and the gains are selected such that the matrices

$$\begin{pmatrix} 0 & 1 & 0 \\ 0 & 0 & 1 \\ k_{p1} & k_{p2} & k_{p3} \end{pmatrix}, \tag{13}$$

are Hurwitz.

On the other hand, each term of $\bar{\tau} := (\bar{\tau}_\phi, \bar{\tau}_\theta, \bar{\tau}_\psi) \in \mathbb{R}^3$ can be designed by any of the following five controllers:

a) PID Controller:

$$\bar{\tau}_q = k_{q1}\bar{e}_q + k_{q2}e_q + k_{q3}\varepsilon_q, \tag{14}$$

where $\bar{e}_q := \int_0^t e_q(\tau)d\tau$, with $q = \phi, \theta, \psi$; and the gains are selected such that the matrices

$$\begin{pmatrix} 0 & 1 & 0 \\ 0 & 0 & 1 \\ k_{q1} & k_{q2} & k_{q3} \end{pmatrix}, \tag{15}$$

are Hurwitz.

b) Continuous Super–Twisting Algorithm (STA) [19]:

$$s_q = \varepsilon_q + k_{q1}e_q, \tag{16a}$$
$$\bar{\tau}_q = v - k_{q2}\lceil s_q \rfloor^{\frac{1}{2}}, \tag{16b}$$
$$\dot{v} = -k_{q3}\lceil s_q \rfloor^0. \tag{16c}$$

A possible selection for the gains is given by [88] and shown in Table 1.

Table 1: STA's gains selection.

Set	k_{q1}	k_{q2}	k_{q3}	ζ
1	> 0	$1.5\zeta^{\frac{1}{2}}$	1.1ζ	> 0

c) Continuous Twisting Control (CTC) [20]:

$$\bar{\tau}_q = v - k_{q1}\lceil e_q \rfloor^{\frac{1}{3}} - k_{q2}\lceil \varepsilon_q \rfloor^{\frac{1}{2}}, \tag{17a}$$
$$\dot{v} = -k_{q3}\lceil e_q \rfloor^0 - k_{q4}\lceil \varepsilon_q \rfloor^0. \tag{17b}$$

One possible choice for gains is given in Table 2.

Table 2: TC's gains selection.

Set	k_{q1}	k_{q2}	k_{q3}	k_{q4}	ζ
1	$25\zeta^{\frac{2}{3}}$	$15\zeta^{\frac{1}{2}}$	2.3ζ	1.1ζ	> 0
2	$19\zeta^{\frac{2}{3}}$	$10\zeta^{\frac{1}{2}}$	2.3ζ	1.1ζ	> 0
3	$13\zeta^{\frac{2}{3}}$	$7.5\zeta^{\frac{1}{2}}$	2.3ζ	1.1ζ	> 0
4	$7\zeta^{\frac{2}{3}}$	$5\zeta^{\frac{1}{2}}$	2.3ζ	1.1ζ	> 0

d) Continuous Singular Terminal Sliding–Mode Control (STSMC) [21]:

$$s_q = \varepsilon_q + k_{q1}\lceil e_q \rfloor^{\frac{2}{3}}, \tag{18a}$$
$$\bar{\tau}_q = v - k_{q2}\lceil s_q \rfloor^{\frac{1}{2}}, \tag{18b}$$
$$\dot{v} = -k_{q3}\lceil s_q \rfloor^0. \tag{18c}$$

A possible selection for gains is given in Table 3.

Table 3: STSMC's gains selection.

Set	k_{q1}	k_{q2}	k_{q3}	ζ
1	> 0	$1.5\zeta^{\frac{1}{2}}$	1.1ζ	> 0

e) Continuous Nonsingular Terminal Sliding–Mode Control (NTSMC) [22]:

$$s_q = e_q + k_{q1}\lceil \varepsilon_q \rfloor^{\frac{3}{2}}, \tag{19a}$$

$$\bar{\tau}_q = \upsilon - k_{q2}\lceil s_q \rfloor^{\frac{1}{3}}, \tag{19b}$$

$$\dot{\upsilon} = -k_{q3}\lceil s_q \rfloor^{0}. \tag{19c}$$

A possible selection for gains is shown in Table 4.

Table 4: NTSMC's gains selection.

Set	k_{q1}	k_{q2}	k_{q3}	ζ
1	$20\zeta^{-\frac{1}{2}}$	$4.4\zeta^{\frac{2}{3}}$	2.5ζ	> 0
2	$28.7\zeta^{-\frac{1}{2}}$	$4.5\zeta^{\frac{2}{3}}$	2ζ	> 0
3	$7.7\zeta^{-\frac{1}{2}}$	$7.5\zeta^{\frac{2}{3}}$	2ζ	> 0
4	$\zeta^{-\frac{1}{2}}$	$16\zeta^{\frac{2}{3}}$	7ζ	> 0

Hence, the following result is recalled.

Theorem 2 [2]. *Let the control* (10) *and* (11) *be applied to system* (5)*, and Assumptions 1, 2 and 3 be satisfied. Suppose that the virtual PID controller gains are such that the matrix* (13) *is Hurwitz, and* $\bar{\tau}_\phi$*,* $\bar{\tau}_\theta$ *and* $\bar{\tau}_\psi$ *are designed according to any of the controllers given in a)-e). Then, at steady state* $(e_\xi, \varepsilon_\xi, e_\eta, \varepsilon_\eta) = 0$*, the tracking error dynamics is* GUES.

The corresponding proofs of the convergence to zero of the tracking error dynamics for the TC, STSMC and NTSMC can be checked in [2]. On the other hand, for the convergence of the robustified PID controller and the STA one can follow exactly the same procedure, given in [2], to show that the tracking error is also exponentially stable.

2.3.3 *Experimental Results*

In the following, experimental results on the QBall2 by Quanser (see Fig. 4), using the CTC given in (17), are shown for the trajectory tracking task of a quad–rotor under wind gusts. Such wind gusts are generated by means of an industrial fan that provides a wind velocity between 2.1[m/s] and 4.2[m/s], over a diagonal of the X–Y–axis, that changes depending on the distance between the fan and the vehicle (see Fig. 44). For more details about the Qball2, the experimental platform, and the parameters of the model (5), please see Appendix B.

The experiments presented in this Section have been implemented with the Euler's integration method and a sampling time equal to $h_s = 0.002$[s]. The parameters for the controllers were selected according to (13) and the Table 2, and are given as $K_{i\xi} =$

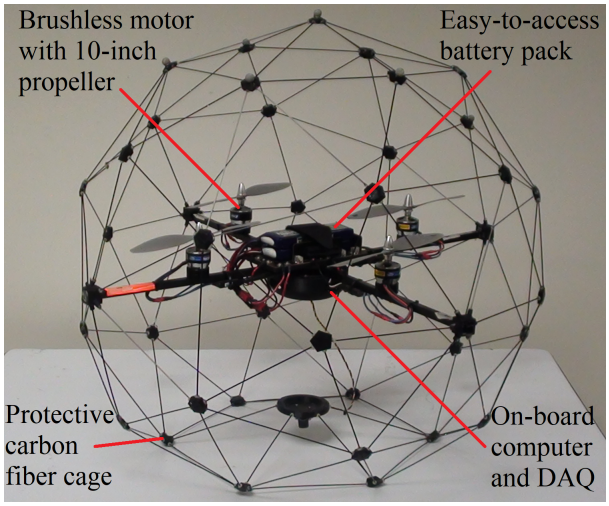

Figure 4: QBall2 by Quanser

$\mathrm{diag}(0.006, 0.006, 0.2)$, $K_{p\xi} = \mathrm{diag}(0.08, 0.08, 0.25)$, $K_{d\xi} = \mathrm{diag}(0.06, 0.06, 0.156)$, $k_{q1} = 0.256$, $k_{q2} = 0.418$, $k_{q3} = 0.016$ and $k_{q4} = 0.006$, with $q = \phi, \theta, \psi$.

Before proceeding with the experimental results, the following expressions are introduced:

$$\bar{\mathcal{F}}(t) = \frac{1}{n_t}\sum_{i=1}^{n_t} \mathcal{F}_i(t), \quad \bar{\mathcal{F}}\text{-Mean} = \frac{1}{n_s}\sum_{j=t_o/h_s}^{n_s} \bar{\mathcal{F}}(jh_s), \tag{20}$$

where $\mathcal{F}_i : \mathbb{R}_+ \to \mathbb{R}$ is a positive function given by the i–th trial test, $\bar{\mathcal{F}} : \mathbb{R}_+ \to \mathbb{R}$ represents the average function given by n_t trial tests, $\bar{\mathcal{F}}$-Mean $\in \mathbb{R}_+$ represents the mean value of the average function, n_s is the number of samples and t_o is the take–off time. For these experimental results $n_t = 10$, $n_s = 30000$ and $t_o = 5$[s].

In order to better illustrate the performance of the CTC, 10 trial tests have been done for each of the controllers. For the sake of clarity, only the average signals are illustrated.

The desired trajectory is given as:

$$\begin{aligned}
x_d(t) =& r(\arctan(\varphi) + \arctan(t-\varphi))\cos(\omega t),\\
y_d(t) =& r(\arctan(\varphi) + \arctan(t-\varphi))\sin(\omega t),\\
z_d(t) =& 0.26(1+\tanh(t-7.5)) + 0.1(1+\tanh((t-35)/3) + 0.28,\\
\psi_d(t) =& 0,
\end{aligned}$$

with $r = 0.2$[m], $\varphi = 15$[rad] and $\omega = \pi/6$[rad/s].

The tracking results are illustrated through are depicted in Fig. 5. In this figure, one can see the real quad–rotor (x, y, z)–position and ψ orientation compared to the corresponding desired trajectory. The corresponding pitch and roll angles are illustrated in Fig. 6 while the control signals are depicted in Fig. 7.

From these figures, one can notice the robust performance in the trajectory tracking, even under the effects of wind gusts. The pitch and roll angles does not exceed ± 4 degrees, and the control signals are bounded.

In order to better illustrate the performance, the following performance index is proposed

$$\mathcal{F}_{RMS}(t) = \left(\frac{1}{\Delta T}\int_{t-\Delta T}^{T} \|\mathcal{F}(\sigma)\|^2 \, d\sigma\right)^{1/2}, \tag{21}$$

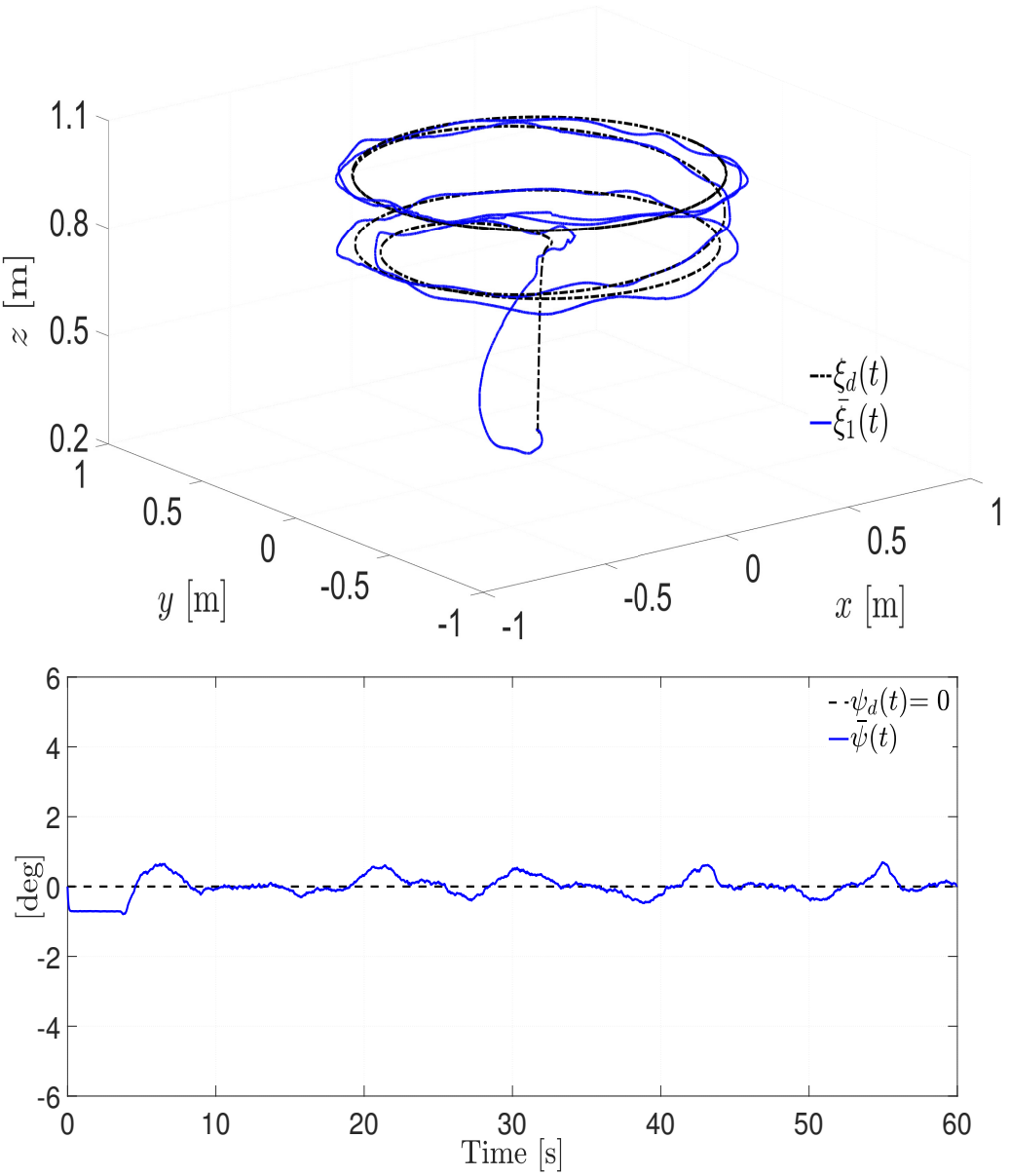

Figure 5: Quad–rotor position and yaw orientation

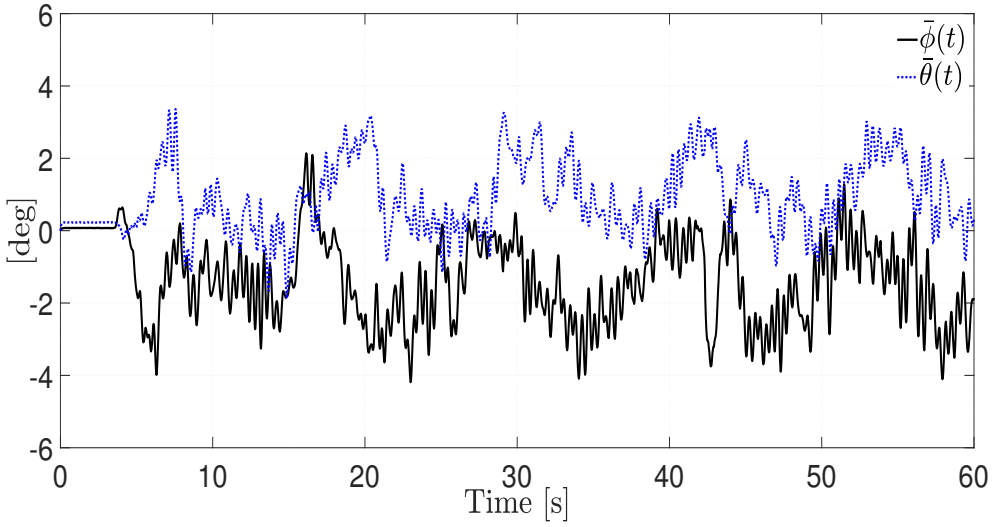

Figure 6: Quad–rotor roll and pitch orientation

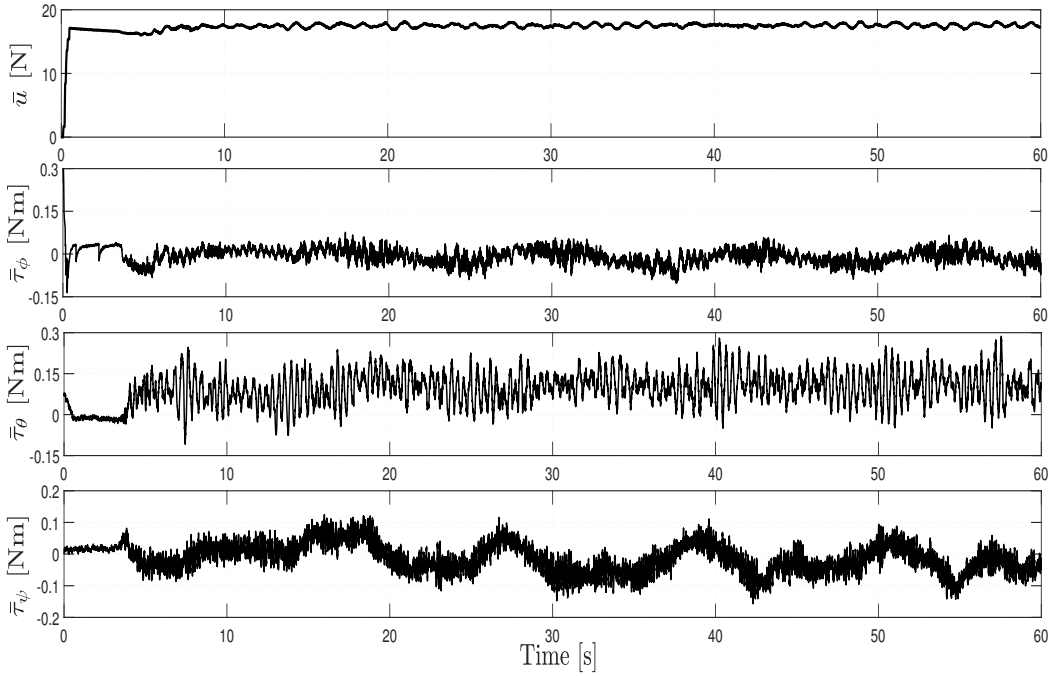

Figure 7: Control signals

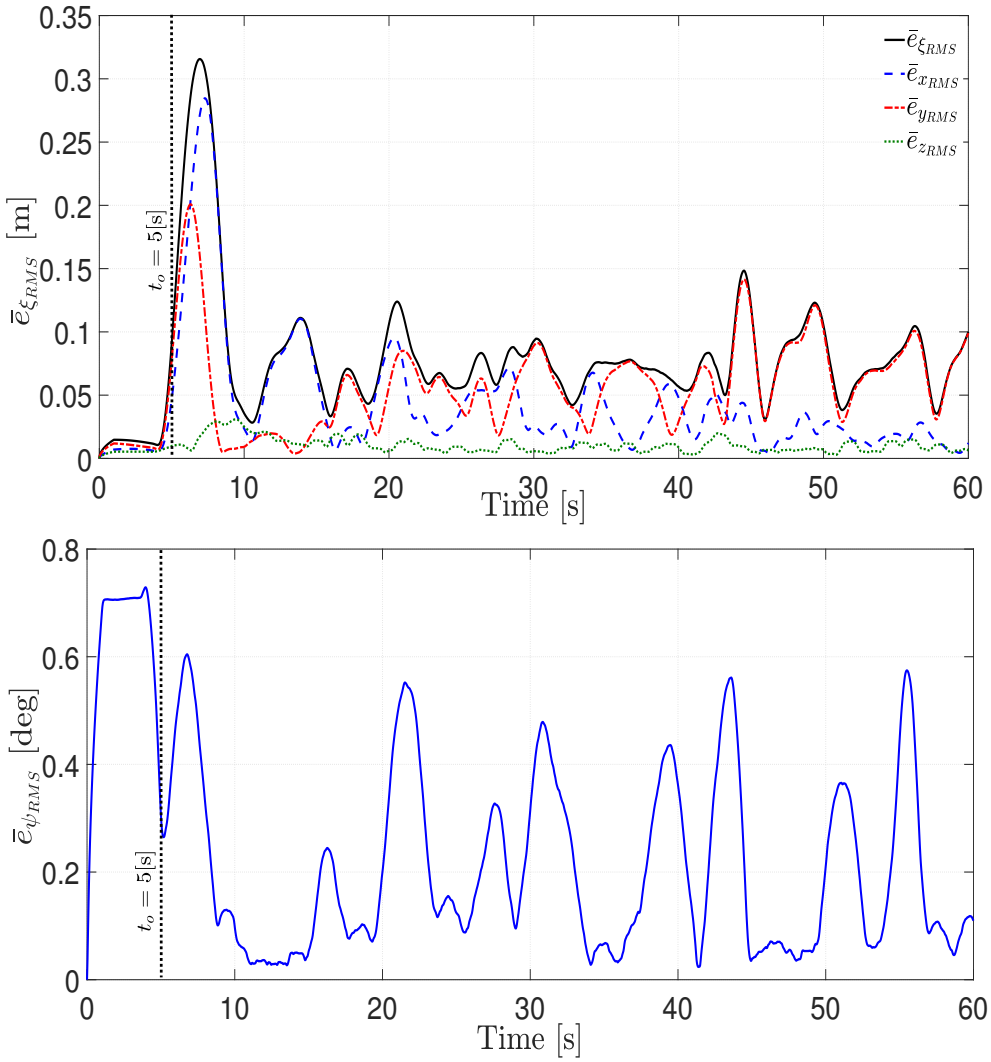

Figure 8: Quad–rotor position and yaw orientation

where $\mathcal{F}_{RMS} : \mathbb{R} \to \mathbb{R}_{\geqslant 0}$ represents the root mean square value of the function $\mathcal{F} : \mathbb{R} \to \mathbb{R}^n$. The results of the performance indexes average for the position tracking error and the yaw angle error, with $\Delta T = 2$, are depicted in Fig. 8.

The take–off of the quad–rotor is a crucial part of the experiments since, due to the quad–rotor cage, there exists a physical contact with the ground provoking some friction effects that could affect the performance of the tests. In this sense, from Fig. 8 one can note that the performance is affected at the beginning of the test.

Based on these results, the CTC strategy provides an acceptable performance despite the wind gusts. To provide a more precise quantitative comparison, some numerical properties of the performance indexes average, *i.e.*, the minimum, the mean and the maximum values, are illustrated in Tab. 5. In order to neglect the initial conditions effect, such values are taken from the take–off time $t_o = 5$[s].

Table 5: CTC performance index properties

Coordinate	$\min(\bar{e}_{RMS})$	$\bar{e}_{RMS}$-Mean	$\max(\bar{e}_{RMS})$
x	0.0044	0.0459	0.2846
y	0.0040	0.0596	0.2008
z	0.0028	0.0107	0.0309
ξ	0.0283	0.0843	0.3156
ψ	0.0238	0.2053	0.6044

2.3.4 *Comparative analysis of continuous sliding–modes control strategies*

It is worth mentioning that a comparative study of the practical performance of the controllers given in (14)–(19) was developed in [44]. In such a study, by using different performance indices (for instance, root mean square values, the minimum, mean and maximum values, convergence time, *etc.*), and through different robustness tests (for instance, tracking task under wind gusts and load disturbances), these controllers were tested.

Due to the robustness of the controllers, all of them have demonstrated an acceptable performance even under wind gusts and load disturbances. However, the study shows that the CTC provides the best performance, according to the proposed indexes. On the other hand, the robustified PID controller gives the worst performance. For more details about this comparative study, please see [44].

2.4 ATTRACTIVE ELLIPSOID–BASED ROBUST CONTROL

The robust tracking control designed in this Section is composed by AEM–based controllers together with a GSTO. Such a proposal is proposed in [3].

Let us write the system (5) in the following compact way

$$\dot{\xi} = A\xi + B(g_\xi(\eta_1)u_m - G - \Lambda_\xi\xi_2 + d_\xi), \tag{22a}$$
$$\dot{\eta} = A\eta + B(J\tau + \Xi w_\eta(\eta_2) - \Lambda_\eta\eta_2 + d_\eta), \tag{22b}$$

where $\xi := (\xi_1^T, \xi_2^T)^T \in \mathbb{R}^6$, $\eta := (\eta_1^T, \eta_2^T)^T \in \mathbb{R}^6$ and the matrices A and B are given as

$$A := \begin{pmatrix} 0_3 & I_3 \\ 0_3 & 0_3 \end{pmatrix} \in \mathbb{R}^{6\times 6}, \; B := \begin{pmatrix} 0_3 \\ I_3 \end{pmatrix} \in \mathbb{R}^{6\times 3}.$$

Let us define the tracking errors as $e_\xi := \xi - (\xi_d^T, \dot{\xi}_d^T)^T \in \mathbb{R}^6$ and $e_\eta := \eta - (\eta_d^T, \dot{\eta}_d^T)^T \in \mathbb{R}^6$. Thus, the tracking error dynamics are given as follows

$$\dot{e}_\xi = Ae_\xi + B(g_\xi(\eta_1)u_m - G - \Lambda_\xi\xi_2 + d_\xi - \ddot{\xi}_d), \tag{23a}$$
$$e_{y_\xi} = Ce_\xi, \tag{23b}$$
$$\dot{e}_\eta = Ae_\eta + B(J\tau + \Xi w_\eta(\eta_2) - \Lambda_\eta\eta_2 + d_\eta - \ddot{\eta}_d), \tag{23c}$$
$$e_{y_\eta} = Ce_\eta, \tag{23d}$$

where $e_{y_\xi} \in \mathbb{R}^3$ and $e_{y_\eta} \in \mathbb{R}^3$ are the output tracking errors, respectively; with $C := (I_3, 0_3) \in \mathbb{R}^{3\times 6}$. As we have mentioned before, due to the under–actuated nature of the system, it is not possible to control all the positions and angles independently. Therefore, the references signals $\theta_\star$ and $\phi_\star$, as well as the control inputs u_m and τ, must be properly designed in order to achieve a desired position ξ_d and a desired angle ψ_d.

To this aim, a virtual control $\nu := (\nu_x, \nu_y, \nu_z)^T \in \mathbb{R}^3$ is introduced once again in the position error dynamics, *i.e.*,

$$\dot{e}_\xi = Ae_\xi + B(\nu + w_\xi(\eta_1, u_m, \nu) - \Lambda_\xi \xi_2 + d_\xi - \ddot{\xi}_d), \tag{24a}$$
$$e_{y_\xi} = Ce_\xi, \tag{24b}$$
$$\dot{e}_\eta = Ae_\eta + B(J\tau + \Xi w_\eta(\eta_2) - \Lambda_\eta \eta_2 + d_\eta - \ddot{\eta}_d), \tag{24c}$$
$$e_{y_\eta} = Ce_\eta, \tag{24d}$$

where $w_\xi(\eta_1, u_m, \nu) = g_\xi(\eta_1)u_m - G - \nu$. In order to calculate the main thrust u_m and the references signals $\phi_\star$ and $\theta_\star$, we can use again the expression given in (10), based on the virtual control ν, which is designed further on.

Thus, the aim now is to design the virtual control ν and the control input τ such that the tracking error dynamics (24) converges to the smallest neighborhood of the origin using only the information of the output tracking errors.

2.4.1 *Finite–Time Sliding–Mode Observer*

Let us introduce the observer, for system (24), that take the following structure

$$\dot{\hat{e}}_\xi = A\hat{e}_\xi + B(\nu + w_\xi(\eta_1, u_m, \nu) - \Lambda_\xi \hat{\xi}_2 - \ddot{\xi}_d) + r_\xi[C\varepsilon_\xi], \tag{25a}$$
$$\dot{\hat{e}}_\eta = A\hat{e}_\eta + B(J\tau + \Xi \hat{w}_\eta(\hat{\eta}_2) - \Lambda_\eta \hat{\eta}_2 - \ddot{\eta}_d) + r_\eta[C\varepsilon_\eta], \tag{25b}$$

where $C\varepsilon_\xi = e_{y_\xi} - C\hat{e}_\xi = (\varepsilon_{\xi 1}, \varepsilon_{\xi 2}, \varepsilon_{\xi 3})^T \in \mathbb{R}^3$ and $C\varepsilon_\eta = e_{y_\eta} - C\hat{e}_\eta = (\varepsilon_{\eta 1}, \varepsilon_{\eta 2}, \varepsilon_{\eta 3})^T \in \mathbb{R}^3$ are the output estimation errors with $\varepsilon_\xi := e_\xi - \hat{e}_\xi = (\varepsilon_{\xi 1}, \ldots, \varepsilon_{\xi 6})^T \in \mathbb{R}^6$ and $\varepsilon_\eta := e_\eta - \hat{e}_\eta = (\varepsilon_{\eta 1}, \ldots, \varepsilon_{\eta 6})^T \in \mathbb{R}^6$ being the state estimation errors; $\hat{\xi}_2 = B^T\hat{e}_\xi + \dot{\xi}_d$, $\hat{w}_\eta(\hat{\eta}_2) = \Upsilon(\hat{\eta}_2)\hat{\eta}_2$ with

$$\Upsilon(\hat{\eta}_2) = \begin{pmatrix} 0 & h\hat{\eta}_2 & 0 \\ h\hat{\eta}_2 & 0 & 0 \\ 0 & \bar{h}\hat{\eta}_2 & 0 \end{pmatrix}, \ \hat{\eta}_2 = (B^T\hat{e}_\eta + \dot{\eta}_d),$$

where $h := (0, 0, 1)$ and $\bar{h} := (1, 0, 0)$; and the nonlinear correction terms $r_\xi : \mathbb{R}^3 \to \mathbb{R}^6$ and $r_\eta : \mathbb{R}^3 \to \mathbb{R}^6$ are given as follows

$$r_\xi := \begin{pmatrix} \hat{K}_{\xi 1}\phi_1(C\varepsilon_\xi) \\ \hat{K}_{\xi 2}\phi_2(C\varepsilon_\xi) \end{pmatrix}, \ r_\eta := \begin{pmatrix} \hat{K}_{\eta 1}\phi_1(C\varepsilon_\eta) \\ \hat{K}_{\eta 2}\phi_2(C\varepsilon_\eta) \end{pmatrix},$$

with $\hat{K}_{\xi 1} = \text{diag}(\hat{k}_{\xi 11}, \hat{k}_{\xi 12}, \hat{k}_{\xi 13})$, $\hat{K}_{\xi 2} = \text{diag}(\hat{k}_{\xi 21}, \hat{k}_{\xi 22}, \hat{k}_{\xi 23})$, $\hat{K}_{\eta 1} = \text{diag}(\hat{k}_{\eta 11}, \hat{k}_{\eta 12}, \hat{k}_{\eta 13})$ and $\hat{K}_{\eta 2} = \text{diag}(\hat{k}_{\eta 21}, \hat{k}_{\eta 22}, \hat{k}_{\eta 23})$ as some gain matrices to be designed; and the nonlinear functions ϕ_1 and ϕ_2 are defined as

$$\phi_1(\mathbf{s}) := \begin{pmatrix} \phi_{11}(s_1) \\ \phi_{12}(s_2) \\ \phi_{13}(s_3) \end{pmatrix} = \begin{pmatrix} \lceil s_1 \rfloor^{\frac{1}{2}} + s_1 \\ \lceil s_2 \rfloor^{\frac{1}{2}} + s_2 \\ \lceil s_3 \rfloor^{\frac{1}{2}} + s_3 \end{pmatrix},$$

$$\phi_2(\mathbf{s}) := \begin{pmatrix} \phi_{21}(s_1) \\ \phi_{22}(s_2) \\ \phi_{23}(s_3) \end{pmatrix} = \begin{pmatrix} \frac{1}{2}\lceil s_1 \rfloor^{0} + \frac{3}{2}\lceil s_1 \rfloor^{\frac{1}{2}} + \frac{1}{2}s_1 \\ \frac{1}{2}\lceil s_2 \rfloor^{0} + \frac{3}{2}\lceil s_2 \rfloor^{\frac{1}{2}} + \frac{1}{2}s_2 \\ \frac{1}{2}\lceil s_3 \rfloor^{0} + \frac{3}{2}\lceil s_3 \rfloor^{\frac{1}{2}} + \frac{1}{2}s_3 \end{pmatrix}.$$

Note that the observers given by (25) preserve the structure of the Generalized Super–Twisting Algorithm (GSTA) described in [71].

Recall that the estimation errors are $\varepsilon_\xi = e_\xi - \hat{e}_\xi$ and $\varepsilon_\eta = e_\eta - \hat{e}_\eta$, respectively. Therefore, the estimation error dynamics is given as follows

$$\dot{\varepsilon}_\xi = A\varepsilon_\xi + B(-\Lambda_\xi B^T \varepsilon_\xi + d_\xi) - r_\xi[C\varepsilon_\xi], \tag{26a}$$

$$\dot{\varepsilon}_\eta = A\varepsilon_\eta + B(\Xi(w_\eta(\eta_2) - \hat{w}_\eta(\hat{\eta}_2)) - \Lambda_\eta B^T \varepsilon_\eta + d_\eta) - r_\eta[C\varepsilon_\eta]. \tag{26b}$$

2.4.2 *Closed–Loop System Dynamics*

The virtual control ν and the control input τ will be designed as feedback controllers based on the state estimation given by the observers (25), *i.e.*,

$$\nu = K_\xi \hat{e}_\xi + \Lambda_\xi \hat{\xi}_2 + \ddot{\xi}_d, \tag{27a}$$

$$\tau = J^{-1}(K_\eta \hat{e}_\eta - \Xi \hat{w}_\eta(\hat{\eta}_2) + \Lambda_\eta \hat{\eta}_2 + \ddot{\eta}_d), \tag{27b}$$

where $K_\xi \in \mathbb{R}^{3\times 6}$ and $K_\eta \in \mathbb{R}^{3\times 6}$ are matrix feedback gains and they will be designed further on. In this way, substituting the control inputs (27) into the tracking error dynamics (24), one obtains

$$\dot{e}_\xi = Ae_\xi + BK_\xi \hat{e}_\xi + B(w_\xi(\eta_1, u_m, \nu) - \Lambda_\xi B^T \varepsilon_\xi + d_\xi), \tag{28a}$$

$$\dot{e}_\eta = Ae_\eta + BK_\eta \hat{e}_\eta + B(\Xi(w_\eta(\eta_2) - \hat{w}_\eta(\hat{\eta}_2)) - \Lambda_\eta B^T \varepsilon_\eta + d_\eta)). \tag{28b}$$

Therefore, the whole closed–loop system dynamics can be expressed as follow

$$\Sigma_\xi : \begin{cases} \dot{e}_\xi = A_\xi e_\xi + B(w_\xi(\eta_1, u_m, \nu) - (\Lambda_\xi B^T + K_\xi)\varepsilon_\xi + d_\xi), \\ \dot{\varepsilon}_\xi = A\varepsilon_\xi + B(d_\xi - \Lambda_\xi B^T \varepsilon_\xi) - r_\xi[C\varepsilon_\xi], \end{cases} \tag{29a}$$

$$\Sigma_\eta : \begin{cases} \dot{e}_\eta = A_\eta e_\eta + B(\Xi\tilde{w}_\eta(\eta_2, \hat{\eta}_2) - (\Lambda_\eta B^T + K_\eta)\varepsilon_\eta + d_\eta), \\ \dot{\varepsilon}_\eta = A\varepsilon_\eta + B(\Xi\tilde{w}_\eta(\eta_2, \hat{\eta}_2) - \Lambda_\eta B^T \varepsilon_\eta + d_\eta) - r_\eta[C\varepsilon_\eta]. \end{cases} \tag{29b}$$

where $\tilde{w}_\eta := (w_\eta - \hat{w}_\eta)$, $A_\xi := A + BK_\xi$ and $A_\eta := A + BK_\eta$. It is evident that the dynamics of ε_ξ and ε_η are decoupled from e_ξ and e_η, respectively. Thus, one can firstly prove that the state estimation errors ε_ξ and ε_η converge to zero in a finite time; and then, optimize the performance of (28) by choice of K_ξ and K_η, respectively.

For this purpose, let us introduce the following constraints over the tracking error dynamics (28).

Assumption 4 *There exist positive and known constants* γ_ξ, γ_η, d_ξ^+, $d_\eta^+ > 0$ *such that the following inequalities hold*

$$\|d_\xi - \Lambda_\xi B^T \varepsilon_\xi\| \leqslant \gamma_\xi \|\varepsilon_\xi\| + d_\xi^+, \tag{30a}$$

$$\|\Xi \tilde{w}_\eta(\eta_2, \hat{\eta}_2) - \Lambda_\eta B^T \varepsilon_\eta + d_\eta\| \leqslant \gamma_\eta \|\varepsilon_\eta\| + d_\eta^+. \tag{30b}$$

Note that (30a) is trivially satisfied due to the linearity of the term $\Lambda_\xi B^T \varepsilon_\xi$ and the boundedness of d_ξ. On the other hand, recall that $\tilde{w}_\eta = (\dot{\phi}\dot{\psi}, \dot{\psi}\dot{\theta}, \dot{\theta}\dot{\phi})^T - \Upsilon(\hat{\eta}_2)\hat{\eta}_2 = (\dot{\phi}\dot{\psi} - \dot{\hat{\phi}}\dot{\hat{\psi}}, \dot{\psi}\dot{\theta} - \dot{\hat{\psi}}\dot{\hat{\theta}}, \dot{\theta}\dot{\phi} - \dot{\hat{\theta}}\dot{\hat{\phi}})^T$. In this sense, taking into account that the quad–rotor is not going to deal with aggressive maneuvers, and due to the to the linearity of the term $\Lambda_\eta B^T \varepsilon_\eta$ and the boundedness of d_η, (30b) is also satisfied.

Let us introduce the following matrices

$$T = \begin{pmatrix} 1 & 0 & 0 & 0 & 0 & 0 \\ 0 & 0 & 1 & 0 & 0 & 0 \\ 0 & 0 & 0 & 0 & 1 & 0 \\ 0 & 1 & 0 & 0 & 0 & 0 \\ 0 & 0 & 0 & 1 & 0 & 0 \\ 0 & 0 & 0 & 0 & 0 & 1 \end{pmatrix}, \ \bar{A} = \begin{pmatrix} 0 & 1 \\ 0 & 0 \end{pmatrix}, \ \bar{b} = \begin{pmatrix} 0 \\ 1 \end{pmatrix}, \ \bar{c} = (1, 0).$$

2.4.3 *Convergence and Stability*

The following theorem describes the finite–time convergence properties of the observers (25).

Theorem 3 [3]. *Let the observer* (25) *be applied to system* (24)*, and Assumptions* 2 *and* 4 *be satisfied. Assume that there exist matrices* $P_\xi = \text{diag}\{P_{\xi i}\}_{i=1}^3 > 0$*, with* $P_{\xi i} = P_{\xi i}^T > 0 \in \mathbb{R}^{6\times 6}$; $P_\eta = \text{diag}\{P_{\eta i}\}_{i=1}^3 > 0$*, with* $P_{\eta i} = P_{\eta i}^T > 0 \in \mathbb{R}^{6\times 6}$; Y_ξ, $Y_\eta \in \mathbb{R}^{6\times 3}$*, and fixed positive constants* α_ξ, $\alpha_\eta > 0$ *such that the following Linear Matrix Inequalities (*LMIs*)*

$$\begin{pmatrix} P_\xi \tilde{A} + \tilde{A}^T P_\xi - Y_\xi \bar{C} & P_\xi \bar{B} & P_\xi \bar{B} \\ -\bar{C}^T Y_\xi^T + \gamma_\xi^2 I_6 + \alpha_\xi P_\xi & & \\ \star & -I_3 & 0_3 \\ \star & \star & -Q_\xi \end{pmatrix} \leqslant 0, \tag{31a}$$

$$\begin{pmatrix} P_\eta \tilde{A} + \tilde{A}^T P_\eta - Y_\eta \bar{C} & P_\eta \bar{B} & P_\eta \bar{B} \\ -\bar{C}^T Y_\eta^T + \gamma_\eta^2 I_6 + \alpha_\eta P_\eta & & \\ \star & -I_3 & 0_3 \\ \star & \star & -Q_\eta \end{pmatrix} \leqslant 0, \tag{31b}$$

are feasible for $\tilde{A} = \text{diag}(\bar{A}, \bar{A}, \bar{A}) \in \mathbb{R}^{6\times 6}$, $\bar{B} = \text{diag}(\bar{b}, \bar{b}, \bar{b}) \in \mathbb{R}^{6\times 3}$, $\bar{C} = \text{diag}(\bar{c}, \bar{c}, \bar{c}) \in \mathbb{R}^{3\times 6}$, $Q_\xi = Q_\xi^T > 0 \in \mathbb{R}^{3\times 3}$ *such that* $d_\xi^+ = \lambda_{\min}^{-\frac{1}{2}}(Q_\xi)$; $Q_\eta = Q_\eta^T > 0 \in \mathbb{R}^{3\times 3}$ *such that* $d_\eta^+ = \lambda_{\min}^{-\frac{1}{2}}(Q_\eta)$*; and some constants* γ_ξ, $\gamma_\eta > 0$*. Then, at the steady state* $\varepsilon_\xi = 0$ *and* $\varepsilon_\eta = 0$*, the state estimation error dynamics are* UFTS *with* $\hat{K}_\xi^T = (\hat{K}_{\xi 1}, \hat{K}_{\xi 2}) = (T\bar{P}_\xi^{-1} Y_\xi)^T$ *and* $\hat{K}_\eta^T = (\hat{K}_{\eta 1}, \hat{K}_{\eta 2}) = (T\bar{P}_\eta^{-1} Y_\eta)^T$*, respectively.*

Now, it will be shown that the ellipsoids $\mathcal{E}(\bar{P}_\xi) := \{e_\xi \in \mathbb{R}^6 \ : \ e_\xi^T \bar{P}_\xi^{-1} e_\xi \leqslant 1 + \lambda_{min}^{-1}(\bar{P}_\eta)\}$ and $\mathcal{E}(\bar{P}_\eta) := \{e_\eta \in \mathbb{R}^6 \ : \ e_\eta^T \bar{P}_\eta^{-1} e_\eta \leqslant 1\}$ are exponentially attractive for the closed–loop system (29).

Theorem 4 [3]. *Let the observer (25) and the linear control (27) be applied to system (24), and Assumptions 1, 2 and 4 be satisfied. Assume that there exist matrices $\bar{P}_\xi = \bar{P}_\xi^T > 0 \in \mathbb{R}^{6\times 6}$, $\bar{P}_\eta = \bar{P}_\eta^T > 0 \in \mathbb{R}^{6\times 6}$, $S_\eta = S_\eta^T > 0 \in \mathbb{R}^{6\times 6}$, $\bar{Y}_\xi$, $\bar{Y}_\eta \in \mathbb{R}^{3\times 6}$ and fixed positive constants $\bar{\alpha}_\xi$, $\bar{\alpha}_\eta > 0$ such that the following* LMIs

$$\begin{pmatrix} \bar{X}_\xi & B & -B(\Lambda_\xi B^T \bar{P}_\xi + \bar{Y}_\xi) & B \\ \star & -I_3 & 0_{3\times 6} & 0_3 \\ \star & \star & -\bar{\alpha}_\xi \bar{P}_\xi & 0_{6\times 3} \\ \star & \star & \star & -\bar{\alpha}_\xi Q_\xi \end{pmatrix} \leqslant 0, \tag{32a}$$

$$\bar{X}_\xi = \bar{P}_\xi A^T + A\bar{P}_\xi + B\bar{Y}_\xi + \bar{Y}_\xi^T B^T + \bar{\alpha}_\xi \bar{P}_\xi,$$

$$\bar{\alpha}_\xi > \bar{\gamma}_\xi^2, \tag{32b}$$

$$\begin{pmatrix} \bar{X}_\eta & B & -B(\Lambda_\eta B^T \bar{P}_\xi + \bar{Y}_\eta) & B \\ \star & -I_3 & 0_{3\times 6} & 0_3 \\ \star & \star & -(\bar{\alpha}_\eta - \gamma_\eta^2) S_\eta & 0_{6\times 3} \\ \star & \star & \star & -\bar{\alpha}_\eta Q_\eta \end{pmatrix} \leqslant 0, \tag{32c}$$

$$\bar{X}_\eta = \bar{P}_\eta A^T + A\bar{P}_\eta + B\bar{Y}_\eta + \bar{Y}_\eta^T B^T + \bar{\alpha}_\eta \bar{P}_\eta,$$

$$\begin{pmatrix} -2\bar{P}_\eta + S_\eta & I_6 \\ I_6 & -I_6 \end{pmatrix} \leqslant 0, \quad \bar{\alpha}_\eta > \gamma_\eta^2, \tag{32d}$$

are feasible for $Q_\xi = Q_\xi^T > 0 \in \mathbb{R}^{3\times 3}$ such that $d_\xi^+ = \lambda_{min}^{-\frac{1}{2}}(Q_\xi)$; $Q_\eta = Q_\eta^T > 0 \in \mathbb{R}^{3\times 3}$ such that $d_\eta^+ = \lambda_{min}^{-\frac{1}{2}}(Q_\eta)$; and some constants $\bar{\gamma}_\xi$, $\gamma_\eta > 0$. Then, the ellipsoids $\mathcal{E}(\bar{P}_\xi)$ and $\mathcal{E}(\bar{P}_\eta)$ are exponentially attractive for the closed–loop system (29) with $K_\xi = \bar{Y}_\xi \bar{P}_\xi^{-1}$ and $K_\eta = \bar{Y}_\eta \bar{P}_\eta^{-1}$.

The corresponding proof of the convergence to zero of the state estimation error for the observer (25), and the proof that the ellipsoids $\mathcal{E}(\bar{P}_\xi)$ and $\mathcal{E}(\bar{P}_\eta)$ are exponentially attractive for the closed–loop system (29) can be checked in [3].

2.4.4 *Experimental Results*

The proposed control strategy is applied to the QBall2 by Quanser, depicted by Fig. 4. For more details about the Qball2, the experimental platform, and the parameters of the model (5), please see Appendix B.

For this experiment, wind gusts are considered as external perturbations. Such wind gusts are generated by means of an industrial fan that provides a wind velocity between 1.84[m/s] and 4[m/s], over a diagonal of the X–Y–axis, that changes depending on the distance between the fan and the vehicle (see Fig. 44).

The desired trajectory is given as

$$\begin{aligned}
x_d(t) &= r(\arctan(\varphi) + \arctan(t-\varphi))\cos(\omega t),\\
y_d(t) &= r(\arctan(\varphi) + \arctan(t-\varphi))\sin(\omega t),\\
z_d(t) &= 0.15(1+\tanh(t-7.5)) + 0.1(1+\tanh((t-35)/3) + 0.3,\\
\psi_d(t) &= 0,
\end{aligned}$$

with $r = 0.2$[m], $\varphi = 15$ and $\omega = \pi/6$[rad/s]. Then, the observer and controller gains can be found by solving the set of LMIs (31) and (32) in SeDuMi solver among YALMIP with $\gamma_\xi = 0.1$, $\gamma_\eta = 0.1$, $\alpha_\eta = 7$,$\alpha_\xi = 3$, $\bar{\gamma}_\xi = 0.1$, $\bar{\alpha}_\xi = 0.75$, $\bar{\alpha}_\eta = 0.75$, $Q_\xi = 2.5I_3$ and $Q_\eta = 1.4085I_3$. The obtained gains are

$$\begin{aligned}
\hat{K}_{\xi 1} &= \mathrm{diag}(5.7372, 5.7372, 5.7372),\\
\hat{K}_{\xi 2} &= \mathrm{diag}(20.1109, 20.1108, 20.1109),\\
\hat{K}_{\eta 1} &= \mathrm{diag}(11.8497, 11.8497, 11.8497),\\
\hat{K}_{\eta 2} &= \mathrm{diag}(67.9953, 67.9938, 67.9956),
\end{aligned}$$

$$K_\xi = \begin{pmatrix}
-4.8011 & 0.0217 & 0.0217 & -5.6533 & 0.0118 & 0.0118\\
0.0217 & -4.8011 & 0.0217 & 0.0118 & -5.6533 & 0.0118\\
0.0217 & 0.0217 & -4.8011 & 0.0118 & 0.0118 & -5.6533
\end{pmatrix},$$

$$K_\eta = \begin{pmatrix}
-2.8502 & 0.0631 & 0.0631 & -2.5392 & 0.2263 & 0.2263\\
0.0631 & -2.8502 & 0.0631 & 0.2263 & -2.5392 & 0.2263\\
0.0631 & 0.0631 & -2.8502 & 0.2263 & 0.2263 & -2.5392
\end{pmatrix}.$$

In order to better illustrate the performance of the proposed control strategy, 10 trial tests have been done. All these experiments have been implemented with the Euler's integration method with a sampling time equal to $h_s = 0.002$[s].

The following experimental results consider the expressions given in (20), with $n_t = 10$, $n_s = 30000$ and $t_o = 5$[s]. In order to better illustrate the performance of the control strategies the performance index introduced in (21) is implemented, where $\Delta T = 2$.

The tracking results are illustrated through the Figs. 9, 10 and 11, where the performance of the proposed AEM is shown. Particularly, in Figs. 9 and 10 it is possible to see the real quad–rotor (x, y, z)–position and ψ orientation, for 10 trial tests as well as its average, compared to the desired (x_d, y_d, z_d)–position and ψ_d orientation. On the other hand, in Fig. 11 one can see one trial test of the tracking position errors that clearly belong to the ellipsoid $\mathcal{E}(\bar{P}_\xi)$ validating the results given by Theorem 4.

It is worth highlighting that the performance indexes $e_{x_{RMS}}$, $e_{y_{RMS}}$ and $e_{z_{RMS}}$ depict the performance of the controllers for each position coordinate, respectively. In order to provide a more precise quantitative comparison, some numerical properties of the performance indexes, *i.e.*, the minimum, the mean and the maximum values, are illustrated in Tab. 6. Such values are taken from the take–off time $t_o = 5$[s] in order to neglect the initial conditions effect.

Note that the proposed robust output–based control is completely constructive since its synthesis (observer and control law) is in terms of LMIs and its computational complexity is more simple. This point is very important when one deals with the output–based control synthesis for quad–rotors since normally it is very difficult to tune the controller parameters.

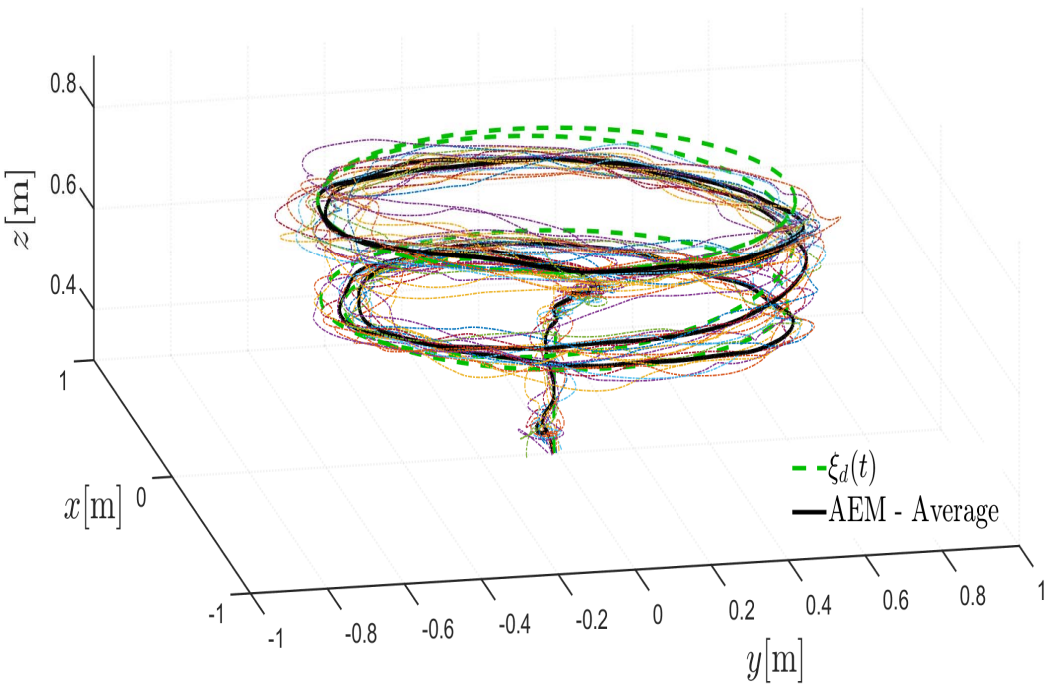

Figure 9: Quad–rotor position – AEM with GSTOs. *The dashed signals represent the results of each of the 10 experimental tests, while the solid line represents the average of these functions*

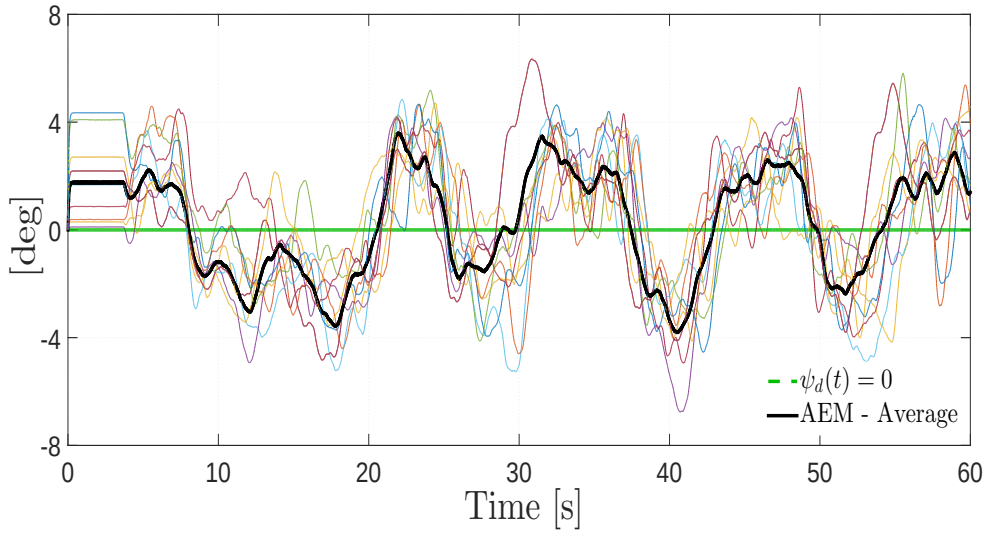

Figure 10: Quad–rotor position and yaw orientation – AEM with GSTOs. *The dashed signals represent the results of each of the 10 experimental tests, while the solid line represents the average of these functions*

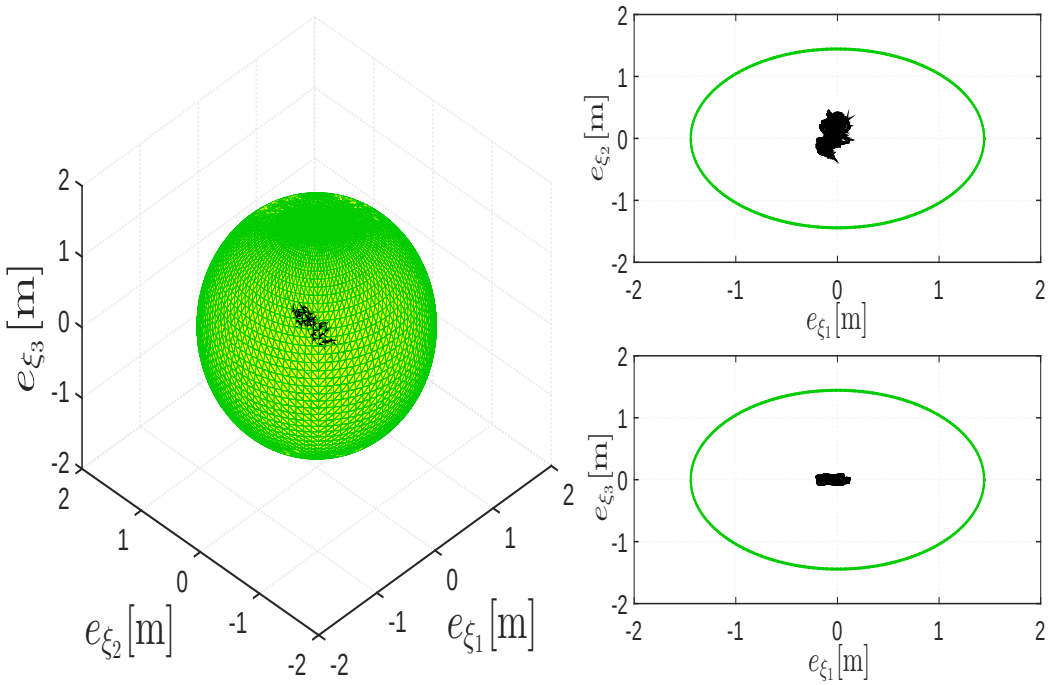

Figure 11: Quad–rotor tracking error – AEM with GSTOs. *The green line corresponds to the ellipsoid* $\mathcal{E}(\bar{P}_\xi)$ *while the black one to the trajectories of the tracking position errors for different projections*

Table 6: AEM performance index properties

Coordinate	$\min(\bar{e}_{RMS})$	$\bar{e}_{RMS}$-Mean	$\max(\bar{e}_{RMS})$
x	0.0192	0.0463	0.1119
y	0.0341	0.1134	0.2775
z	0.0110	0.0241	0.0977
ξ	0.0590	0.1342	0.2815

3

FAULT DIAGNOSIS STRATEGY

Summary. *In this chapter, the problem statement about the FD is formally introduced. Afterward, an FT–SMO is designed in order to estimate some states of the quad–rotor and provide fault information through a set of auxiliary variables, i.e., residual signals. Based on these residuals, an FD strategy is proposed, and through different algorithms, the detection, isolation and identification of multiple faults are achieved. Experimental results show the effectiveness of this strategy.*

3.1 PROBLEM STATEMENT

Let us recall the quad–rotor dynamics:

$$\dot{\xi}_1 = \xi_2, \tag{33a}$$
$$\dot{\xi}_2 = g_\xi(\eta_1)u_m - G - \Lambda_\xi \xi_2 + d_\xi, \tag{33b}$$
$$\dot{\eta}_1 = \eta_2, \tag{33c}$$
$$\dot{\eta}_2 = J\tau + \Xi w_\eta(\eta_2) - \Lambda_\eta \eta_2 + d_\eta, \tag{33d}$$

where $\xi_1 := (x, y, z)^T \in \mathbb{R}^3$, $\xi_2 := (\dot{x}, \dot{y}, \dot{z})^T \in \mathbb{R}^3$, $\eta_1 := (\phi, \theta, \psi)^T \in \mathbb{R}^3$ and $\eta_2 := (\dot{\phi}, \dot{\theta}, \dot{\psi})^T \in \mathbb{R}^3$ represent the quad–rotor positions, linear velocities, angles and angular velocities , respectively. The term $u_m := u_z/m$, with $u_z \in \mathbb{R}$ representing the main thrust and $m \in \mathbb{R}_+$ the mass of the quad–rotor. $\tau := (\tau_\phi, \tau_\theta, \tau_\psi)^T \in \mathbb{R}^3$ represents the angular moment vector with τ_ϕ, τ_θ and $\tau_\psi \in \mathbb{R}$ as the roll, pitch and yaw angular moments, respectively. $d_\xi := (d_x, d_y, d_z)^T \in \mathbb{R}^3$ and $d_\eta := (d_\phi, d_\theta, d_\psi)^T \in \mathbb{R}^3$ represent disturbances given by uncertainties and external perturbations, *e.g.*, some unmodeled dynamics and wind gusts.

The relation between the control inputs u_z, τ_ϕ, τ_θ, τ_ψ and the thrusts T_i, generated by the i–th rotor, is given by

$$\underbrace{\begin{bmatrix} u_z \\ \tau_\phi \\ \tau_\theta \\ \tau_\psi \end{bmatrix}}_{u} = \underbrace{\begin{bmatrix} 1 & 1 & 1 & 1 \\ 0 & 0 & L & -L \\ L & -L & 0 & 0 \\ K_\tau & K_\tau & -K_\tau & -K_\tau \end{bmatrix}}_{M} \underbrace{\begin{bmatrix} T_1 \\ T_2 \\ T_3 \\ T_4 \end{bmatrix}}_{T}, \tag{34}$$

where u is the control input vector, T is the thrust vector and M is the full rank matrix that relates the control signals to the thrusts. The constant L represents the distance between the motors and the center of mass of the quad–rotor, while K_τ represents the thrust coefficient.

Therefore, in presence of faults, the current command thrust $\bar{T}$ is given as

$$\bar{T}(t) = (I_4 - \Gamma(t))\,T(t) = T(t) - f(t), \tag{35}$$

where $\Gamma(t) := \mathrm{diag}(\gamma_1(t), \gamma_2(t), \gamma_3(t), \gamma_4(t)) \in \mathbb{R}^{4\times4}$ is the LOE matrix and $f(t) = \Gamma(t)T(t) := (f_1(t), f_2(t), f_3(t), f_4(t))^T \in \mathbb{R}^4$ is the fault vector. The term $\gamma_i(t) \in (0, 1)$

represents the case of an LOE fault in the i–th rotor. The case of $\gamma_i(t) = 0$ represents a healthy rotor, while $\gamma_i(t) = 1$ means that the i–th actuator is fully damaged. Note that the current command thrust $\bar{T}$ is not measured and therefore is unknown.

The goal in this chapter is to design an FD method to detect (discern if there are faults or not), isolate (if there are faults, determine which rotors are faulty) and identify the magnitude of each LOE, despite some uncertainties and external perturbations. It is assumed that only the positions and angles of the vehicle are measurable.

Before proceeding, the following assumptions and definitions are introduced.

Assumption 5 *The faults are uniformly bounded and Lipschitz, i.e.,* $f \in \mathcal{L}_{F_1}$, $\dot{f} \in \mathcal{L}_{F_2}$, *with known positive constants* F_1 *and* F_2.

Definition 3 [45] *The fault* f_i *is strongly detectable if there exists a stable residual generator* $r(t)$ *such that it reaches a non–zero steady–state value for a fault signal that has a bounded final value different from zero.*

Assumptions 5 characterizes the class of faults that the proposed approach will be able to deal with.

Let us define $\chi_1 := (z, \phi, \theta, \psi)^T \in \mathbb{R}^4$ and $\chi_2 := (\dot{z}, \dot{\phi}, \dot{\theta}, \dot{\psi})^T \in \mathbb{R}^4$. Note that the actuator faults directly affect the control signals. Therefore, we just analyze the dynamics of χ_1 and χ_2 in order to see the effect of the actuator faults. Then, considering (34) and (35), the dynamics of χ_1 and χ_2 are given as

$$\dot{\chi}_1 = \chi_2, \tag{36a}$$

$$\dot{\chi}_2 = \zeta(\chi_1) M (I_4 - \Gamma(t)) T(t) + \vartheta(\chi_2) + d, \tag{36b}$$

where $\zeta(\chi_1) := \operatorname{diag}(c\phi c\theta/m, J) \in \mathbb{R}^{4\times 4}$, $\vartheta(\chi_2) := (-a_z \dot{z} - g, (\Xi w_\eta(\eta_2) - \Lambda_\eta \eta_2)^T)^T \in \mathbb{R}^4$ and the vector of disturbances $d := \left(d_z, d_\eta^T\right)^T \in \mathbb{R}^4$.

Note that the faults and disturbances act in the same way on the quad–rotor dynamics, *i.e.*, as unknown forces that affect the acceleration of the system.

3.2 REDUCED FINITE–TIME SLIDING–MODE OBSERVER

Let us introduce the following constraint.

Assumption 6 *The term* $\vartheta(\chi_2)$ *is Lipschitz, i.e.,* $\|\vartheta(\chi_2) - \vartheta(\hat{\chi}_2)\|_\infty \leqslant L_\vartheta \|\chi_2 - \hat{\chi}_2\|_\infty$, *for any* $\chi_2, \hat{\chi}_2 \in \mathbb{R}^4$.

Note that, similar to Assumption 3, the previous constraint is satisfied as long as the quad–rotor does not perform aggressive maneuvers, *i.e.*, any trajectory for which the roll and pitch angles exceed $\pm\pi/2$ [rad], and whose angular velocities growth faster than a linear rate.

In this sense, Assumption 6 implies that the pitch and roll angles must hold $|\phi| < \pi/2$ and $|\theta| < \pi/2$, respectively; and this could be possible if the desired trajectories are Lipschitz; therefore, the angular velocities do not growth faster than a linear rate.

The FT–SMO has the following structure [18]

$$\dot{\hat{\chi}}_1 = \hat{\chi}_2 + \hat{K}_1 \varphi_1(e_\chi), \tag{37a}$$

$$\dot{\hat{\chi}}_2 = \zeta(\chi_1) MT + \vartheta(\hat{\chi}_2) + \hat{\chi}_3 + \hat{K}_2 \varphi_2(e_\chi), \tag{37b}$$

$$\dot{\hat{\chi}}_3 = \hat{K}_3 \varphi_3(e_\chi), \tag{37c}$$

where $e_\chi := \chi_1 - \hat{\chi}_1 \in \mathbb{R}^4$ is the output error, the nonlinear output injections φ_1, φ_2, $\varphi_3 : \mathbb{R}^4 \to \mathbb{R}^4$ are given as $\varphi_1(\mathbf{s}) := \lceil \mathbf{s} \rfloor^{\frac{2}{3}}$, $\varphi_2(\mathbf{s}) := \lceil \mathbf{s} \rfloor^{\frac{1}{3}}$ and $\varphi_3(\mathbf{s}) := \lceil \mathbf{s} \rfloor^0$, for any $\mathbf{s} \in \mathbb{R}^4$, and $\hat{K}_r = \mathrm{diag}(\hat{k}_{r1}, \hat{k}_{r2}, \hat{k}_{r3}, \hat{k}_{r4}) \in \mathbb{R}^{4\times4}$, $r = \overline{1,3}$, are some gain matrices to be designed.

Define the state estimation error as $\hat{e}_\chi := (e_\chi, \varepsilon_\chi, \sigma_\chi) \in \mathbb{R}^{12}$, where $\varepsilon_\chi := \chi_2 - \hat{\chi}_2 \in \mathbb{R}^4$ is the estimation error of the velocities, and $\sigma_\chi := \Delta(t) - \hat{\chi}_3 \in \mathbb{R}^4$ is the estimation error of the total uncertainty given by $\Delta(t) = \Phi(t) + \vartheta(\chi_2) - \vartheta(\hat{\chi}_2)$, with $\Phi(t) = d - \zeta(\chi_1)Mf(t)$. Due to Assumptions 2 (Lipschitz external perturbations), 5 and 6, such an uncertainty is bounded and Lipschitz, *i.e.*, $\Delta \in \mathcal{L}_\delta$ and $\dot{\Delta} \in \mathcal{L}_{\bar{\delta}}$, with known positive constants δ and $\bar{\delta}$, respectively.

The following theorem describes the finite–time convergence properties of the FT–SMO.

Theorem 5 [18] *Let the observer* (37) *be applied to system* (36). *Suppose that Assumptions 2, 5 and 6 hold, and that the observer gains are selected as* $\hat{K}_1 = 2\bar{\delta}^{\frac{1}{3}} I_4$, $\hat{K}_2 = 1.5\bar{\delta}^{\frac{1}{2}} I_4$, $\hat{K}_3 = 1.1\bar{\delta} I_4$; *then,* $\hat{e}_\chi = 0$ *is* UFTS.

Remark 1 *Consider the occurrence of a fault at time* $t_f > \mathcal{T}_0 > 0$, *where* $\mathcal{T}_0$ *is the convergence time before a fault occurrence. In the presence of a sudden fault, an aggressive transient may take place, and as a consequence, the observer may lose the exact estimation. However, the observer will converge again at a time* $\mathcal{T}_1 > t_f$, *satisfying the detection time requirements.*

According to Theorem 5, $\hat{e}_\chi = 0$ is UFTS, which implies that $\hat{\chi}_1(t) = \chi_1(t)$, $\hat{\chi}_2(t) = \chi_2(t)$ and $\hat{\chi}_3(t) = \Delta(t)$, for all $t \geqslant \mathcal{T}_1 > 0$. Therefore, if Assumptions 2, 5 and 6 hold, the FT–SMO (37) provides the following residuals

$$\hat{\chi}_3(t) = \left(\hat{\chi}_z(t), \hat{\chi}_\phi(t), \hat{\chi}_\theta(t), \hat{\chi}_\psi(t)\right)^T = \Phi(t), \ \forall t \geqslant \mathcal{T}_1 > 0. \tag{38}$$

3.3 FINITE–TIME CONVERGENCE OF THE RESIDUALS

Since the quad–rotor dynamics is relatively fast, the detection delay plays a major role in order to avoid dangerous situations, as well as the propagation of the fault [89]. In this sense, the convergence time of the scheme is an important requirement of the FD, where the faults must be detected at a very early stage. Moreover, the convergence time must comply with the presence of disturbances and sudden actuator faults.

In the proposed FD strategy, the proper tuning of the proposed FT–SMO gains is essential in order to build the residual signals given in (38). By selecting higher gains, a faster convergence of the residuals to their exact values is achieved [18]. However, if there is noise in the measurement, there is a trade–off between the accuracy of the residuals and the convergence time speed. In this sense, if the gains are properly designed, according to [18], the FT–SMO (37) provides the best possible accuracy in the presence of bounded noise with a finite–time convergence to a region proportional to the noise.

For this reason, the proposed FT–SMO is suitable to minimize detection delay, due to its capability to converge in a finite time, which can be done arbitrarily small; its insensitivity properties against some class of disturbances and to achieve accuracy in the residual generation.

3.4 FAULT DETECTION

In order to detect if there is an actuator fault, the following proposition is introduced.

Proposition 1 *Suppose that Assumptions 2, 5 and 6 hold, and assume that the fault f satisfies*

$$\|f\|_f > 2\|M^{-1}\zeta^{-1}(\chi_1)D\|_f, \tag{39}$$

with $D := (D_3, D_4, D_5, D_6)^T$, and $\|\cdot\|_f = esssup_{t\in[t_f,+\infty)}\|\cdot\|$, with t_f as the instant of time in which the fault occurs. Then, if

$$\|\hat{\chi}_3\|_\infty > \|D\|, \tag{40}$$

the fault f is strongly detectable.

The proof of Proposition 1 is postponed to the Appendix.

Note that the matrix ζ^{-1} always exists and is well–defined for all $\phi \in (-\pi/2, \pi/2)$ and $\theta \in (-\pi/2, \pi/2)$. Such constraints are satisfied as long as the quad–rotor does not perform aggressive maneuvers. The fault detection consists in verifying the inequality (40).

3.5 FAULT ISOLATION

Once faults are detected, the next step is to isolate them. Due to Assumption 2 (Lipschitz external perturbations), and the estimation properties of the FT–SMO, one can establish the following constraints for the external perturbations:

$$\underline{d}_z \leqslant d_z(t), \qquad \underline{d}_\phi \leqslant d_\phi(t) \leqslant \overline{d}_\phi \ \forall t \geqslant 0, \tag{41a}$$

$$\underline{d}_\theta \leqslant d_\theta(t) \leqslant \overline{d}_\theta, \qquad \underline{d}_\psi \leqslant d_\psi(t) \leqslant \overline{d}_\psi \ \forall t \geqslant 0, \tag{41b}$$

where $\underline{d}_z$, $\underline{d}_\phi$, $\overline{d}_\phi$, $\underline{d}_\theta$, $\overline{d}_\theta$, $\underline{d}_\psi$, $\overline{d}_\psi \in \mathbb{R}$ are known constants. These constants can be estimated by means of the FT–SMO through experimental tests under nominal conditions, *i.e.*, free of faults. Then, the following functions are introduced:

$$\sigma_z(t) = \begin{cases} 0, & \text{if } \|\hat{\chi}_z\|_\infty \leqslant D_3, \\ \underline{d}_z, & \text{if } \|\hat{\chi}_z\|_\infty > D_3, \end{cases} \tag{42a}$$

$$\sigma_\phi(t) = \begin{cases} 0, & \text{if } \|\hat{\chi}_\phi\|_\infty \leqslant D_4, \\ \overline{d}_\phi, & \text{if } \|\hat{\chi}_\phi\|_\infty > D_4 \wedge \hat{\chi}_\phi(t) > 0, \\ \underline{d}_\phi, & \text{if } \|\hat{\chi}_\phi\|_\infty > D_4 \wedge \hat{\chi}_\phi(t) < 0, \end{cases} \tag{42b}$$

$$\sigma_\theta(t) = \begin{cases} 0, & \text{if } \|\hat{\chi}_\theta\|_\infty \leqslant D_5, \\ \overline{d}_\theta, & \text{if } \|\hat{\chi}_\theta\|_\infty > D_5 \wedge \hat{\chi}_\theta(t) > 0, \\ \underline{d}_\theta, & \text{if } \|\hat{\chi}_\theta\|_\infty > D_5 \wedge \hat{\chi}_\theta(t) < 0, \end{cases} \tag{42c}$$

$$\sigma_\psi(t) = \begin{cases} 0, & \text{if } \|\hat{\chi}_\psi\|_\infty \leqslant D_6, \\ \overline{d}_\psi, & \text{if } \|\hat{\chi}_\psi\|_\infty > D_6 \wedge \hat{\chi}_\psi(t) > 0, \\ \underline{d}_\psi, & \text{if } \|\hat{\chi}_\psi\|_\infty > D_6 \wedge \hat{\chi}_\psi(t) < 0. \end{cases} \tag{42d}$$

Consider the following functions

$$\rho_1(t) = \frac{\sigma_z(t) - \hat{\chi}_z(t)}{4m^{-1}c\phi(t)c\theta(t)} + \frac{\sigma_\psi(t) - \hat{\chi}_\psi(t)}{4J_z^{-1}K_\tau} + \frac{\sigma_\theta(t) - \hat{\chi}_\theta(t)}{2J_y^{-1}L}, \tag{43a}$$

$$\rho_2(t) = \frac{\sigma_z(t) - \hat{\chi}_z(t)}{4m^{-1}c\phi(t)c\theta(t)} + \frac{\sigma_\psi(t) - \hat{\chi}_\psi(t)}{4J_z^{-1}K_\tau} - \frac{\sigma_\theta(t) - \hat{\chi}_\theta(t)}{2J_y^{-1}L}, \tag{43b}$$

$$\rho_3(t) = \frac{\sigma_z(t) - \hat{\chi}_z(t)}{4m^{-1}c\phi(t)c\theta(t)} - \frac{\sigma_\psi(t) - \hat{\chi}_\psi(t)}{4J_z^{-1}K_\tau} + \frac{\sigma_\theta(t) - \hat{\chi}_\theta(t)}{2J_x^{-1}L}, \tag{43c}$$

$$\rho_4(t) = \frac{\sigma_z(t) - \hat{\chi}_z(t)}{4m^{-1}c\phi(t)c\theta(t)} - \frac{\sigma_\psi(t) - \hat{\chi}_\psi(t)}{4J_z^{-1}K_\tau} - \frac{\sigma_\theta(t) - \hat{\chi}_\theta(t)}{2J_x^{-1}L}, \tag{43d}$$

$$\lambda_1(t) = \frac{\sigma_z(t) - \hat{\chi}_z(t) - D_z}{2m^{-1}c\phi(t)c\theta(t)} + \frac{\sigma_\psi(t) - \hat{\chi}_\psi(t) - D_\psi}{2J_z^{-1}K_\tau}, \tag{43e}$$

$$\lambda_2(t) = \frac{\sigma_z(t) - \hat{\chi}_z(t) - D_z}{2m^{-1}c\phi(t)c\theta(t)} + \frac{\hat{\chi}_\psi(t) - \sigma_\psi(t) - D_\psi}{2J_z^{-1}K_\tau}. \tag{43f}$$

Note that all the previous functions depend on known or estimated variables. Moreover, the functions σ_n, with $n = z, \phi, \theta, \psi$, given in (42) provide an approximation of the disturbances taken into account the sign of the residuals signals. For instance, σ_z is equal to 0, when $\|\hat{\chi}_z\|_\infty \leqslant D_3$, since d_z cannot be distinguished from the faults; and equal to $\underline{d}_z$, when $\|\hat{\chi}_z\|_\infty > D_3$, since the effect of the faults is distinguished from d_z. Then, the following proposition is introduced.

Proposition 2 *Suppose that Assumptions 2, 5 and 6 hold, and assume that the fault f_i is strongly detectable, i.e.,*

$$\|f_1\|_{f_1} > 2Q_1(\chi_1)\|I_\theta D\|, \tag{44a}$$

$$\|f_2\|_{f_2} > 2Q_2(\chi_1)\|I_\theta D\|, \tag{44b}$$

$$\|f_3\|_{f_3} > 2Q_3(\chi_1)\|I_\phi D\|, \tag{44c}$$

$$\|f_4\|_{f_4} > 2Q_4(\chi_1)\|I_\phi D\|, \tag{44d}$$

where $\|\cdot\|_{f_i} = esssup_{t\in[t_{f_i},+\infty)}\|\cdot\|$, with t_{f_i} as the instant at which the fault of the i–th rotor has occurred, and

$$\begin{aligned} Q_1(\chi_1) &= \|I_\theta M^{-1}\zeta^{-1}(\chi_1)\|_{f_1}, \\ Q_2(\chi_1) &= \|I_\theta M^{-1}\zeta^{-1}(\chi_1)\|_{f_2}, \\ Q_3(\chi_1) &= \|I_\phi M^{-1}\zeta^{-1}(\chi_1)\|_{f_3}, \\ Q_4(\chi_1) &= \|I_\phi M^{-1}\zeta^{-1}(\chi_1)\|_{f_4}, \end{aligned}$$

with $I_\theta := \text{diag}(1, 0, 1, 1) \in \mathbb{R}^{4\times4}$ and $I_\phi := \text{diag}(1, 1, 0, 1) \in \mathbb{R}^{4\times4}$. Then, the Algorithms 1 and 2 provide the isolation of the i–th fault with the warning signals $\mathcal{A}_i$, indicating the occurrence of a fault in the i–th rotor when $\mathcal{A}_i = 1$, or indicating that the rotor is healthy when $\mathcal{A}_i = 0$.

***Algorithm 1**: Rotors 1 and 2*

Input: $\hat{\chi}_\theta$, D_5, ρ_1, ρ_2, λ_1;
Output: $\mathcal{A}_1$, $\mathcal{A}_2$;

if $\|\hat{\chi}_\theta\|_\infty > D_5 \wedge \hat{\chi}_\theta < 0$ $\rightarrow \mathcal{A}_1 = 1$;
  if $\rho_2 > 0 \rightarrow \mathcal{A}_2 = 1$;
  else$\rightarrow \mathcal{A}_2 = 0$;
  end
elseif $\|\hat{\chi}_\theta\|_\infty > D_5 \wedge \hat{\chi}_\theta > 0$ $\rightarrow \mathcal{A}_2 = 1$;
  if $\rho_1 > 0 \rightarrow \mathcal{A}_1 = 1$;
  else$\rightarrow \mathcal{A}_1 = 0$;
  end
elseif $\|\hat{\chi}_\theta\|_\infty < D_5 \wedge \lambda_1 > 0$ $\rightarrow \mathcal{A}_1 = \mathcal{A}_2 = 1$;
else$\rightarrow \mathcal{A}_1 = \mathcal{A}_2 = 0$;
end

***Algorithm 2**: Rotors 3 and 4*

Input: $\hat{\chi}_\phi$, D_4, ρ_3, ρ_4, λ_2;
Output: $\mathcal{A}_3$, $\mathcal{A}_4$;

if $\|\hat{\chi}_\phi\|_\infty > D_4 \wedge \hat{\chi}_\phi < 0$ $\rightarrow \mathcal{A}_3 = 1$;
  if $\rho_4 > 0 \rightarrow \mathcal{A}_4 = 1$;
  else$\rightarrow \mathcal{A}_4 = 0$;
  end
elseif $\|\hat{\chi}_\phi\|_\infty > D_4 \wedge \hat{\chi}_\phi > 0$ $\rightarrow \mathcal{A}_4 = 1$;
  if $\rho_3 > 0 \rightarrow \mathcal{A}_3 = 1$;
  else$\rightarrow \mathcal{A}_3 = 0$;
  end
elseif $\|\hat{\chi}_\phi\|_\infty < D_4 \wedge \lambda_2 > 0$ $\rightarrow \mathcal{A}_3 = \mathcal{A}_4 = 1$;
else$\rightarrow \mathcal{A}_3 = \mathcal{A}_4 = 0$;
end

The proof of Proposition 2 is postponed to the Appendix.

Note that each Q_i depends on the system parameters, and the pitch and roll angles. Therefore, each Q_i depends on the maneuvers of the vehicle. However, taking into account that the quad–rotor does not perform aggressive maneuvers, such variables are clearly bounded. The warning signal $\mathcal{A}_i$ indicates a fault in the i–th rotor, and prevents from providing a wrong fault identification.

3.6 FAULT IDENTIFICATION

The detection and isolation schemes do not determine the magnitude of the fault. For active FTCs, the fault identification is necessary to compensate the effect of the faults.

For this purpose consider the fault isolation matrix $\mathcal{A}(t) := \text{diag}(\mathcal{A}_1(t), \mathcal{A}_2(t), \mathcal{A}_3(t), \mathcal{A}_4(t)) \in \mathbb{R}^{4\times 4}$ and the vector $\sigma(t) := (\sigma_z(t), \sigma_\phi(t), \sigma_\theta(t), \sigma_\psi(t))^T \in \mathbb{R}^4$. Then, the following proposition establishes the fault identification scheme.

Proposition 3 *Suppose that Assumptions 2, 5 and 6 hold, and assume that the fault f_i is strongly detectable and it has been isolated. Then, the identification of the fault vector f is given by*

$$\hat{f}(t) = \mathcal{A}(t) M^{-1} \zeta^{-1}(\chi_1) \left(\sigma(t) - \hat{\chi}_3(t)\right). \tag{45}$$

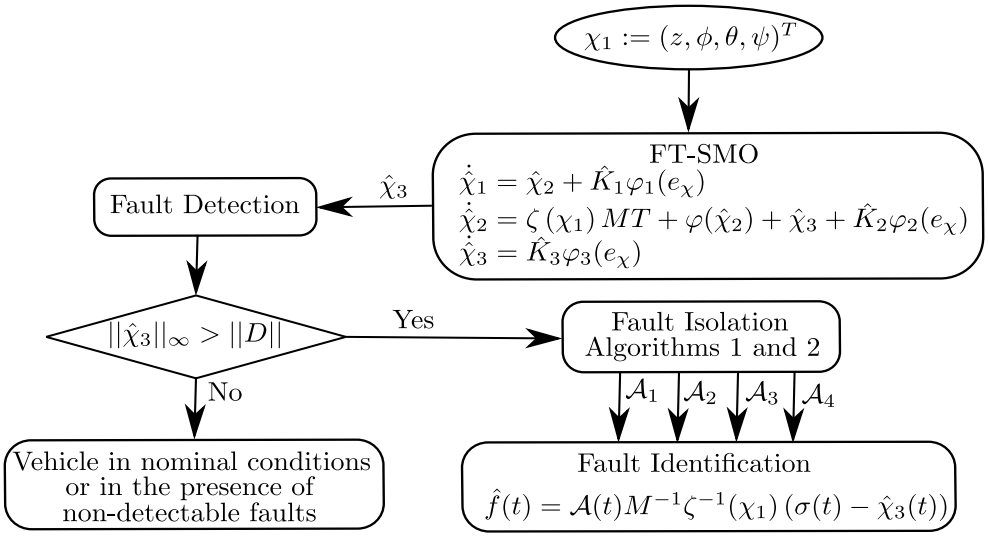

Figure 12: Flowchart of the proposed FD strategy

Moreover, the identification errors satisfy

$$Q_1(\chi_1)\left[\|I_\theta D\| - \left\|\begin{pmatrix}\underline{d}_z\\ \underline{d}_\theta\\ \underline{d}_\psi\end{pmatrix}\right\|\right] \leqslant \|f_1 - \hat{f}_1\|_{f_1} \leqslant Q_1(\chi_1)\,\|I_\theta D\|\,, \tag{46a}$$

$$Q_2(\chi_1)\left[\|I_\theta D\| - \left\|\begin{pmatrix}\underline{d}_z\\ \overline{d}_\theta\\ \underline{d}_\psi\end{pmatrix}\right\|\right] \leqslant \|f_2 - \hat{f}_2\|_{f_2} \leqslant Q_2(\chi_1)\,\|I_\theta D\|\,, \tag{46b}$$

$$Q_3(\chi_1)\left[\|I_\phi D\| - \left\|\begin{pmatrix}\underline{d}_z\\ \underline{d}_\phi\\ \overline{d}_\psi\end{pmatrix}\right\|\right] \leqslant \|f_3 - \hat{f}_3\|_{f_3} \leqslant Q_3(\chi_1)\,\|I_\phi D\|\,, \tag{46c}$$

$$Q_4(\chi_1)\left[\|I_\phi D\| - \left\|\begin{pmatrix}\underline{d}_z\\ \overline{d}_\phi\\ \overline{d}_\psi\end{pmatrix}\right\|\right] \leqslant \|f_4 - \hat{f}_4\|_{f_4} \leqslant Q_4(\chi_1)\,\|I_\phi D\|\,. \tag{46d}$$

The proof of Proposition 3 is postponed to the Appendix.

In order to better illustrate the proposed FD strategy, the flowchart, depicted in Fig. 12, provides a clear idea of the workflow that the proposed strategy carries out to detect, isolate, and identify faults in multiple actuators.

3.7 COMMENTS ON THE FAULT DIAGNOSIS STRATEGY

- According to Definition 3, faults that do not satisfy (39) are not detectable. This implies that the effect of such faults cannot be distinguished from the effect of disturbances. However, it is always possible to design robust controllers to compensate such non–detectable faults (for more details, see, *e.g.*, [2] and [3]).

- The parameters of the proposed strategy are composed by the observer gains, which are selected according to [18], as it is mentioned in Theorem 5, and the parameters of the proposed FD, *i.e.*, the upper and lower bounds of the disturbances given in (41), which are obtained by means of the FT–SMO through multiple experimental tests under nominal conditions, *i.e.*, free of faults.

- The quad–rotor dynamics do not posses analytical redundancy that is independent of the disturbances, *i.e.*, the faults and the disturbances are matched.

- To obtain the identification of the i–th LOE, the relation $\hat{\gamma}_i(t) = \hat{f}_i(t)/T_i(t)$ can be used. Note that, due to the effect of disturbances, it is not possible to provide an exact identification of the LOE.

- The proposed FD approach is able to detect, isolate and identify any type of strongly detectable, bounded and Lipschitz faults, *i.e.*, faults satisfying Assumption 5. For instance, a compound fault given by bias, or freezing control signals, and LOE faults. Nevertheless, the proposed FD will not be capable of distinguishing the effect of each of them.

- The proposed method can also be applied to other nonlinear systems with the same FD problem, *i.e.*, with disturbances and faults acting on the same input channel. However, it is required that the disturbances, faults and control inputs could be taken to a linear form as in (76).

- The proposed FD is not limited by the number of faults but by the type of faults. Evidently, if there does not exist a controller ensuring a certain level of performance, and the quad–rotor crashes, the proposed FD is senseless. But not only the proposed FD, any FD approach is meaningless in such a situation. In this sense, a certain performance level should be a priori guaranteed by a robust controller.

- To the best of our knowledge, there are very few works related to the development of fault diagnosis methodologies for the quad–rotor system, addressing the problem of distinguishing between faults and disturbances. The most similar work is given in [25]. However, a linearized model of the quad–rotor is considered, neglecting the nonlinearities and coupled dynamics that characterize this system. Moreover, disturbances are only considered in the attitude subsystem, and only simulation results are provided. In this sense, there is not a fair comparison framework.

3.8 EXPERIMENTAL RESULTS

The proposed FD strategy is applied to the QBall2 by Quanser depicted by Fig. 4. For more details about the Qball2, the experimental platform, and the parameters of the model (33), please see Appendix B.

Multiple experimental tests have been implemented under nominal conditions in order to obtain the upper and lower bounds of the disturbances given in (41). Once the FD parameters are obtained, many experimental tests have been carried out to validate the performance of the proposed FD strategy. The results from 5 experiments are shown in the following.

Two LOE are considered, one in rotor 1 with an LOE of 20% starting at $t_{f_1} = 15\,[s]$ and finishing at $t^{\star}_{f_1} = 60\,[s]$, and another one in rotor 2 with an LOE of 30% starting at $t_{f_2} = 45\,[s]$. The faults are injected by software through the command thrusts before sending them to the vehicle.

The continuous STSMC, given by (10), (11) and (18) (where a possible selection for the gains is in Table 3), is designed for its robust properties, as is shown in [2]. For these experiments, wind gusts are considered as external perturbations. Such wind gusts are generated by means of an industrial fan that provides a wind velocity approximately of 4[m/s], over a diagonal of the X–Y–axis (see Fig. 44).

The desired trajectory is given as

$$x_d(t) = 0.2(\arctan(15) + \arctan(t-15))\cos(\pi t/6), \tag{47a}$$
$$y_d(t) = 0.2(\arctan(15) + \arctan(t-15))\sin(\pi t/6), \tag{47b}$$
$$z_d(t) = 0.63 + 0.25\tanh(t-7.5) + 0.1\tanh(t/3-12), \tag{47c}$$
$$\psi_d(t) = 0, \tag{47d}$$

and, the gains of the FT–SMO (37) are designed according to Theorem 5, *i.e.*, $K_1 = 6.463I_4$, $K_2 = 4.743I_4$ and $K_3 = 11I_4$, with $\bar{\delta} = 10$.

The following experimental results consider the expressions given in (20), with $n_t = 10$ and $n_s = 50000$. All the experiments have been implemented with the Euler's integration method with a sampling–time equal to $h_s = 0.002$[s]. The following figures show the results corresponding to 5 tests, where the average data are depicted by a solid line and are represented as the variable with a bar. In order to obtain the upper and lower bounds of the disturbances, 10 tests in nominal conditions were performed.

In order to diminish the noise effect in the residual signals $\hat{\chi}_n$, with $n = z, \phi, \theta, \psi$, provided by the FT–SMO, these are evaluated through the following test function [45]

$$\mu(\hat{\chi}_n(t)) = \frac{1}{\Delta T}\int_{t-\Delta T}^{t} \hat{\chi}_n(\tau)\,d\tau,$$

which provides a filtered version of each residual signal. The behavior of these signals, with $\Delta T = 1$, is shown in Fig. 13. In order to improve the performance of the proposed FD, a threshold of 100 samples, *i.e.*, 0.2 seconds, gives an estimated mean time between false alarms and potential faults (for more details see Chpt. 6 in [45]).

After the occurrence of the fault f_1 at $t_{f_1} = 15\,[s]$, the residual signals $\hat{\chi}_z$ and $\hat{\chi}_\theta$ are notably affected. When f_2 occurs, at $t_{f_2} = 45\,[s]$, the effect on $\hat{\chi}_z$ is even greater, $\hat{\chi}_\psi$ is notably affected, while the effect of both faults is compensated in the residual $\hat{\chi}_\theta$. Once rotor 1 is recovered at $t^{\star}_{f_1} = 60\,[s]$, the residuals $\hat{\chi}_z$ and $\hat{\chi}_\psi$ decrease, approaching their lower thresholds, while the effect on $\hat{\chi}_\theta$ is greater. The residual $\hat{\chi}_\phi$ remains within its thresholds throughout all tests, where the roll angle ϕ is not affected by faults on rotors 1 and 2.

The detection scheme described in (40) is shown in Fig. 14, where $\|\bar{\hat{\chi}}_3\|_\infty$ exceeds the value of $\|D\|$ in an average time $\bar{t}_d = 15.42$[s], indicating the existence of an actuator fault.

The alert signals of the isolation scheme are shown in Fig. 15 where the alert signals $\mathcal{A}_3$ and $\mathcal{A}_4$ remain deactivated during all tests, $\mathcal{A}_1$ is activated in an average time $\bar{t}_1 = 15.42\,[s]$ and deactivated at $\bar{t}^{\star}_1 = 60.52\,[s]$, while $\mathcal{A}_2$ is activated in an average time $\bar{t}_2 = 45.53\,[s]$.

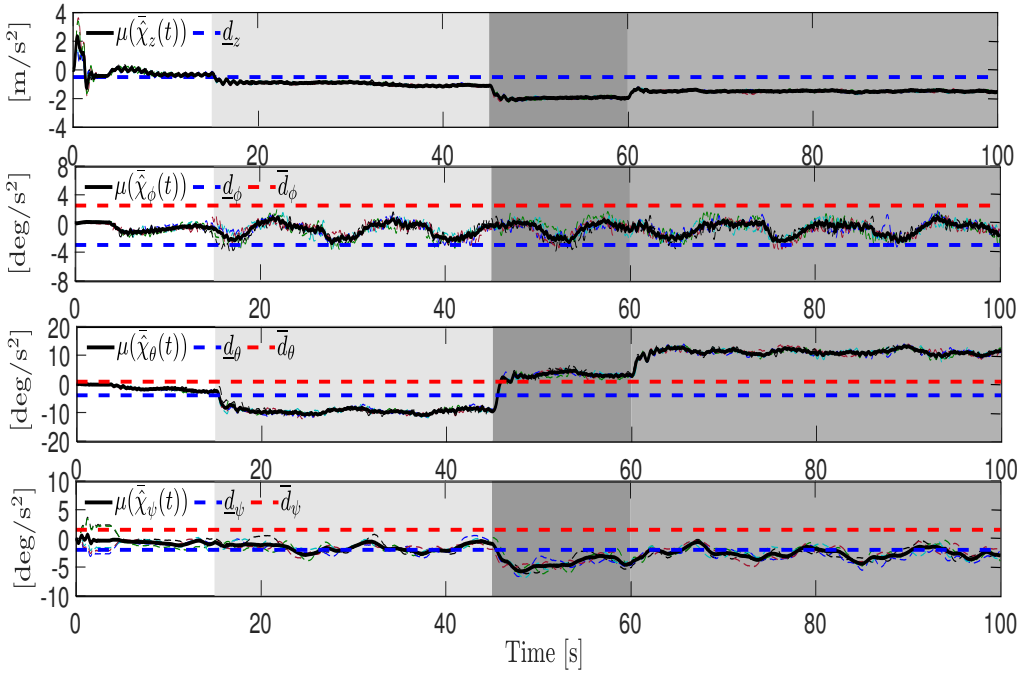

Figure 13: Residual signals generated by the FT–SMO. *The dashed signals represent the results of each of the 5 experimental tests, while the solid line represents the average of these functions. The shaded light gray area depicts the time when fault f_1 is active, the gray area when fault f_2 is active, and the dark gray when both of them are active*

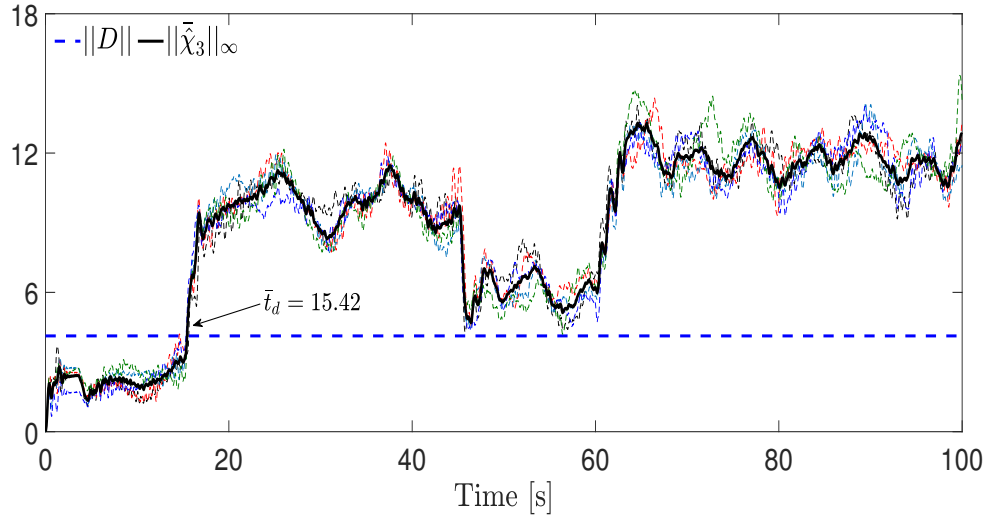

Figure 14: Fault detection. *The dashed signals represent the results of each of the 5 experimental tests, while the solid line represents the average of these functions*

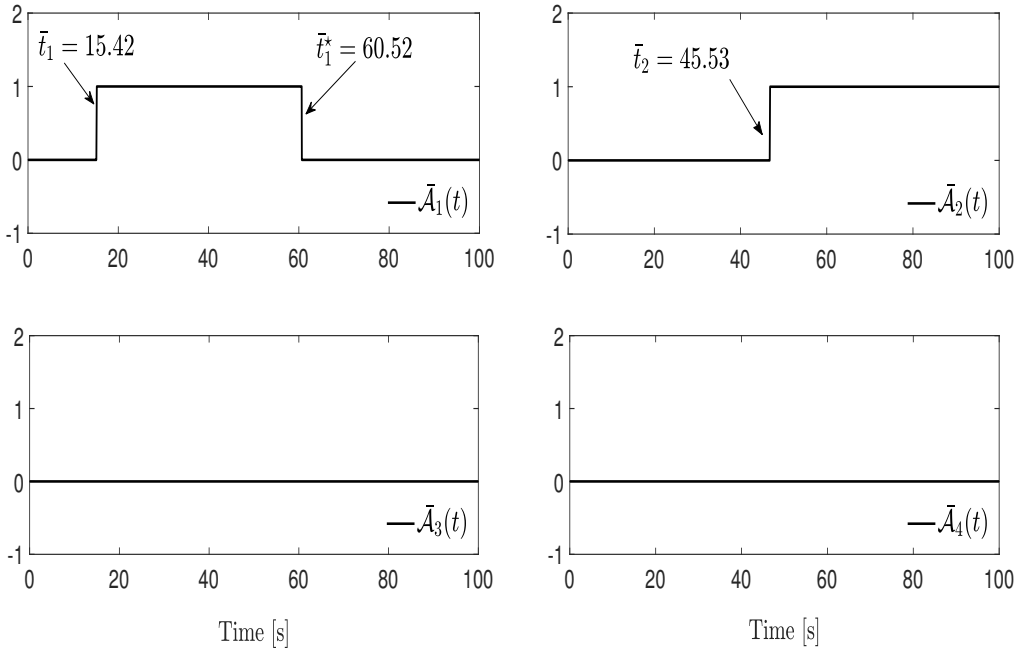

Figure 15: Fault isolation

Table 7: Properties of the performance indexes $\bar{e}_{1RMS}(t)$ and $\bar{e}_{2RMS}(t)$

LOE	**Mean–e_{RMS}**	**Mean–e%**	**min–e_{RMS}**
$\hat{\gamma}_1$	0.018	9%	0.011
$\hat{\gamma}_2$	0.021	7%	0.010

The fault identification scheme is implemented through (45), and its performance is shown in Fig. 16, for the LOE on rotor 1, and in Fig. 17, for the LOE on rotor 2.

In order to better illustrate the performance, the following performance index is proposed

$$\mathcal{F}_{RMS}(t) = \left(\frac{1}{\Delta T} \int_{t-\Delta T}^{T} \|\mathcal{F}(\sigma)\|^2 \, d\sigma \right)^{1/2}, \tag{48}$$

where $\mathcal{F}_{RMS} : \mathbb{R} \to \mathbb{R}_{\geqslant 0}$ represents the root mean square value of the function $\mathcal{F} : \mathbb{R} \to \mathbb{R}^n$. The results of the performance indexes for the identification errors $e_1(t) = \gamma_1(t) - \hat{\gamma}_1(t)$ and $e_2(t) = \gamma_2(t) - \hat{\gamma}_2(t)$, with $\Delta T = 1$, are depicted in Fig. 18. Also, the minimum, the mean value and the mean percentage error, are computed and illustrated in Tab. 7.

These results show that, moments after the existence of a fault, the proposed FD scheme successfully detects, isolates and identifies the faults, which allows us to apply corrective actions for an active FTC.

For illustrative purposes, the control objective is shown in Fig. 19, *i.e.*, the trajectory tracking of x, y, z and ψ, where the quad–rotor fulfills the trajectory task being a passive fault–tolerant control given by the robustness of the controller, however, it is notorious that the tracking error is greater due to the faults present in the actuators.

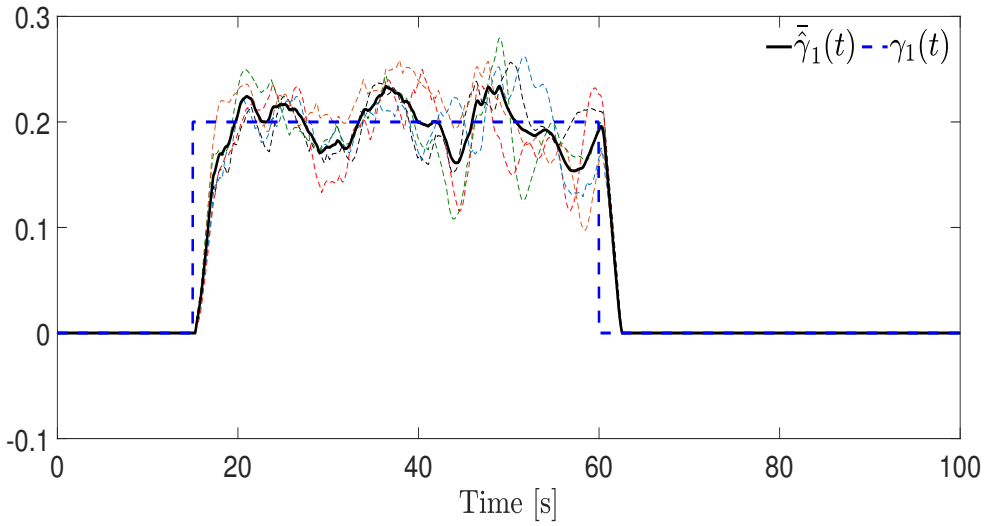

Figure 16: Fault identification on rotor 1. *The dashed signals represent the results of each of the 5 experimental tests, while the solid line represents the average of these functions*

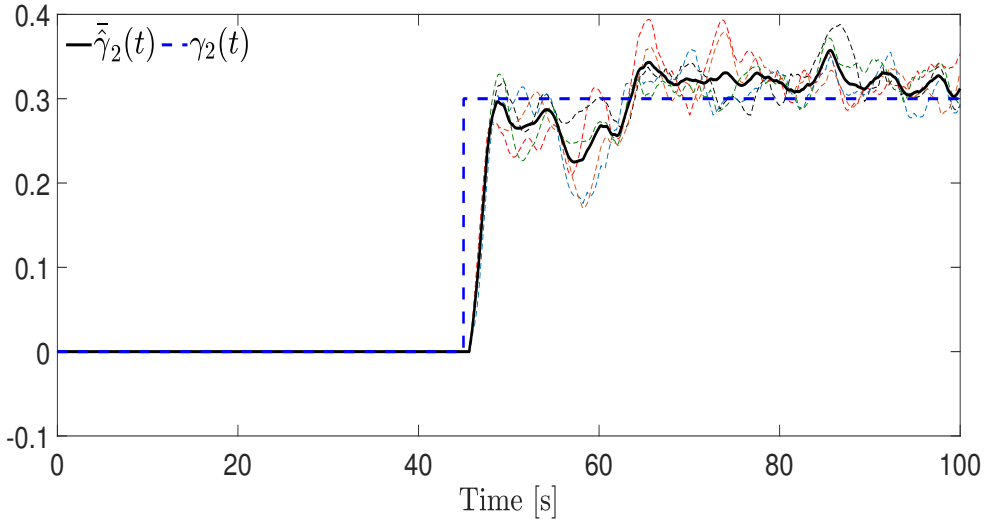

Figure 17: Fault identification on rotor 2. *The dashed signals represent the results of each of the 5 experimental tests, while the solid line represents the average of these functions*

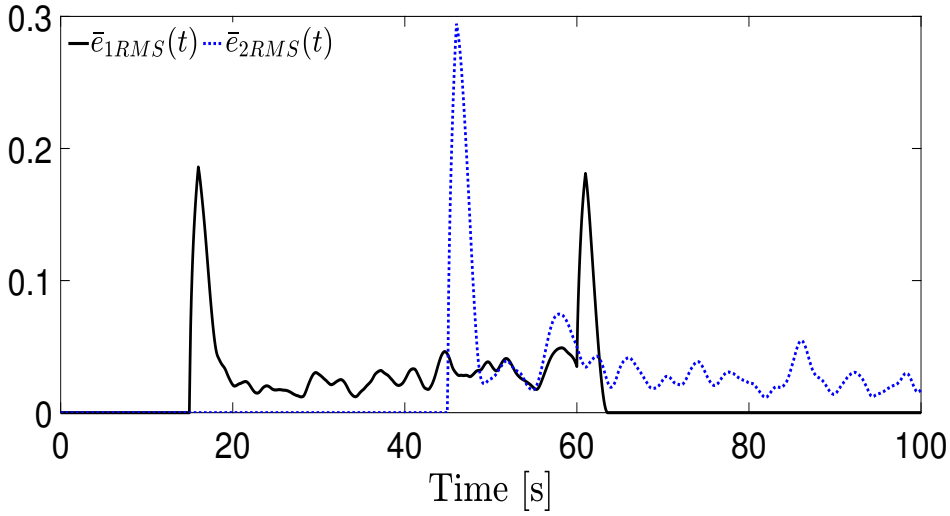

Figure 18: LOE error indexes

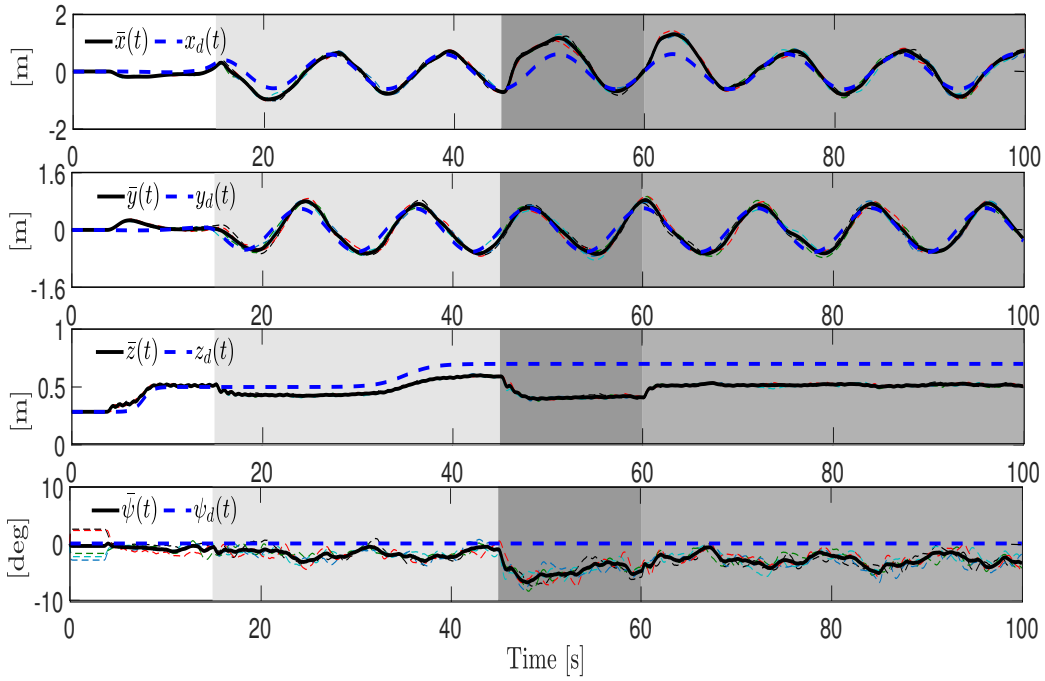

Figure 19: Position and attitude of the QBall2. *The dashed signals represent the results of each of the 5 experimental tests, while the solid line represents the average of these functions. The shaded light gray area depicts the time when fault f_1 is active, the gray area when fault f_2 is active, and the dark gray when both of them are active*

4

ACTIVE FAULT ACCOMMODATION CONTROL DESIGN

Summary. *In this chapter, the problem statement about the design of a controller to counteract the effect of multiple faults is formally introduced. Then, an active FTC, that makes use of the FD designed in Chapter 3, is designed based on the actuator fault accommodation methodology to partially compensate the effect of possible multiple LOEs despite the presence of disturbances. The proposed FAC is independent of the control–loop, allowing the usage of a baseline robust–nominal controller. Such a baseline controller is designed as the HOSMCs given in Chapter 2. Experimental results show the effectiveness of this strategy.*

4.1 PROBLEM STATEMENT

Let us recall the quad–rotor dynamics:

$$\dot{\xi}_1 = \xi_2, \tag{49a}$$
$$\dot{\xi}_2 = g_\xi(\eta_1)u_m - G - \Lambda_\xi \xi_2 + d_\xi, \tag{49b}$$
$$\dot{\eta}_1 = \eta_2, \tag{49c}$$
$$\dot{\eta}_2 = J\tau + \Xi w_\eta(\eta_2) - \Lambda_\eta \eta_2 + d_\eta, \tag{49d}$$

where $\xi_1 := (x, y, z)^T \in \mathbb{R}^3$, $\xi_2 := (\dot{x}, \dot{y}, \dot{z})^T \in \mathbb{R}^3$, $\eta_1 := (\phi, \theta, \psi)^T \in \mathbb{R}^3$ and $\eta_2 := (\dot{\phi}, \dot{\theta}, \dot{\psi})^T \in \mathbb{R}^3$ represents the quad–rotor positions, linear velocities, angles and angular velocities , respectively. The term $u_m := u_z/m$, with $u_z \in \mathbb{R}$ representing the main thrust and $m \in \mathbb{R}_+$ the mass of the quad–rotor. $\tau := (\tau_\phi, \tau_\theta, \tau_\psi)^T \in \mathbb{R}^3$ represent the angular moment vector with τ_ϕ, τ_θ and $\tau_\psi \in \mathbb{R}$ as the roll, pitch and yaw angular moments, respectively. $d_\xi := (d_x, d_y, d_z)^T \in \mathbb{R}^3$ and $d_\eta := (d_\phi, d_\theta, d_\psi)^T \in \mathbb{R}^3$ represent disturbances given by uncertainties and external perturbations, *e.g.*, some unmodeled dynamics and wind gusts.

The relation between the control inputs u_z, τ_ϕ, τ_θ, τ_ψ and the thrusts T_i, generated by the i–th rotor, is given by

$$\underbrace{\begin{bmatrix} u_z \\ \tau_\phi \\ \tau_\theta \\ \tau_\psi \end{bmatrix}}_{u} = \underbrace{\begin{bmatrix} 1 & 1 & 1 & 1 \\ 0 & 0 & L & -L \\ L & -L & 0 & 0 \\ K_\tau & K_\tau & -K_\tau & -K_\tau \end{bmatrix}}_{M} \underbrace{\begin{bmatrix} T_1 \\ T_2 \\ T_3 \\ T_4 \end{bmatrix}}_{T}, \tag{50}$$

where u is the control input vector, T is the thrust vector and M is the full rank matrix that relates the control signals to the thrusts. The constant L represents the distance between the motors and the center of mass of the quad–rotor, while K_τ represents the thrust coefficient.

Therefore, in presence of faults, the current command thrust $\bar{T}$ is given as

$$\bar{T}(t) = (I_4 - \Gamma(t))\, T(t) = T(t) - f(t), \tag{51}$$

where $\Gamma(t) := \text{diag}(\gamma_1(t), \gamma_2(t), \gamma_3(t), \gamma_4(t)) \in \mathbb{R}^{4\times4}$ is the LOE matrix and $f(t) = \Gamma(t)T(t) := (f_1(t), f_2(t), f_3(t), f_4(t))^T \in \mathbb{R}^4$ is the fault vector. The term $\gamma_i(t) \in (0, 1)$ represents the case of an LOE fault in the i–th rotor. The case of $\gamma_i(t) = 0$ represents a healthy rotor, while $\gamma_i(t) = 1$ means that the i–th actuator is fully damaged. Note that the current command thrust $\bar{T}$ is not measured and therefore is unknown.

The goal in this chapter is to design an FAC to achieve the tracking of a desired trajectory under the influence of possible multiple LOEs, uncertainties and external perturbations. It is assumed that only the positions and angles of the vehicle are measurable.

In this sense, the proposed FAC uses the FD information in a baseline robust–nominal controller to increase its fault tolerance through the fault identification, *i.e.*,

$$T(t) = M^{-1}u(t) + \hat{f}(t), \tag{52}$$

where u is the nominal control input vector. Hence, the current command thrust, given in (51), can be written as $\bar{T}(t) = M^{-1}u(t) - \tilde{f}(t)$, with $\tilde{f} = f - \hat{f}$.

In order to apply the proposed fault accommodation strategy, a baseline robust–nominal control is designed based on the HOSMCs given in Chapter 2.

4.2 BASELINE ROBUST–NOMINAL CONTROL DESIGN

In order to highlight the fault accommodation properties, baseline robust–nominal controllers are proposed based on a combination between PID controllers (for the position subsystem) and CTCs (for the attitude subsystem) (for more details, please refer to [2]).

However, it is possible to apply different HOSMCs for the design of the attitude controllers, as it was described in Section 2, such as the STSMC, the NTSNC, or some HOSMC based on discontinuous integral action (see, *e.g.*, [90], and [91]).

Recall that the tracking error vectors are given as

$$e_\xi = (e_x, e_y, e_z)^T = \xi_1 - \xi_d, \quad e_\eta = \left(e_\phi, e_\theta, e_\psi\right)^T = \eta_1 - \eta_d,$$

$$\varepsilon_\xi = (\varepsilon_x, \varepsilon_y, \varepsilon_z)^T = \xi_2 - \dot{\xi}_d, \quad \varepsilon_\eta = \left(\varepsilon_\phi, \varepsilon_\theta, \varepsilon_\psi\right)^T := \eta_2 - \dot{\eta}_d,$$

where $\xi_d = (x_d, y_d, z_d)^T \in \mathbb{R}^3$ and $\eta_d = (\phi_\star, \theta_\star, \psi_d)^T \in \mathbb{R}^3$ are the desired position and attitude vectors, respectively.

The references signals $\phi_\star$ and $\theta_\star$ must be properly designed in order to achieve the tracking trajectory task. Such as in Chapter 2, Section 2.3.2, a virtual control $\nu = (\nu_x, \nu_y, \nu_z)^T \in \mathbb{R}^3$ is introduced in the position error dynamics, *i.e.*,

$$\dot{e}_\xi = \varepsilon_\xi, \tag{53a}$$

$$\dot{\varepsilon}_\xi = \nu + w_\xi(\eta_1, u_z, \nu) - \Lambda_\xi\xi_2 + d_\xi - \ddot{\xi}_d, \tag{53b}$$

$$\dot{e}_\eta = \varepsilon_\eta, \tag{53c}$$

$$\dot{\varepsilon}_\eta = J\tau + \Xi w_\eta(\eta_2) - \Lambda_\eta\eta_2 + d_\eta - \ddot{\eta}_d, \tag{53d}$$

where the disturbance term $w_\xi(\eta_1, u_z, \nu) = u_m g_\xi(\eta_1) - G - \nu$. Thus, selecting appropriately the virtual control ν, the command signals u_z, $\phi_\star$ and $\theta_\star$ can be computed as in (10).

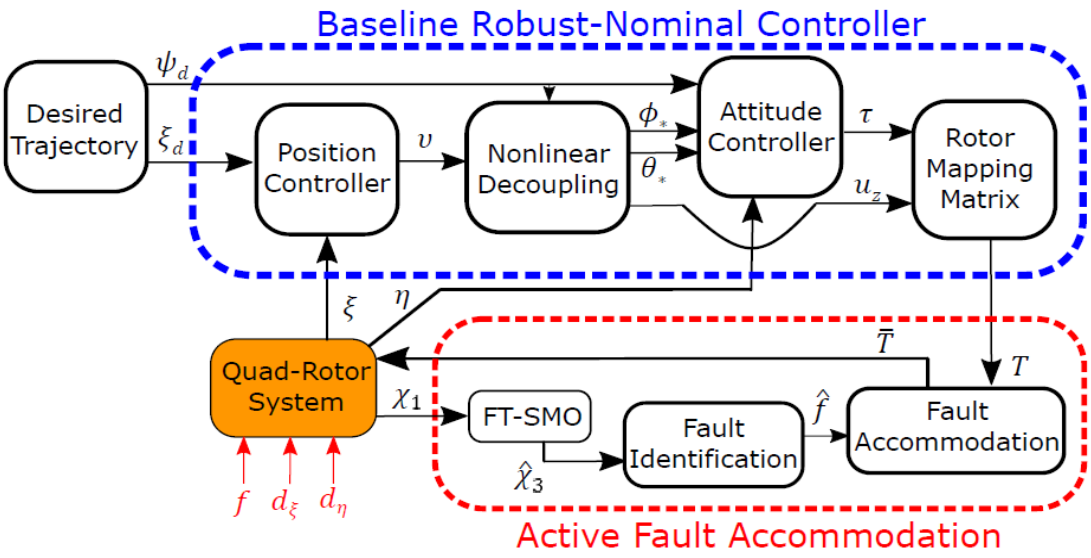

Figure 20: Flowchart of the proposed FAC strategy

Then, the virtual controllers $\nu = (\nu_x, \nu_y, \nu_z)^T$, and the angular moment vector τ are designed as

$$\nu = \nu_\star + \frac{g_\xi(\eta_1)}{m} \sum_{i=1}^{4} \hat{f}_i(t), \tag{54a}$$

$$\tau = \tau_\star + I_\eta M \hat{f}(t), \tag{54b}$$

where $I_\eta := (0_{3\times 1}, I_3) \in \mathbb{R}^{3\times 4}$, and the fault estimation $\hat{f}$ is computed through the FD described in Section 3. Such a term $\hat{f}$ represents the fault accommodation. The baseline robust–nominal controllers are given as

$$\nu_\star = \bar{\nu} + \Lambda_\xi \xi_2 + \ddot{\xi}_d, \tag{55a}$$

$$\tau_\star = J^{-1}(\bar{\tau} - \Xi w_\eta(\eta_2) + \Lambda_\eta \eta_2 + \ddot{\eta}_d). \tag{55b}$$

The term $\bar{\nu}$ is designed as the PID controller given in (12), while each term of $\bar{\tau} := (\bar{\tau}_\phi, \bar{\tau}_\theta, \bar{\tau}_\psi) \in \mathbb{R}^3$ is designed as the CTC given in (17). Such baseline robust–nominal controllers have an intrinsic passive fault tolerance due to its robustness properties [2].

Then, the following result can be established.

Theorem 6 *Let the FAC (54) and the baseline robust–nominal controllers (55) be applied to system (49). Suppose that Assumptions 1, 2, 3 and 5 hold. Then, the position tracking error dynamics is* ISS *with respect to* d_ξ *and* $\tilde{f}$*; while the attitude tracking error* $(e_\eta, \varepsilon_\eta) = 0$ *is UFTS.*

The proof of Theorem 6 is postponed to the Appendix.

To summarize, the proposed strategy allows us to achieve the trajectory tracking for a quad–rotor under the presence of LOE on the rotors and disturbances. A flowchart of the proposed actuator FAC is depicted by Fig. 20.

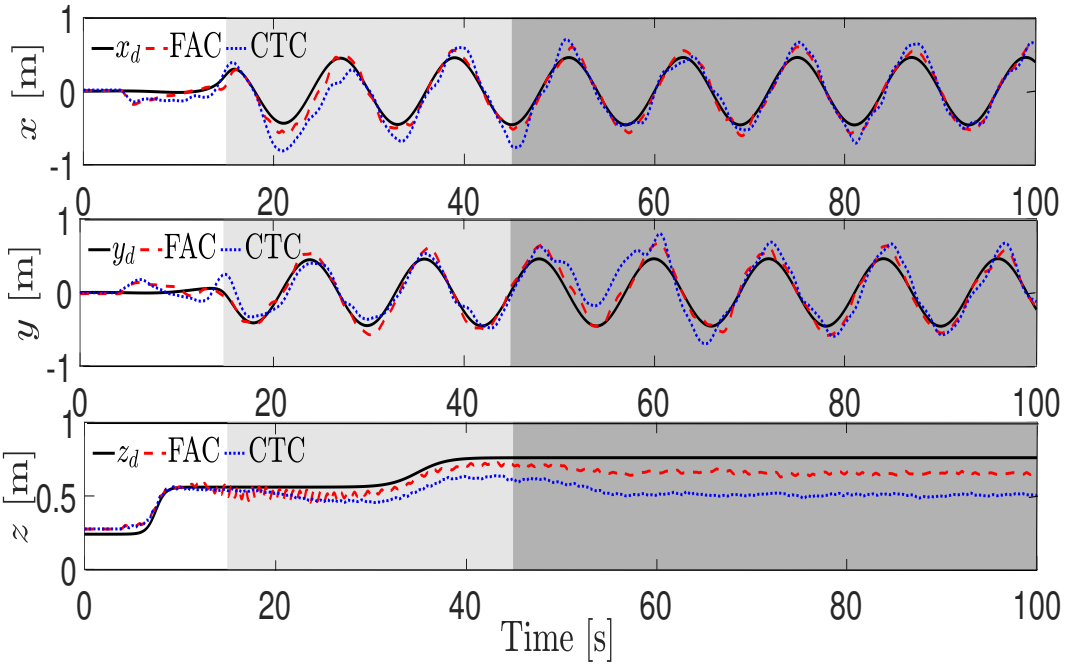

Figure 21: Trajectories of the quad–rotor. Position. *The shaded light gray area depicts the time when fault f_1 is active, and the dark gray when both faults are active*

4.3 EXPERIMENTAL RESULTS

In order to show the performance of the proposed FAC, experimental tests are presented on the QBall2 by Quanser depicted by Fig. 4. For more details about the Qball2, the experimental platform, and the parameters of the model (49), please see Appendix B. For this purpose, a comparison is presented between the baseline robust–nominal controller, given by the combination of the PID controllers and the CTCs, and the proposed FAC. Both controllers are subject to the same faults and they are designed using the same gains.

The desired tracking task is given by the helical trajectory given in (47). The rotor LOE faults are considered as

$$\gamma_1(t) = \begin{cases} 0, & \forall t < 15, \\ 0.2, & \forall t \geqslant 15, \end{cases} \qquad \gamma_3(t) = \begin{cases} 0, & \forall t < 45, \\ 0.2, & \forall t \geqslant 45, \end{cases}$$

while the rotors 2 and 4 are fault–free. The experiment has been implemented with the Euler's integration method with a sampling–time equal to $h_s = 0.002[s]$.

The tracking task, in the translational coordinates and in the yaw angle, is illustrated in Figs. 21 and 22, respectively. Despite the LOE faults, both controllers make the quad–rotor track the desired trajectory. However, adding the fault allocation scheme in the baseline robust–nominal controller, the position and yaw tracking performance and the yaw angle is evidently improved.

To obtain the identification of the i–th LOE, the relation $\hat{\gamma}_i(t) = \hat{f}_i(t)/T_i(t)$ can be used. The fault identification of each fault is depicted in Figs. 23 and 24. Once a fault occurs, the fault identification module approximates the magnitude of each fault. On

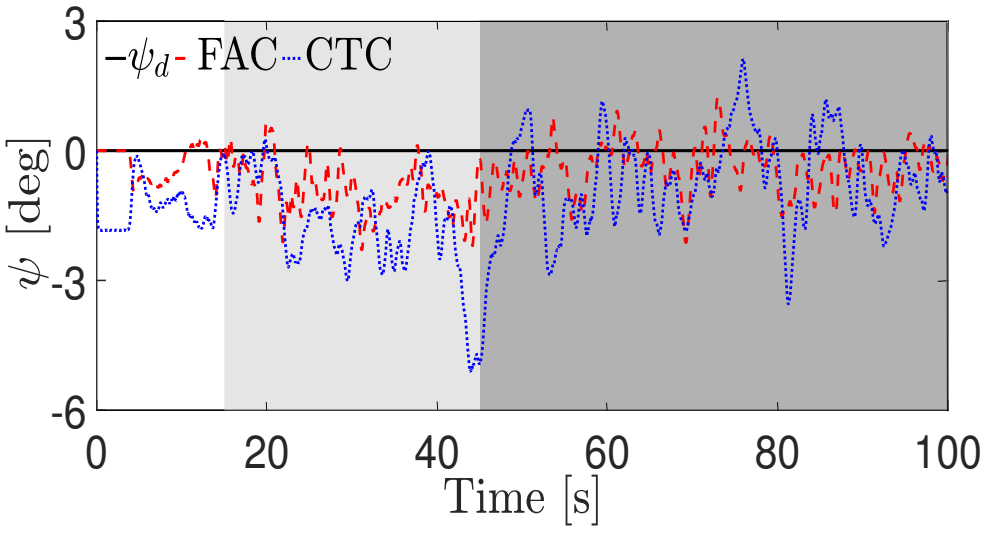

Figure 22: Quad–rotor yaw angle. *The shaded light gray area depicts the time when fault* f_1 *is active, and the dark gray when both faults are active*

Table 8: Properties of the tracking performance indexes e_{xRMS}, e_{yRMS}, e_{zRMS} and $\bar{e}_{\psi RMS}$.

Controller	x	y	z	ψ
FAC	**0.0683**	**0.0750**	**0.0754**	**0.7092**
CTC	0.1158	0.1323	0.1695	1.3391

the other hand, the thrust generated by each rotor is shown in Fig. 25, where the control effort in the FAC is more aggressive.

In order to better illustrate the performance, the following performance index is proposed

$$\mathcal{F}_{RMS}(t) = \left(\frac{1}{\Delta T} \int_{t-\Delta T}^{T} \|\mathcal{F}(\sigma)\|^2 \, d\sigma \right)^{1/2}, \tag{56}$$

where $\mathcal{F}_{RMS} : \mathbb{R} \to \mathbb{R}_{\geqslant 0}$ represents the root mean square value of the function $\mathcal{F} : \mathbb{R} \to \mathbb{R}^n$. In this sense, the average value of the root mean square of each position error signal and the yaw angle error are computed and they are illustrated in Tab. 8. The first 5 seconds of each experimental test are not taken into account in order to avoid the initial condition effect. Note that using the same controller gains, and under the effect of the same faults, the FAC improves the performance in each coordinate.

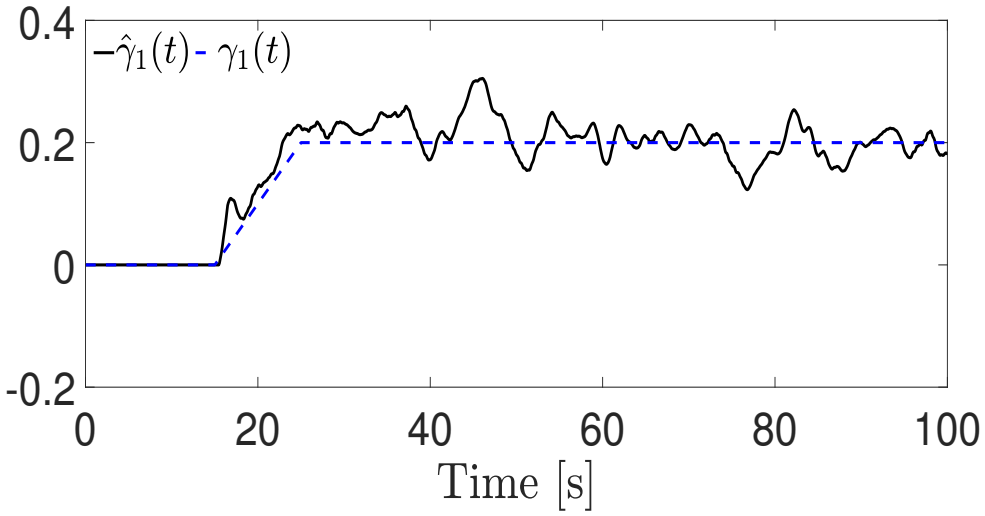

Figure 23: Fault identification on rotor 1

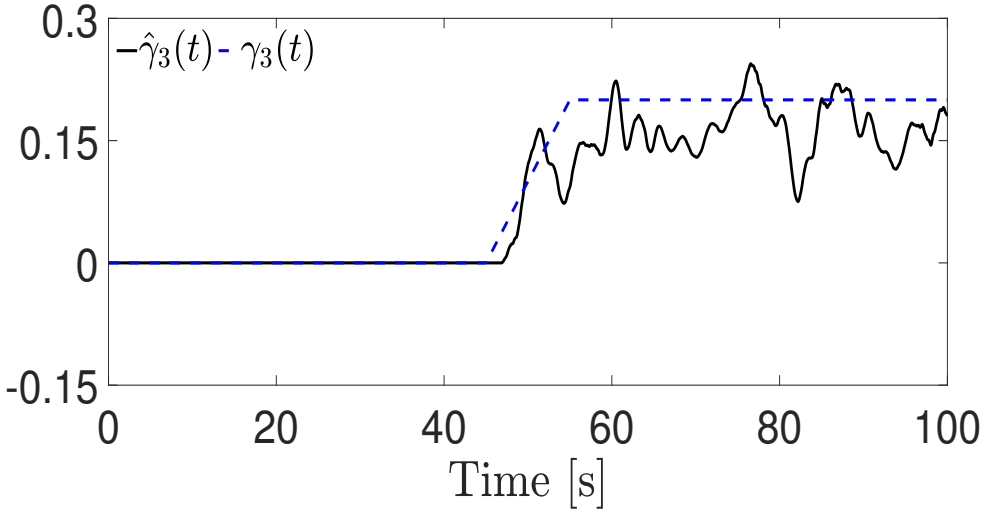

Figure 24: Fault identification on rotor 3

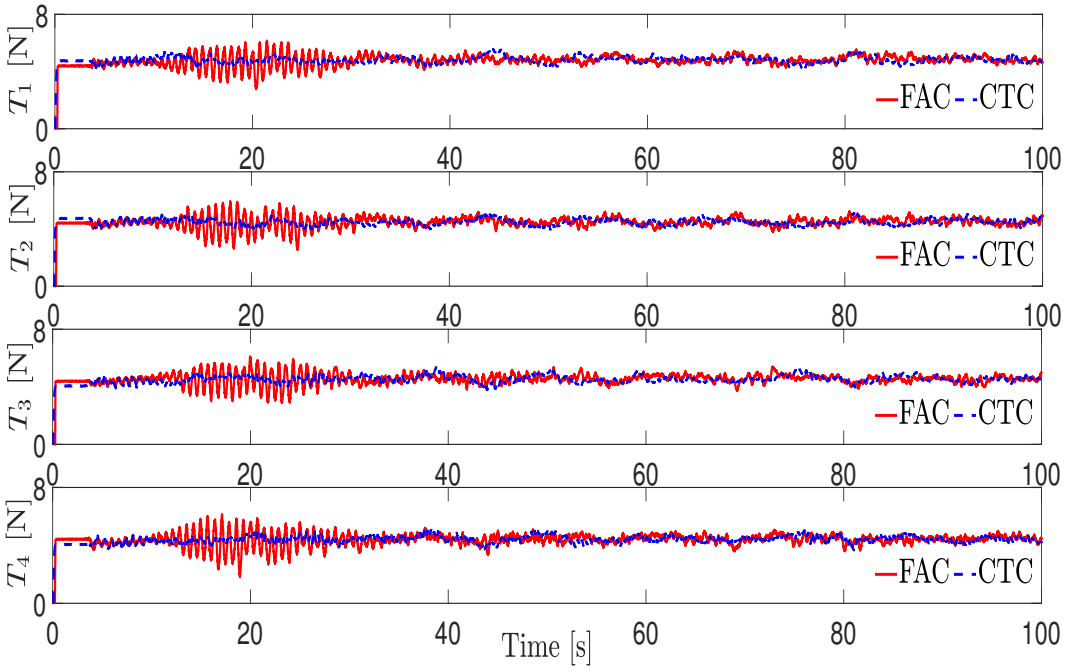

Figure 25: Rotor thrusts

5

FAULT–TOLERANT CONTROL FOR A ROTOR FAILURE

Summary. *In this chapter, the problem statement about the design of a controller to counteract the effect of a rotor failure is formally introduced. Afterward, an active FTC is designed to deal with the trajectory tracking problem in a quad–rotor under a rotor failure and in the presence of disturbances. The rotor failure is isolated using the FD designed in Chapter 3, and then, a combination of an FT–SMO, PID controllers, and HOSMCs is proposed. Such a strategy allows the position tracking without breaking physical restrictions, such as the sign of pitch and roll moments. Numerical simulations show the feasibility of the proposed strategy.*

5.1 PROBLEM STATEMENT

Let us recall the quad–rotor dynamics:

$$\dot{\xi}_1 = \xi_2, \tag{57a}$$
$$\dot{\xi}_2 = g_\xi(\eta_1)u_m - G - \Lambda_\xi \xi_2 + d_\xi, \tag{57b}$$
$$\dot{\eta}_1 = \eta_2, \tag{57c}$$
$$\dot{\eta}_2 = J\tau + \Xi w_\eta(\eta_2) - \Lambda_\eta \eta_2 + d_\eta, \tag{57d}$$

where $\xi_1 := (x, y, z)^T \in \mathbb{R}^3$, $\xi_2 := (\dot{x}, \dot{y}, \dot{z})^T \in \mathbb{R}^3$, $\eta_1 := (\phi, \theta, \psi)^T \in \mathbb{R}^3$ and $\eta_2 := (\dot{\phi}, \dot{\theta}, \dot{\psi})^T \in \mathbb{R}^3$ represent the quad–rotor positions, linear velocities, angles and angular velocities , respectively. The term $u_m := u_z/m$, with $u_z \in \mathbb{R}$ representing the main thrust and $m \in \mathbb{R}_+$ the mass of the quad–rotor. $\tau := (\tau_\phi, \tau_\theta, \tau_\psi)^T \in \mathbb{R}^3$ represents the angular moment vector with τ_ϕ, τ_θ and $\tau_\psi \in \mathbb{R}$ as the roll, pitch and yaw angular moments, respectively. $d_\xi := (d_x, d_y, d_z)^T \in \mathbb{R}^3$ and $d_\eta := (d_\phi, d_\theta, d_\psi)^T \in \mathbb{R}^3$ represent disturbances given by uncertainties and external perturbations, *e.g.*, some unmodeled dynamics and wind gusts.

The relation between the control inputs u_z, τ_ϕ, τ_θ, τ_ψ and the thrusts T_i, generated by the i–th rotor, is given by

$$\underbrace{\begin{bmatrix} u_z \\ \tau_\phi \\ \tau_\theta \\ \tau_\psi \end{bmatrix}}_{u} = \underbrace{\begin{bmatrix} 1 & 1 & 1 & 1 \\ 0 & 0 & L & -L \\ L & -L & 0 & 0 \\ K_\tau & K_\tau & -K_\tau & -K_\tau \end{bmatrix}}_{M} \underbrace{\begin{bmatrix} T_1 \\ T_2 \\ T_3 \\ T_4 \end{bmatrix}}_{T}, \tag{58}$$

where u is the control input vector, T is the thrust vector and M is the full rank matrix that relates the control signals to the thrusts. The constant L represents the distance between the motors and the center of mass of the quad–rotor, while K_τ represents the thrust coefficient.

Therefore, in presence of failures, the current command thrust $\bar{T}$ is given as

$$\bar{T}(t) = (I_4 - \Gamma(t))\, T(t) = T(t) - f(t), \tag{59}$$

where $\Gamma(t) := \text{diag}(\gamma_1(t), \gamma_2(t), \gamma_3(t), \gamma_4(t)) \in \mathbb{R}^{4\times4}$ is the failure matrix and $f(t) = \Gamma(t)T(t) := (f_1(t), f_2(t), f_3(t), f_4(t))^T \in \mathbb{R}^4$ is the fault vector. The binary term $\gamma_i(t)$ represents the presence or absence of a failure in the i–th rotor. The case of $\gamma_i(t) = 0$ represents a healthy rotor, while $\gamma_i(t) = 1$ means that the i–th actuator is fully damaged. Note that the current command thrust $\bar{T}$ is not measured and therefore is unknown.

Note that in a rotor failure scenario, relation (58) ceases to be bijective. For instance, in case of a failure on T_1, the relation between the control inputs and the remaining thrusts is given by

$$\begin{pmatrix} u_z \\ \tau_\phi \\ \tau_\theta \\ \tau_\psi \end{pmatrix} = \begin{pmatrix} 1 & 1 & 1 \\ 0 & L & -L \\ -L & 0 & 0 \\ K_\tau & -K_\tau & -K_\tau \end{pmatrix} \begin{pmatrix} T_2 \\ T_3 \\ T_4 \end{pmatrix}. \tag{60}$$

Then, a rotor failure implies the loss of a degree of freedom. Among these, the roll and pitch angles are vital since they are essential for the x–y translational trajectory tracking. Moreover, in order to avoid a possible ground collision, the altitude must be controllable. On the other hand, the impossibility to control the yaw angle implies loosing the heading of the vehicle, which is not essential in accomplishing a tracking task.

Therefore, from (60), it is easy to see that the control input τ_ψ is now linearly dependent on u_z and τ_θ, *i.e.*,

$$\tau_\psi(t) = K_\tau \left(-u_z(t) - 2\frac{\tau_\theta(t)}{L} \right), \forall t \geqslant t_{f1}, \tag{61}$$

where t_{f1} represents the instant at which the rotor 1 failure has occurred. Similar expressions can be obtained by considering a failure on the rotors 2, 3 or 4, respectively, as

$$\tau_\psi(t) = K_\tau \left(-u_z(t) + 2\frac{\tau_\theta(t)}{L} \right), \forall t \geqslant t_{f2}, \tag{62a}$$

$$\tau_\psi(t) = K_\tau \left(u_z(t) + 2\frac{\tau_\phi(t)}{L} \right), \forall t \geqslant t_{f3}, \tag{62b}$$

$$\tau_\psi(t) = K_\tau \left(u_z(t) - 2\frac{\tau_\phi(t)}{L} \right), \forall t \geqslant t_{f4}, \tag{62c}$$

where t_{fi} represents the instant at which the failure of the i–th rotor has occurred. Therefore, the FTC design is carried out taking into account such a linear dependence caused by a single rotor failure.

In this sense, the goal in this chapter is to design an active FTC to achieve the tracking of a desired trajectory under the influence of a rotor failure, uncertainties and external perturbations. It is assumed that only the positions and angles of the vehicle are measurable.

The proposed strategy is composed of a full FT–SMO, that provides a full state estimation from the measurable output and identifies some type of disturbances, and a combination of PID controllers (in order to generate the main thrust and the desired pitch an roll angles) and Continuous HOSMCs (for the angular moments). Firstly, the design of the FT–SMO is presented.

It is important to mention that the following FT–SMO makes use of the FD designed in Chapter 3 in order to isolate and identify the current failure.

5.2 FULL FINITE–TIME SLIDING–MODE OBSERVER

An additionally full state FT–SMO, based on the FD scheme, is proposed [18]

$$\dot{\hat{\xi}}_1 = \hat{\xi}_2 + \hat{K}_1 \varphi_1(\hat{e}_\xi), \tag{63a}$$

$$\dot{\hat{\xi}}_2 = \frac{1}{m}\sum_{i=1}^{4}\left(T_i(t) - \hat{f}_i\right) g_\xi(\eta_1) - G - \Lambda_\xi \hat{\xi}_2 + \hat{\xi}_3 + \hat{K}_2 \varphi_2(\hat{e}_\xi), \tag{63b}$$

$$\dot{\hat{\xi}}_3 = \hat{K}_3 \varphi_3(\hat{e}_\xi), \tag{63c}$$

$$\dot{\hat{\eta}}_1 = \hat{\eta}_2 + \hat{K}_4 \varphi_1(\hat{e}_\eta), \tag{63d}$$

$$\dot{\hat{\eta}}_2 = J I_\eta M(T(t) - \hat{f}) + \Xi w_\eta(\hat{\eta}_2) - \Lambda_\eta \hat{\eta}_2 + \hat{\eta}_3 + \hat{K}_5 \varphi_2(\hat{e}_\eta), \tag{63e}$$

$$\dot{\hat{\eta}}_3 = \hat{K}_6 \varphi_3(\hat{e}_\eta), \tag{63f}$$

where $I_\eta := (0_{3\times 1}, I_3) \in \mathbb{R}^{3\times 4}$; $\hat{e}_\xi = \xi_1 - \hat{\xi}_1 \in \mathbb{R}^3$ and $\hat{e}_\eta = \eta_1 - \hat{\eta}_1 \in \mathbb{R}^3$ are the output errors, respectively; the nonlinear output injections φ_1, φ_2, $\varphi_3 : \mathbb{R}^3 \to \mathbb{R}^3$ are given as $\varphi_1(\mathbf{s}) := \lceil \mathbf{s} \rfloor^{\frac{2}{3}}$, $\varphi_2(\mathbf{s}) := \lceil \mathbf{s} \rfloor^{\frac{1}{3}}$ and $\varphi_3(\mathbf{s}) := \lceil \mathbf{s} \rfloor^{0}$, for any $\mathbf{s} \in \mathbb{R}^3$, with some design diagonal gain matrices $\hat{K}_j = \operatorname{diag}(\hat{k}_{j1}, \hat{k}_{j2}, \hat{k}_{j3}) \in \mathbb{R}^{3\times 3}$ with $j = \overline{1,6}$.

Define the state estimation error as $\hat{e}_f := (\hat{e}_\xi, \hat{\varepsilon}_\xi, \hat{e}_\eta, \hat{\varepsilon}_\eta, \hat{e}_\xi, \hat{e}_\eta)^T \in \mathbb{R}^{18}$, where $\hat{\varepsilon}_\xi := \xi_2 - \hat{\xi}_2 \in \mathbb{R}^3$ and $\hat{\varepsilon}_\eta := \eta_2 - \hat{\eta}_2 \in \mathbb{R}^3$ are the linear and angular velocity estimation errors, respectively, while $\hat{e}_\xi := d_\xi - \hat{\xi}_3$ and $\hat{e}_\eta := d_\eta - \hat{\eta}_3$ are the estimation errors of the disturbances. In this sense, the total uncertainty affecting the estimation error between system (57) and the FT–SMO (63) is given by

$$\Delta = \begin{pmatrix} \Delta_\xi \\ \Delta_\eta \end{pmatrix} := \begin{pmatrix} d_\xi - \Lambda_\xi \hat{\varepsilon}_\xi \\ d_\eta - \Lambda_\eta \hat{\varepsilon}_\eta + \Xi(w_\eta(\eta_2) - w_\eta(\hat{\eta}_2)) \end{pmatrix}.$$

Due to Assumptions 2 and 3, such uncertainties are bounded and Lipschitz, *i.e.*, $\Delta \in \mathcal{L}_\delta$ and $\dot{\Delta} \in \mathcal{L}_{\bar{\delta}}$, with known positive constants δ and $\bar{\delta}$.

The following theorem describes the finite–time convergence properties of the FT–SMO (63).

Theorem 7 [18] *Let the observer* (63) *be applied to system* (57). *Suppose that Assumptions* 2, 3 *and* 5 *hold, assume that the failure has been isolated, and that the observer gains are selected as* $\hat{K}_1 = \hat{K}_4 = 2\bar{\delta}^{\frac{1}{3}} I_3$, $\hat{K}_2 = \hat{K}_5 = 1.5\bar{\delta}^{\frac{1}{2}} I_3$ *and* $\hat{K}_3 = \hat{K}_6 = 1.1\bar{\delta} I_3$; *then, at steady state* $\hat{e}_f = 0$, *the state estimation error dynamics is* UFTS.

Remark 2 *The observer* (63) *is insensitive to the effect of both, disturbances and faults. However, the control inputs* u_z *and* τ, *used in the observer, are the real ones, i.e., taking into account the fault identification given in Chapter* 3, *Section* 3.6, *depending on the rotor failure. Therefore, the proposed FT–SMO provides an estimation only of the disturbances.*

Taking into account the Remark 1 (convergence time of the observer before the failure occurrence), and according to Theorem 7, $\hat{e}_f = 0$ is UFTS, which implies that $\hat{\xi}_1(t) = \xi_1(t)$, $\hat{\xi}_2(t) = \xi_2(t)$, $\hat{\xi}_3(t) = d_\xi(t)$, $\hat{\eta}_1(t) = \eta_1(t)$, $\hat{\eta}_2(t) = \eta_2(t)$ and $\hat{\eta}_3(t) = d_\eta(t)$, for all $t \geqslant \mathcal{T}_2$, where $\mathcal{T}_2$ is the observer convergence time. Therefore, if Assumptions 2, 3 and 5 hold, the FT–SMO (63) provides the following disturbance identifications for all $t \geqslant \mathcal{T}_2$

$$\hat{\xi}_3(t) = (\hat{\xi}_x(t), \hat{\xi}_y(t), \hat{\xi}_z(t))^T = d_\xi(t), \tag{64a}$$

$$\hat{\eta}_3(t) = (\hat{\eta}_\phi(t), \hat{\eta}_\theta(t), \hat{\eta}_\psi(t))^T = d_\eta(t). \tag{64b}$$

5.3 CONTROL STRATEGY

Due to the under–actuated nature of the quad–rotor and the failure of one of the rotors, it is not possible to control all the positions and angles, independently. Moreover, based on (61) and (62), it is not possible to stabilize the yaw angle due to the effect of the failure. Hence, the proposed control strategy is designed in order to allow the yaw angular velocity to remain bounded and the position tracking to be achieved even in the presence of some disturbances.

The proposed strategy is based on two cascading loops. The internal loop controls the attitude of the vehicle, while the external loop contains the controllers of the translational coordinates. In this way, the external loop generates a desired roll and pitch angles, that the internal loop will use in the attitude control.

Define the tracking error vectors as

$$\begin{aligned} e_\xi &= (e_x, e_y, e_z)^T = \xi_1 - \xi_d, \\ \varepsilon_\xi &= (\varepsilon_x, \varepsilon_y, \varepsilon_z)^T = \xi_2 - \dot{\xi}_d, \\ \bar{e}_\eta &:= (e_\phi, e_\theta)^T = H\eta_1 - \bar{\eta}_d, \\ \bar{\varepsilon}_\eta &:= (\varepsilon_\phi, \varepsilon_\theta)^T = H\eta_2 - \dot{\bar{\eta}}_d, \end{aligned}$$

with

$$H := \begin{pmatrix} 1 & 0 & 0 \\ 0 & 1 & 0 \end{pmatrix},$$

and where $\xi_d = (x_d, y_d, z_d)^T \in \mathbb{R}^3$ and $\bar{\eta}_d = (\phi_\star, \theta_\star)^T \in \mathbb{R}^2$ are the desired position and attitude vectors, respectively.

The references signals $\phi_\star$ and $\theta_\star$, as well as the control input u_z, must be properly designed in order to achieve a desired position ξ_d. To do this, a virtual control $\nu := (\nu_x, \nu_y, \nu_z)^T \in \mathbb{R}^3$ is introduced in the position error dynamics, *i.e.*,

$$\dot{e}_\xi = \varepsilon_\xi, \tag{65a}$$
$$\dot{\varepsilon}_\xi = \nu + w_\xi(\eta_1, u_z, \nu) - \Lambda_\xi \xi_2 + d_\xi - \ddot{\xi}_d, \tag{65b}$$
$$\dot{\bar{e}}_\eta = \bar{\varepsilon}_\eta, \tag{65c}$$
$$\dot{\bar{\varepsilon}}_\eta = H(J\tau + \Xi w_\eta(\eta_2) - \Lambda_\eta \eta_2 + d_\eta) - \ddot{\bar{\eta}}_d, \tag{65d}$$

where the disturbance term $w_\xi(\eta_1, u_z, \nu) = (w_x, w_y, w_z) = u_m g_\xi(\eta_1) - G - \nu$. Thus, the virtual control ν may be chosen as follows

$$\nu_x = u_m(c\phi_\star s\theta_\star c\psi + s\phi_\star s\psi), \tag{66a}$$
$$\nu_y = u_m(c\phi_\star s\theta_\star s\psi - s\phi_\star c\psi), \tag{66b}$$
$$\nu_z = u_m c\phi_\star c\theta_\star - g. \tag{66c}$$

Note that, different from (10), the measured yaw angle ψ is considered in the previous set of expressions.

The main thrust u_z, as well as the references signals $\phi_\star$ and $\theta_\star$, are calculated from (66), *i.e.*,

$$u_z = m\sqrt{\nu_x^2 + \nu_y^2 + (\nu_z + g)^2}, \tag{67a}$$
$$\phi_\star = \arcsin\left[u_m^{-1}(\nu_x s\psi - \nu_y c\psi)\right], \tag{67b}$$
$$\theta_\star = \arctan[(\nu_z + g)^{-1}(\nu_x c\psi + \nu_y s\psi)]. \tag{67c}$$

Therefore, the objective now is to design the virtual controller ν and the angular moments τ_ϕ and τ_θ such that the tracking error vector $e := (e_\xi, \varepsilon_\xi, \bar{e}_\eta, \bar{\varepsilon}_\eta) \in \mathbb{R}^{10}$ converges to zero despite the complete loss of a rotor and disturbances. In order to fulfill such an objective, it will be demonstrated that system (65a)–(65b) is ISS with respect to w_ξ and that system (65c)–(65d) is UFTS. Then the behavior of w_ξ will be discussed, and finally, the yaw dynamics will be analyzed.

5.3.1 *Position Control Design*

Let us propose the following PID virtual controller for as

$$\nu = K_{i\xi}\bar{e}_\xi + K_{p\xi}e_\xi + K_{d\xi}\varepsilon_\xi + \Lambda_\xi\xi_2 - \hat{\xi}_3 + \ddot{\xi}_d, \tag{68}$$

where $K_{i\xi} = \text{diag}(k_{x1}, k_{y1}, k_{z1}) \in \mathbb{R}^{3\times3}$, $K_{p\xi} = \text{diag}(k_{x2}, k_{y2}, k_{z2}) \in \mathbb{R}^{3\times3}$, $K_{d\xi} = \text{diag}(k_{x3}, k_{y3}, k_{z3}) \in \mathbb{R}^{3\times3}$ and $\bar{e}_\xi := (\bar{e}_x, \bar{e}_y, \bar{e}_z)^T \in \mathbb{R}^3$ with $\bar{e}_x := \int_0^t e_x(\tau)d\tau$, $\bar{e}_y := \int_0^t e_y(\tau)d\tau$ and $\bar{e}_z := \int_0^t e_z(\tau)d\tau$. Then, the following result can be established.

Lemma 1 [2] *Let the control* (68) *be applied to system* (57)*, and assume that Assumptions 1, 2 and 3 hold. Then, system* (65a)–(65b) *is ISS with respect to* w_ξ*.*

5.3.2 *Pitch and Roll Control Design*

The attitude tracking error dynamics (65c)–(65d) can be viewed as a decoupled dynamics with two independent control inputs. Since the rotor thrust T_i is proportional to the square of the rotation speed Ω_i, *i.e.*, $T_i = k_i\Omega_i^2$, with k_i as a positive constant, then $T_i \geqslant 0$. Therefore, after the complete loss of a single rotor, the angular moments $\tau_\theta = L(T_1 - T_2)$ and $\tau_\phi = L(T_3 - T_4)$ are severely affected.

In the occurrence of a failure in the first rotor, it follows that $\tau_\theta(t) = -LT_2 \leqslant 0$, for all $t \geqslant t_{f1}$. Consequently, such a control must be negative. A failure in the second rotor requires a positive control since $\tau_\theta(t) = LT_1 \geqslant 0$, for all $t \geqslant t_{f2}$. In the same way, a failure in the third rotor requires a negative control since $\tau_\phi(t) = -LT_4 \leqslant 0$, for all $t \geqslant t_{f3}$, while a failure in the fourth rotor requires a positive control since $\tau_\phi(t) = LT_3 \geqslant 0$, for all $t \geqslant t_{f4}$. Therefore, such sign constraints must be taken into account for the attitude control design.

Consider the functions

$$f_\phi(\eta_2, \hat{\eta}_\phi, \ddot{\phi}_\star) := -b_\phi\dot{\theta}\dot{\psi} + \frac{a_\phi}{J_x}\dot{\phi} - \hat{\eta}_\phi + \ddot{\phi}_\star,$$
$$f_\theta(\eta_2, \hat{\eta}_\theta, \ddot{\theta}_\star) := -b_\theta\dot{\phi}\dot{\psi} + \frac{a_\theta}{J_y}\dot{\theta} - \hat{\eta}_\theta + \ddot{\theta}_\star.$$

Then, in order to satisfy the sign conditions, τ_ϕ and τ_θ are designed according to Algorithm 1.

Algorithm 3: Pitch and Roll Control Design

Input: $\bar{\tau}_\phi$, $\bar{\tau}_\theta$, f_ϕ, f_θ

Output: τ_ϕ, τ_θ

1: **if** $\gamma_1 = 0$
2: $\quad \tau_\phi = J_x(\bar{\tau}_\phi + f_\phi(\eta_2, \hat{\eta}_3, \ddot{\phi}_\star))$
3: $\quad \tau_\theta = \frac{J_y}{2}(\bar{\tau}_\theta + f_\theta(\eta_2, \hat{\eta}_3, \ddot{\theta}_\star) - |\bar{\tau}_\theta + f_\theta(\eta_2, \hat{\eta}_3, \ddot{\theta}_\star)|)$
4: **elseif** $\gamma_2 = 0$
5: $\quad \tau_\phi = J_x(\bar{\tau}_\phi + f_\phi(\eta_2, \hat{\eta}_3, \ddot{\phi}_\star))$
6: $\quad \tau_\theta = \frac{J_y}{2}(\bar{\tau}_\theta + f_\theta(\eta_2, \hat{\eta}_3, \ddot{\theta}_\star) + |\bar{\tau}_\theta + f_\theta(\eta_2, \hat{\eta}_3, \ddot{\theta}_\star)|)$
7: **elseif** $\gamma_3 = 0$
8: $\quad \tau_\phi = \frac{J_x}{2}(\bar{\tau}_\phi + f_\phi(\eta_2, \hat{\eta}_3, \ddot{\phi}_\star) - |\bar{\tau}_\theta + f_\phi(\eta_2, \hat{\eta}_3, \ddot{\phi}_\star)|)$
9: $\quad \tau_\theta = J_y(\bar{\tau}_\theta + f_\theta(\eta_2, \hat{\eta}_3, \ddot{\theta}_\star))$
10: **elseif** $\gamma_4 = 0$
11: $\quad \tau_\phi = \frac{J_x}{2}(\bar{\tau}_\phi + f_\phi(\eta_2, \hat{\eta}_3, \ddot{\phi}_\star) + |\bar{\tau}_\theta + f_\phi(\eta_2, \hat{\eta}_3, \ddot{\phi}_\star)|)$
12: $\quad \tau_\theta = J_y(\bar{\tau}_\theta + f_\theta(\eta_2, \hat{\eta}_3, \ddot{\theta}_\star))$
13: **end**

Note that the isolation of the failure required in Algorithm 3 is provided by the FD strategy described in Section 3.

The terms $\bar{\tau}_\phi$ and $\bar{\tau}_\theta$ are designed by the CTC [20] given in (17), and a possible selection for the gains is in Table 2. Then, the following result can be established.

Lemma 2 *Let the attitude control signals, given in Algorithm 3, be applied to system (57), and assume that Assumptions 1, 2 and 3 hold. Suppose that the disturbances d_θ and d_ϕ satisfy the following constraints*

$$d_\theta(t) \geqslant \frac{a_\theta}{J_y}\dot{\theta}(t) - b_\theta\dot{\phi}(t)\dot{\psi}(t) + \ddot{\theta}_\star,\ \forall t \geqslant t_{f1}, \tag{69a}$$

$$d_\theta(t) \leqslant \frac{a_\theta}{J_y}\dot{\theta}(t) - b_\theta\dot{\phi}(t)\dot{\psi}(t) + \ddot{\theta}_\star,\ \forall t \geqslant t_{f2}, \tag{69b}$$

$$d_\phi(t) \geqslant \frac{a_\phi}{J_x}\dot{\phi}(t) - b_\theta\dot{\phi}(t)\dot{\psi}(t) + \ddot{\phi}_\star,\ \forall t \geqslant t_{f3}, \tag{69c}$$

$$d_\phi(t) \leqslant \frac{a_\phi}{J_x}\dot{\phi}(t) - b_\phi\dot{\theta}(t)\dot{\psi}(t) + \ddot{\phi}_\star,\ \forall t \geqslant t_{f4}, \tag{69d}$$

for a particular rotor failure. Then, at steady state $(\bar{e}_\eta, \bar{\varepsilon}_\eta) = 0$, the system (65c)-(65d) is UFTS.

The proof of Lemma 2 is postponed to the Appendix.

The constraints (69) characterize the set of admissible disturbances and desired trajectories that the quad–rotor can tolerate, under the effect of a rotor failure, in order to ensure that the thrusts on the rotors are always positive. In order to verify such constraints, the information of the finite–time disturbance estimation, given by $\hat{\eta}_3$ in (64b), is used. For the fault–free case, τ_ϕ and τ_θ are designed according to lines 2 and 9 of Algorithm 3, *i.e.*, as in [2].

As mentioned in Lemma 2, the attitude tracking error dynamics strictly depends on the constraints given in (69). Such constraints depend on both, the desired trajectory and the magnitude of the disturbance. Disturbances are intrinsically unknown and it is

not possible to manipulate them for convenience. However, the theoretically established bounds, given in (69), can be manipulated by changing the desired trajectory. For illustration purpose, consider the following example.

Example 1. *Consider that the first rotor has failed; a tracking task given by* $x_d = y_d = 0$ *and* $z_d = 1$*; and assume the disturbances are such that* $d_\xi = 0$, $d_\phi \in \mathcal{L}_{D_4}$, $d_\theta \geqslant 0$ *and* $d_\psi \in \mathcal{L}_{D_6}$.

Then, since the position tracking error is UES*, based on* (68)*, it follows that*

$$\lim_{t\to\infty} \nu_x(t) = \lim_{t\to\infty} \nu_y(t) = \lim_{t\to\infty} \nu_z(t) = 0,$$

and based on (67)*, one obtains*

$$\lim_{t\to\infty} \phi_\star(t) = \lim_{t\to\infty} \theta_\star(t) = \lim_{t\to\infty} \dot{\phi}_\star(t) = \lim_{t\to\infty} \dot{\theta}_\star(t) = 0.$$

Thus, due to the fact that the attitude error dynamics is UFTS*, the constraint* (69a) *is equivalent to*

$$d_\theta(t) \geqslant \frac{a_\theta}{J_y}\dot{\theta}_\star(t) - b_\theta\dot{\phi}_\star(t)\dot{\psi} + \ddot{\theta}_\star(t) = 0.$$

Therefore, (69a) *holds if and only if* $d_\theta(t) \geqslant 0$*. This example perfectly illustrates the fact that constraints* (69) *could be manipulated by means of the desired trajectory in order to ensure its fulfillment.*

It is possible to apply different HOSMCs for the design of the angular moments $\bar{\tau}_\phi$ and $\bar{\tau}_\theta$, as it was described in Section 2, such as the STSMC, the NTSNC, or some HOSMC based on discontinuous integral action (see, *e.g.*, [90], and [91]).

5.3.3 *Virtual Control Disturbance Term*

According to Lemma 1, it is given that the dynamics for e_ξ and ε_ξ is ISS with respect to w_ξ. Now, let us recall that such a disturbance term can be written as

$$w_\xi(\eta_1, u, \nu) = \frac{u_z}{m}\left[\begin{pmatrix} c\phi s\theta c\psi + s\phi s\psi \\ c\phi s\theta s\psi - s\phi c\psi \\ c\phi c\theta \end{pmatrix} - \begin{pmatrix} c\phi_\star s\theta_\star c\psi + s\phi_\star s\psi \\ c\phi_\star s\theta_\star s\psi - s\phi_\star c\psi \\ c\phi_\star c\theta_\star \end{pmatrix}\right].$$

Such a function is Lipschitz in η_1 and continuous in u_z, then it follows that $\|w_\xi\| \leqslant L_w\|\bar{e}_\eta\|$, for all $\eta_1, \nu \in \mathbb{R}^3$ and $u_z \in \mathbb{R}$, for some positive $L_w > 0$. Then, as a result of Lemma 2, it follows that $\bar{e}_\eta(t) = 0$, for all $t \geqslant \mathcal{T}_\eta > 0$. Therefore, the disturbance term w_ξ vanishes when $\bar{e}_\eta = 0$. Moreover, the previous statement implies that $(e_\xi, \varepsilon_\xi) = 0$ will be UES.

5.3.4 *Yaw Dynamics*

The yaw dynamics, which cannot be controlled in the occurrence of a rotor failure due to the linear dependence of τ_ψ with respect to u_z, τ_ϕ and τ_θ, as shown in (61) and (62); is given by

$$\ddot{\psi} = \frac{\tau_\psi}{J_z} + b_\psi\dot{\phi}\dot{\theta} - \frac{a_\psi}{J_z}\dot{\psi} + d_\psi. \tag{70}$$

Based on the results given by Theorem 7 and Lemmas 1 and 2, the angular velocities $\dot{\phi}$ and $\dot{\theta}$, the desired angular accelerations $\ddot{\phi}_\star$ and $\ddot{\theta}_\star$, as well as the disturbance identification $\hat{\eta}_3$, are bounded, *i.e.*, $\|\dot{\phi}\|_\infty \leqslant \delta_\phi$, $\|\dot{\theta}\|_\infty \leqslant \delta_\theta$, $\|\ddot{\phi}_\star\|_\infty \leqslant \delta_{\phi\star}$, $\|\ddot{\theta}_\star\|_\infty \leqslant \delta_{\theta\star}$, $\|\hat{\eta}_\phi\|_\infty \leqslant D_4$ and $\|\hat{\eta}_\theta\|_\infty \leqslant D_5$, with positive constants δ_ϕ, δ_θ, $\delta_{\phi\star}$, $\delta_{\theta\star}$, D_4 and D_5. Furthermore, at steady state $(e_\xi, \varepsilon_\xi) = 0$, the virtual control inputs satisfy $\nu_x = a_x\dot{x} - \hat{\xi}_x + \ddot{x}_d$, $\nu_y = a_y\dot{y} - \hat{\xi}_y + \ddot{y}_d$ and $\nu_z = a_z\dot{z} - \hat{\xi}_z + \ddot{z}_d$, which are bounded, and therefore

$$\lim_{t\to\infty} \sqrt{\nu_x^2(t) + \nu_y^2(t) + (\nu_z(t) + g)^2} \leqslant L_\nu,$$

with a positive constant L_ν. Consider the following expressions

$$L_{\psi 1} = b_\psi \delta_\phi \delta_\theta + D_6 + \frac{mK_\tau}{J_z} L_\nu + \frac{2K_\tau}{LJ_z}(a_\theta \delta_\theta + J_y(D_5 + \delta_{\theta\star})),$$
$$L_{\psi 2} = b_\psi \delta_\phi \delta_\theta + D_6 + \frac{mK_\tau}{J_z} L_\nu + \frac{2K_\tau}{LJ_z}(a_\phi \delta_\phi + J_x(D_4 + \delta_{\phi\star})).$$

Then, let us introduce the following result.

Lemma 3 *Let the position control* (68) *and the attitude control signals given in Algorithm 3 be applied to system* (57)*, and assume that Assumptions 1, 2 and 3 hold. If the angular velocity bounds δ_ϕ and δ_θ satisfy*

$$\|\delta_\phi\|_\infty \leqslant \frac{La_\psi}{2K_\tau J_y b_\theta}, \quad \|\delta_\theta\|_\infty \leqslant< \frac{La_\psi}{2K_\tau J_x b_\phi}, \tag{71}$$

then, after a single rotor failure, the yaw angular velocity satisfies

$$\lim_{t\to\infty} \|\dot{\psi}\|_{fl} \leqslant L_{\psi 1}, \text{ or } \lim_{t\to\infty} \|\dot{\psi}\|_{fk} \leqslant L_{\psi 2}, \tag{72}$$

in the occurrence of a failure in rotors $l = 1, 2$; or in the occurrence of a failure in rotors $k = 3, 4$, respectively.

The proof of Lemma 3 is postponed to the Appendix.

The constraint (71) limits the admissible angular velocities in pitch and roll under the corresponding rotor failure. However, since these bounds for the angular velocities, *i.e.*, δ_ϕ and δ_θ, depend on the desired trajectory, it is possible to ensure the fulfillment of (71). Moreover, since the vehicle does not deal with aggressive maneuvers, the angular velocities in pitch and roll are always bounded.

In this way, based on all the previous statements, the main result is established by the following theorem.

Theorem 8 *Let the expression* (67)*, the position control* (68) *and the attitude control given in Algorithm 3 be applied to system* (57)*. If Assumptions 1, 2, 3 and constraints* (69) *and* (71) *are satisfied; then, after the complete loss of a single rotor, at steady state $(e_\xi, \varepsilon_\xi, \bar{e}_\eta, \bar{\varepsilon}_\eta) = 0$, the system* (65) *is* UES *and the yaw angular velocity is bounded.*

In the following Section some numerical simulations are depicted. It is worth mentioning that comparisons are not provided due to the fact that the literature does not offer FTC schemes that take into account the same rotor failure issues considered in this work.

For instance, in [64] the FTC approach does not consider the presence of disturbances and the gravity center must be shifted. In [67], the proposed FTC only deals with regulations tasks and does not care about disturbances. The proposed FTC given in [69] cannot guarantee the generation of positive thrusts. In this sense, a comparison would be unfair and does not illustrate the advantages of the proposed fault–tolerant controller.

5.4 SIMULATION RESULTS

In order to show the performance and effectiveness of the proposed FTC strategy, numerical simulations using MATLAB/SIMULINK are presented. For more details about the parameters of the model (57), please see Appendix B.

All the simulations consider the failure of the first rotor at $t_{f_1} = 50[s]$. Once the failure has occurred, a fault diagnosis approach helps us to know that the rotor fails, and then, the proposed approach is applied. Initial conditions are given as $\xi_1(0) = \xi_2(0) = \eta_1(0) = \eta_2(0) = 0$, and have been implemented with the Euler's integration method with a sampling method equal to $0.001[s]$.

5.4.1 *Case 1*

The desired trajectory and disturbances are such that the constraints given on Lemma 1 are satisfied.

The desired trajectory is given as

$$x_d(t) = r[\arctan(\varphi) + \arctan(t-\varphi)]\cos(\omega t), \tag{73a}$$
$$y_d(t) = r[\arctan(\varphi) + \arctan(t-\varphi)]\sin(\omega t), \tag{73b}$$
$$z_d(t) = 1.5[1 + \tanh(t-\varphi/2)], \tag{73c}$$

with $r = 0.4[m]$, $\varphi = 15[rad]$ and $\omega = \pi/10[rad/s]$, while the disturbances are given as

$$d_x(t) = 0.2 + 0.1[\sin(\omega_1 t) + \cos(\omega_6 t)], \tag{74a}$$
$$d_y(t) = -0.2 + 0.1[\sin(\omega_5 t) - \cos(\omega_2 t)], \tag{74b}$$
$$d_z(t) = -2 - \sin(\omega_3 t) + \cos(\omega_4 t), \tag{74c}$$
$$d_\phi(t) = -2 - 0.5[\cos(\omega_3 t) + \sin(\omega_6 t)], \tag{74d}$$
$$d_\theta(t) = 3 - 0.5[\sin(\omega_1 t) - \cos(\omega_5 t)], \tag{74e}$$
$$d_\psi(t) = 1.5 + 0.5[\sin(\omega_2 t) + \cos(\omega_4 t)], \tag{74f}$$

where $\omega_1 = 0.2\,[rad/s]$, $\omega_2 = 0.3\,[rad/s]$, $\omega_3 = 0.4\,[rad/s]$, $\omega_4 = 2\,[rad/s]$, $\omega_5 = 3\,[rad/s]$ and $\omega_6 = 4\,[rad/s]$.

The position tracking task is illustrated in Fig. 26 where, despite the failure of the first rotor at $t_{f_1} = 50[s]$, and the presence of disturbances, the quad–rotor tracks the desired trajectory. The pitch, roll and yaw angles, as well as the yaw velocity, are depicted in Fig. 30. The yaw angle ψ, after the occurrence of the failure, begins to increase, while the angular velocity $\dot{\psi}$ is bounded. The disturbance identification for the translational and rotational disturbances are shown in Figs. 27 and 28, respectively. Then, using the information of given by $\hat{\eta}_3$, the disturbance constraint (69a), as well as the angular velocity constraint (71), are shown in Fig. 29. It is easy to see that these constraints hold since there does not exist a crossing between the curves throughout the whole simulation. Finally, the thrusts for each rotor are shown in Fig. 31, where, after the failure of the first rotor, the proposed FTC makes the thrust of rotor 2 near to zero in order to maintain a pitch angle balance due to the loss of the first rotor at $t_{f_1} = 50[s]$, while the thrust on rotors 3 and 4 are increased slightly to achieve the required main thrust.

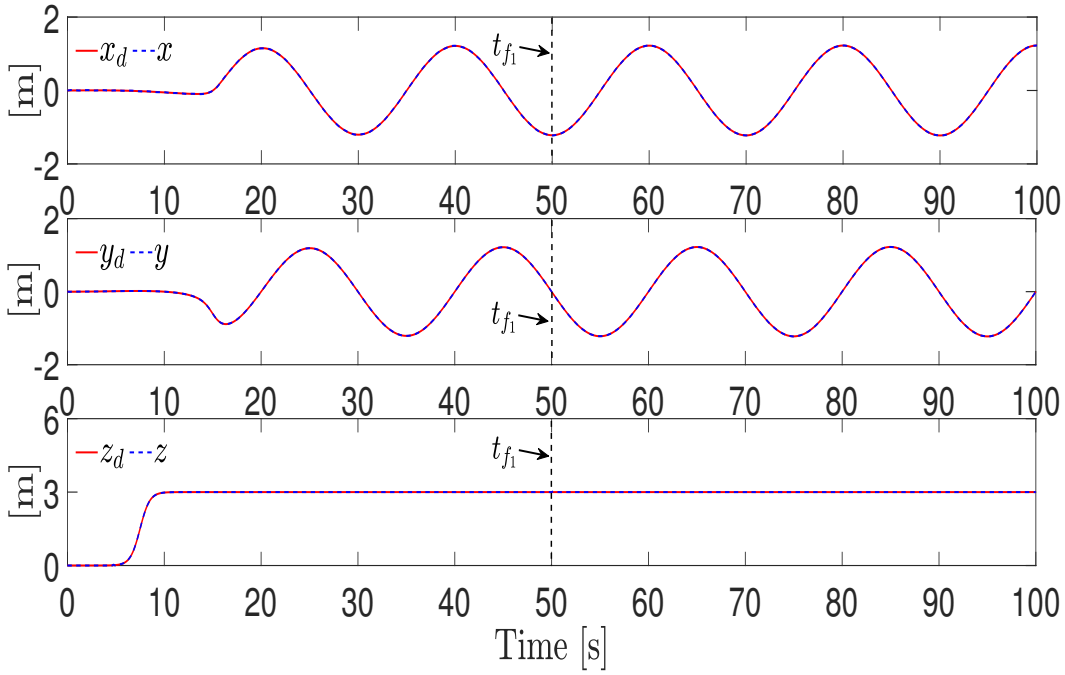

Figure 26: Trajectories of the quad–rotor. Position. Case 1

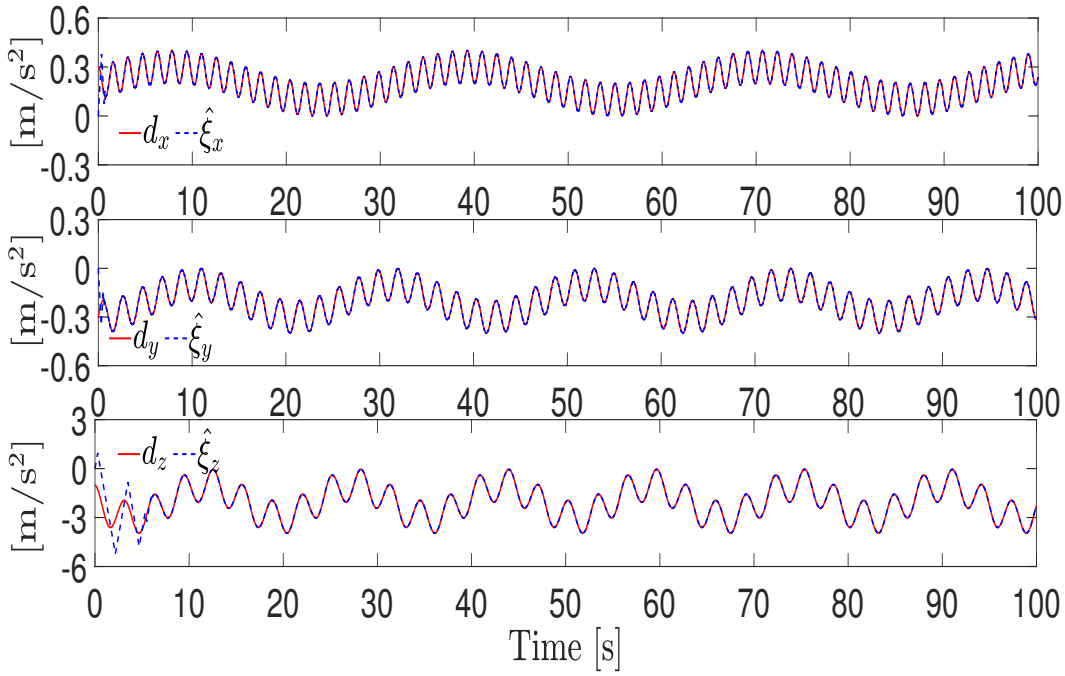

Figure 27: Disturbance identification. Position. Case 1

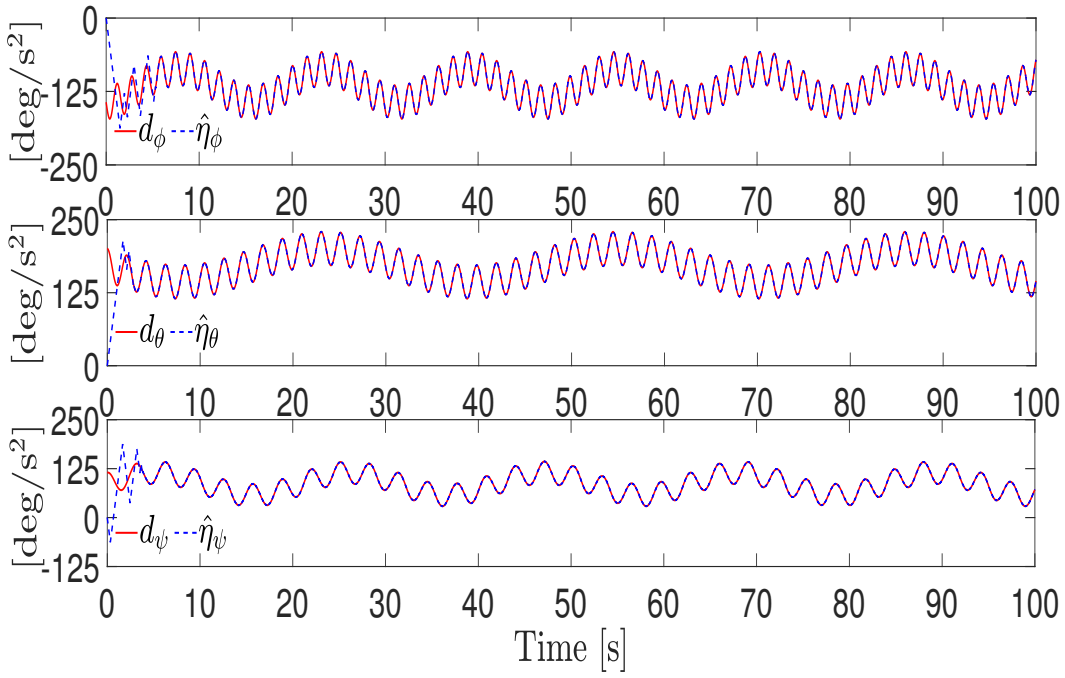

Figure 28: Disturbance identification. Orientation. Case 1

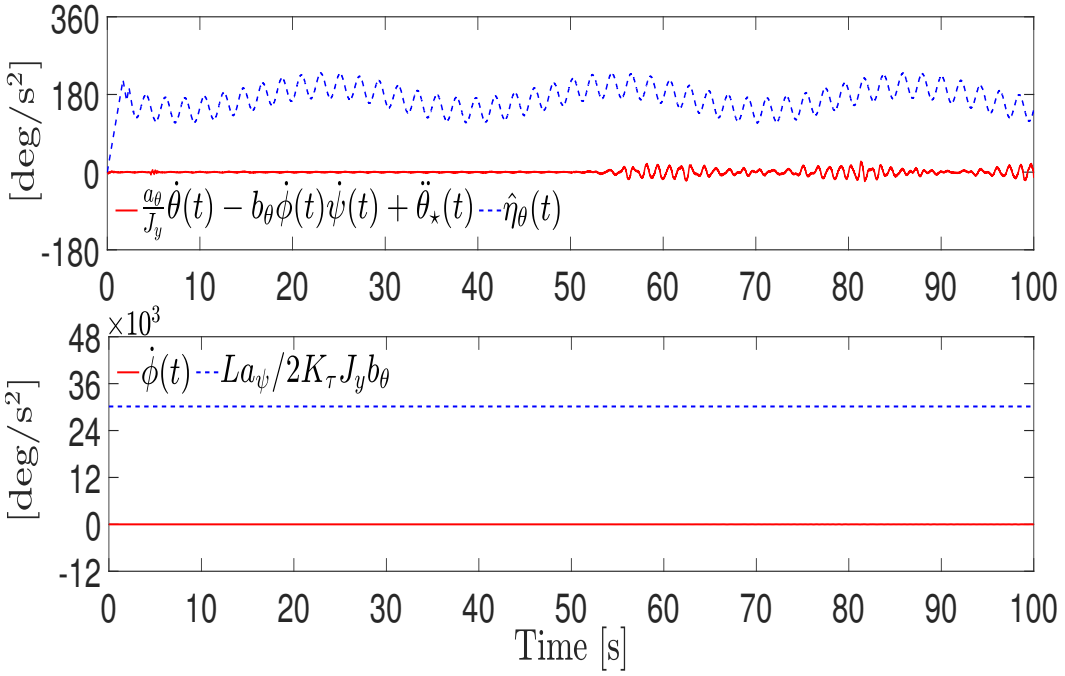

Figure 29: Disturbance and angular velocity constraints. Case 1

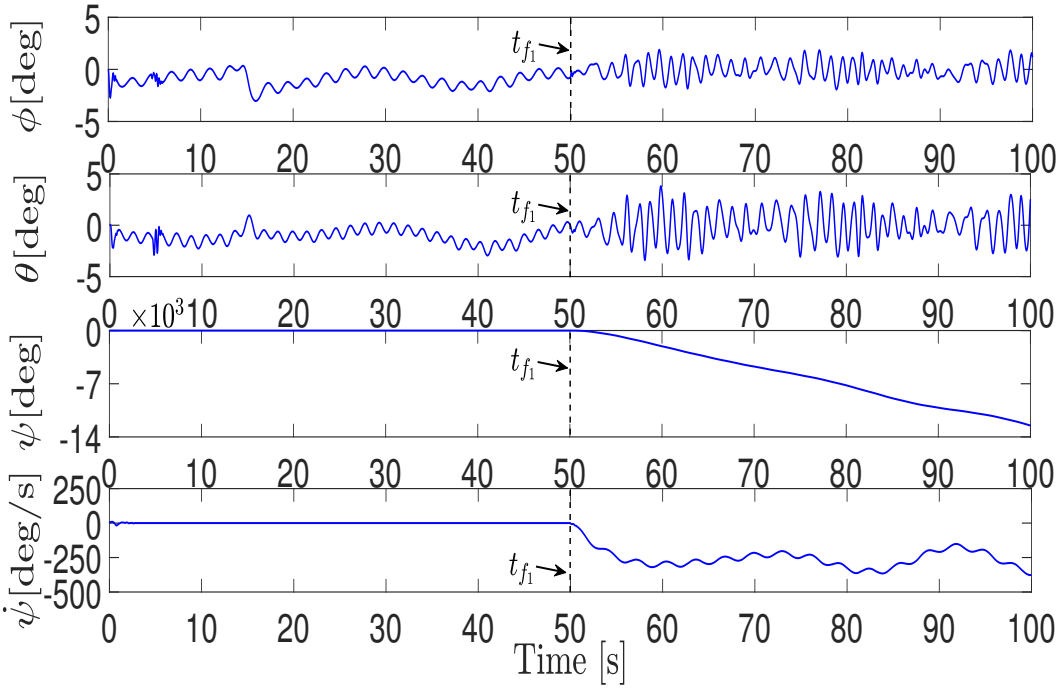

Figure 30: Trajectories of the quad–rotor. Orientation. Case 1

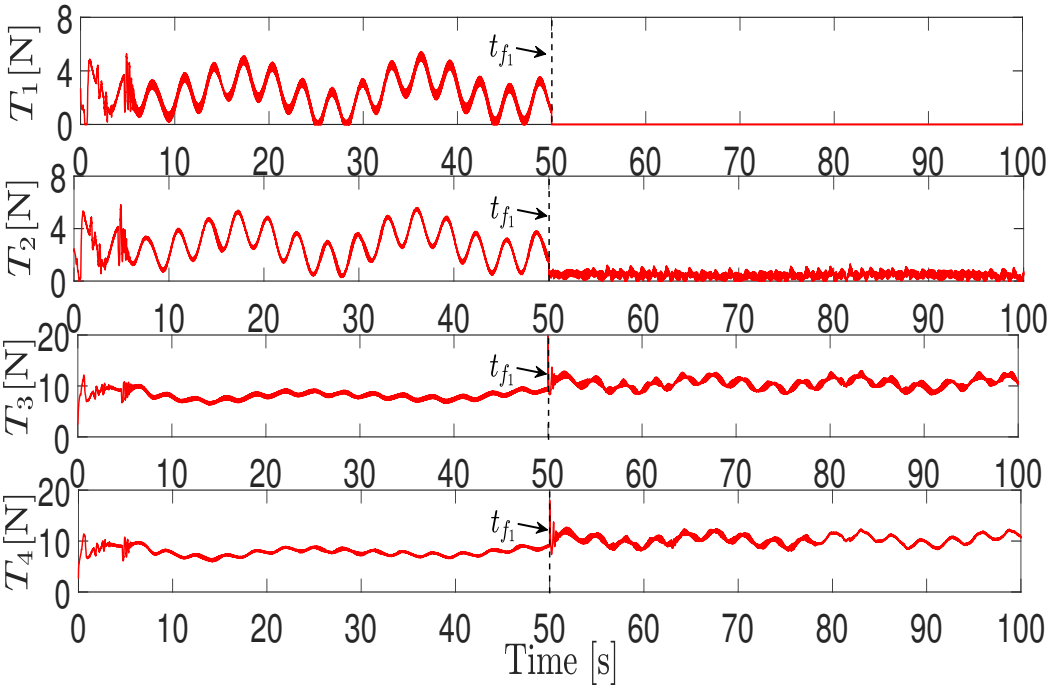

Figure 31: Rotor thrusts. Case 1

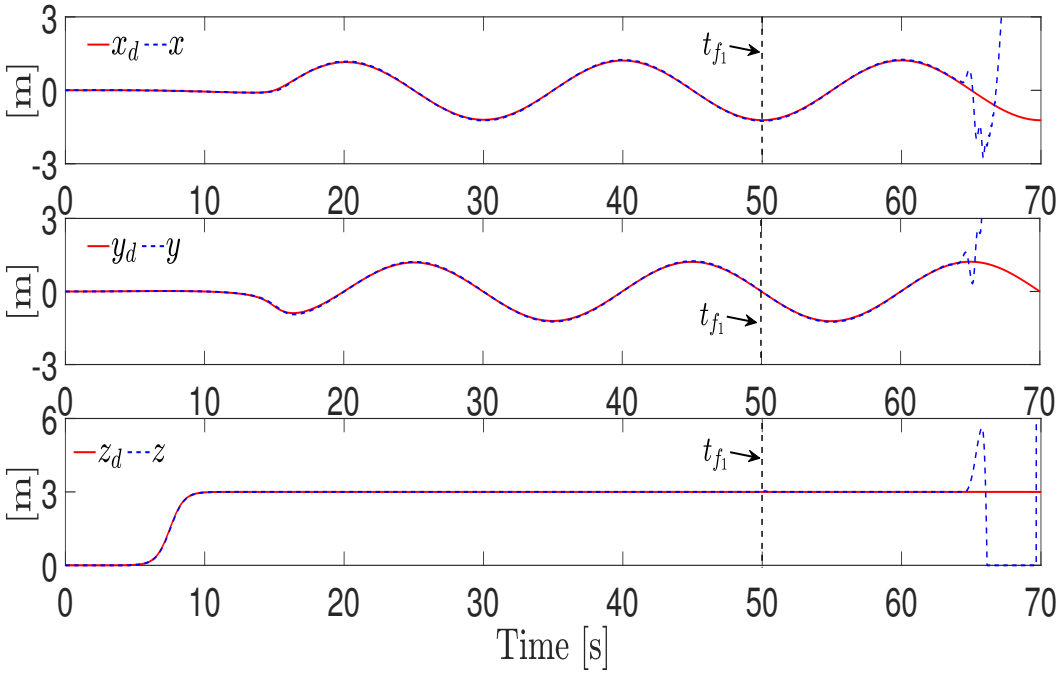

Figure 32: Trajectories of the quad–rotor. Position. Case 2

5.4.2 *Case 2*

The desired trajectory and disturbances are such that the constraints given on Lemma 2 are no longer satisfied.

The desired trajectory is the same than (73), while the disturbances are taken as in (74) but (74e) is given as

$$d_\theta(t) = 2 - 0.5[\sin(\omega_1 t) - \cos(\omega_5 t)]. \tag{75}$$

The position tracking task is illustrated in Fig. 32 where the vehicle stops fulfilling the task around 66.3 [s], losing control a few moments later. The pitch, roll and yaw angles, as well as the yaw velocity, are depicted in Fig. 36. The pitch and roll angles are severely affected, and the angular velocity $\dot{\psi}$ is unbounded in this scenario. The disturbance identification for the translational and rotational disturbances are shown in Figs. 33 and 34, respectively. It is clear that the observer keeps identifying the disturbances throughout the whole simulation. The disturbance constraint (69a) and the angular velocity constraint (71) are shown in Fig. 35. One can see that the disturbance constraint is no longer satisfied after 66.3 [s], while the angular velocity constraint holds throughout the whole simulation. Finally, the thrusts for each rotor are shown in Fig. 37 where, after the failure of the first rotor, the proposed FTC makes the thrust of rotor 2 begins to turn off by time intervals due to the requirement of negative thrusts, while the thrust on rotors 3 and 4 are increased abruptly after loss of control.

5.4.3 *Case 3*

In this case, the same scenario given in Case 2 is performed. Nevertheless, when the failure occurs, the desired trajectory is changed in order to perform an emergency landing, and therefore, rescue the vehicle from a collision.

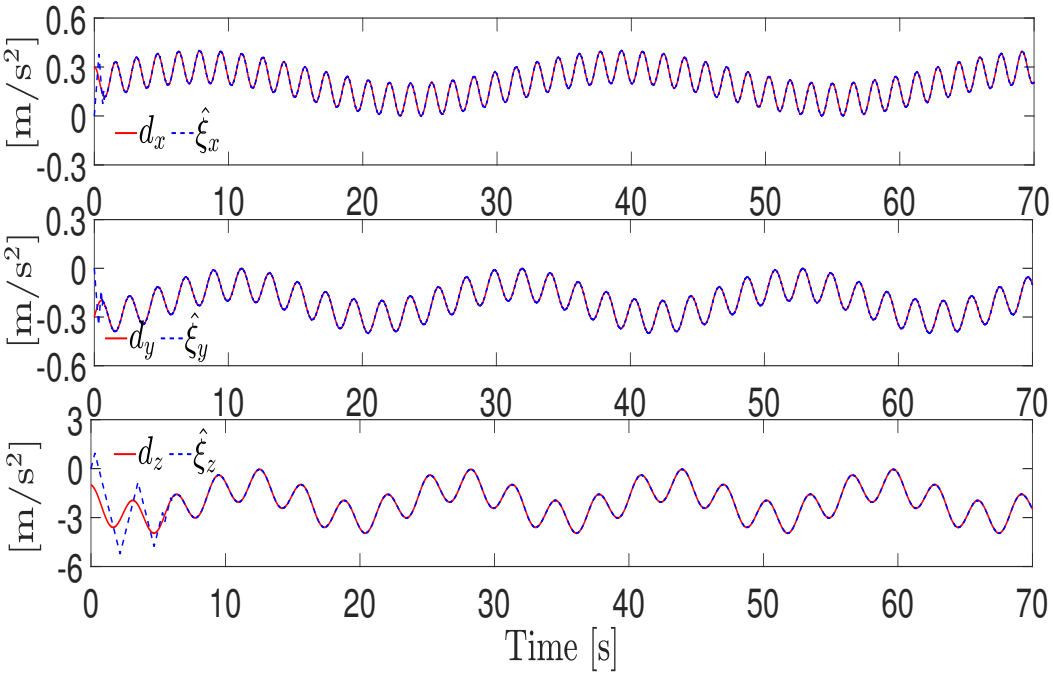

Figure 33: Disturbance identification. Position. Case 2

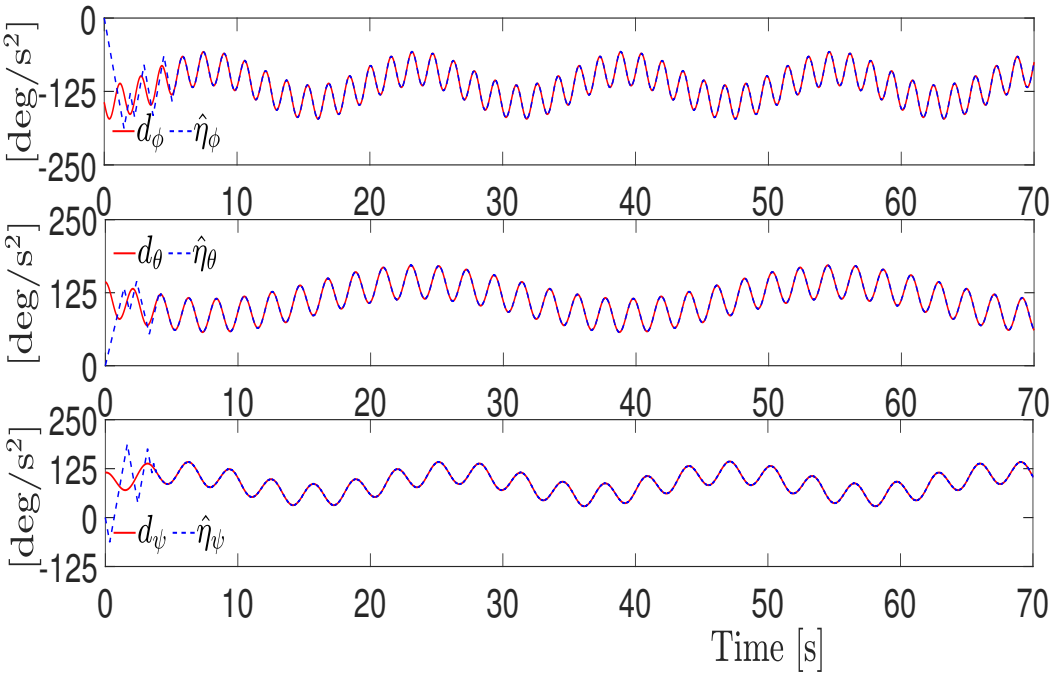

Figure 34: Disturbance identification. Orientation. Case 2

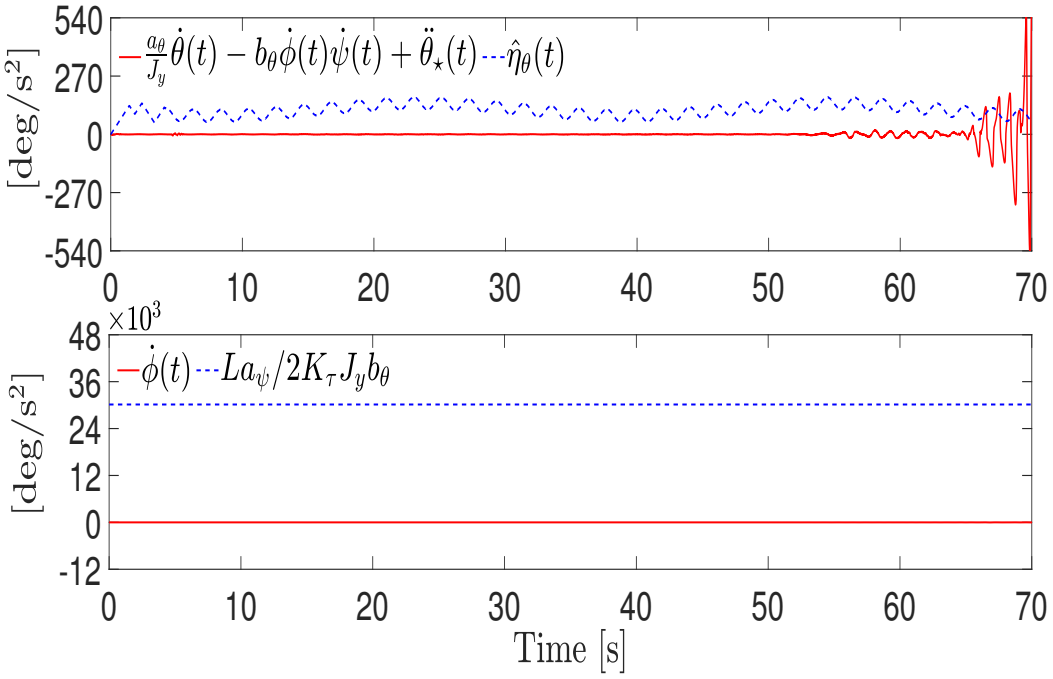

Figure 35: Disturbance and angular velocity constraints. Case 2

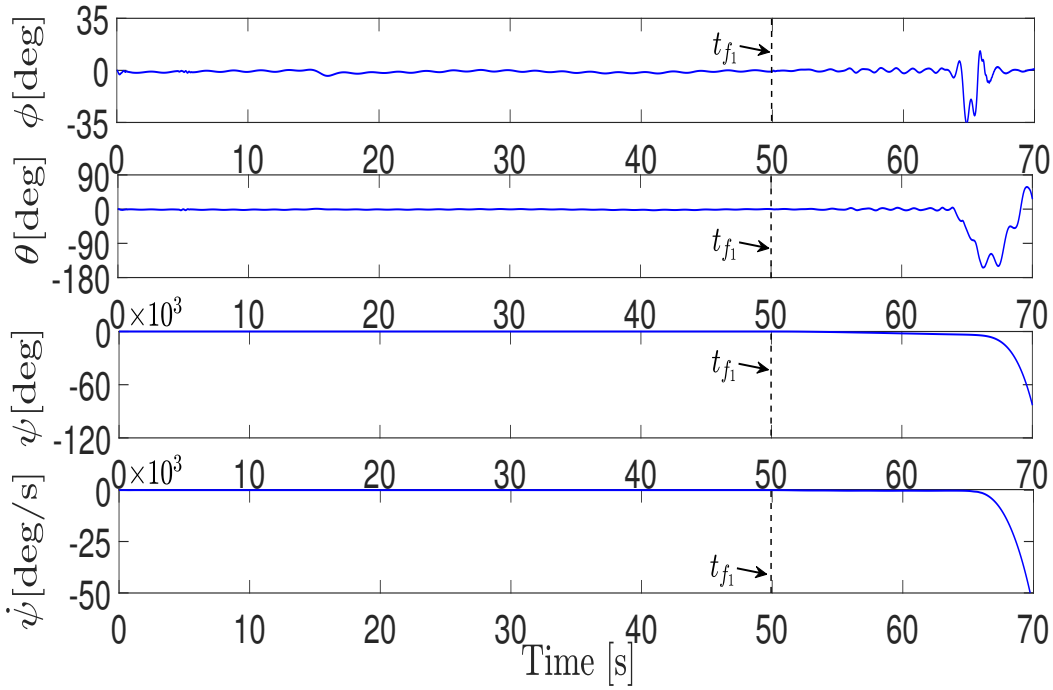

Figure 36: Trajectories of the quad–rotor. Orientation. Case 2

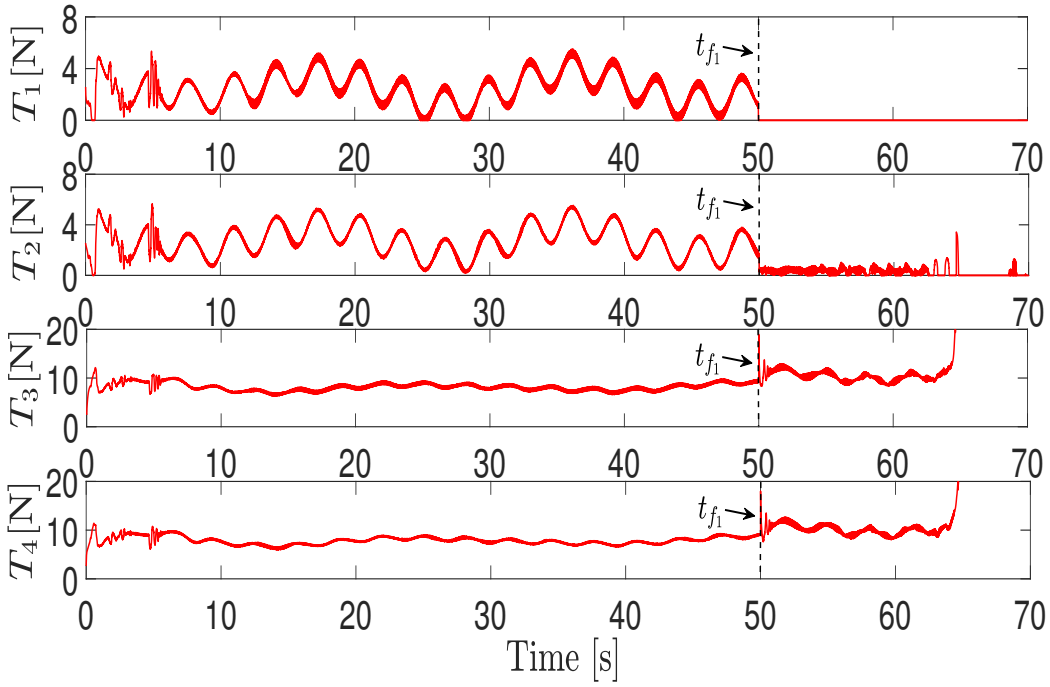

Figure 37: Rotor thrusts. Case 2

The desired trajectory is given as

$$\begin{aligned} x_d(t) &= r[\arctan(\varphi) + \arctan(t-\varphi)]\cos(\omega t)\vartheta(t), \\ y_d(t) &= r[\arctan(\varphi) + \arctan(t-\varphi)]\sin(\omega t)\vartheta(t), \\ z_d(t) &= 1.5[\tanh(t-\varphi/2) - \tanh((t-t_f-40)/3)], \end{aligned}$$

with

$$\vartheta(t) = \begin{cases} 1, & \text{if } t \leqslant t_{f_1}, \\ e^{-0.1(t-t_f)}, & \text{otherwise.} \end{cases}$$

The position tracking task is illustrated in Fig. 38 where, despite the failure of the first rotor at $t_{f_1} = 50$[s], and disturbances, the quad–rotor tracks the desired trajectory and performs an emergency landing. On the other hand, the pitch, roll and yaw angles, as well as the yaw velocity, are depicted in Fig. 42. Similar to Case 1, the yaw angle ψ, after the occurrence of the failure, begins to increase, while the angular velocity $\dot{\psi}$ is bounded. The disturbance identification for the translational and rotational disturbances are shown in Figs. 39 and 40, respectively. Then, using the information given by $\hat{\eta}_3$, the disturbance constraint (69a), as well as the angular velocity constraint (71), are shown in Fig. 41. Compared to Case 2, the disturbance constraint is satisfied throughout the whole simulation. Finally, the thrusts for each rotor are shown in Fig. 43, where, after the failure of the first rotor, the proposed FTC makes the thrust of rotor 2 near to zero in order to maintain a pitch angle balance due to the loss of the first rotor at $t_{f_1} = 50$[s], while the thrust on rotors 3 and 4 are increased slightly to achieve the required main thrust.

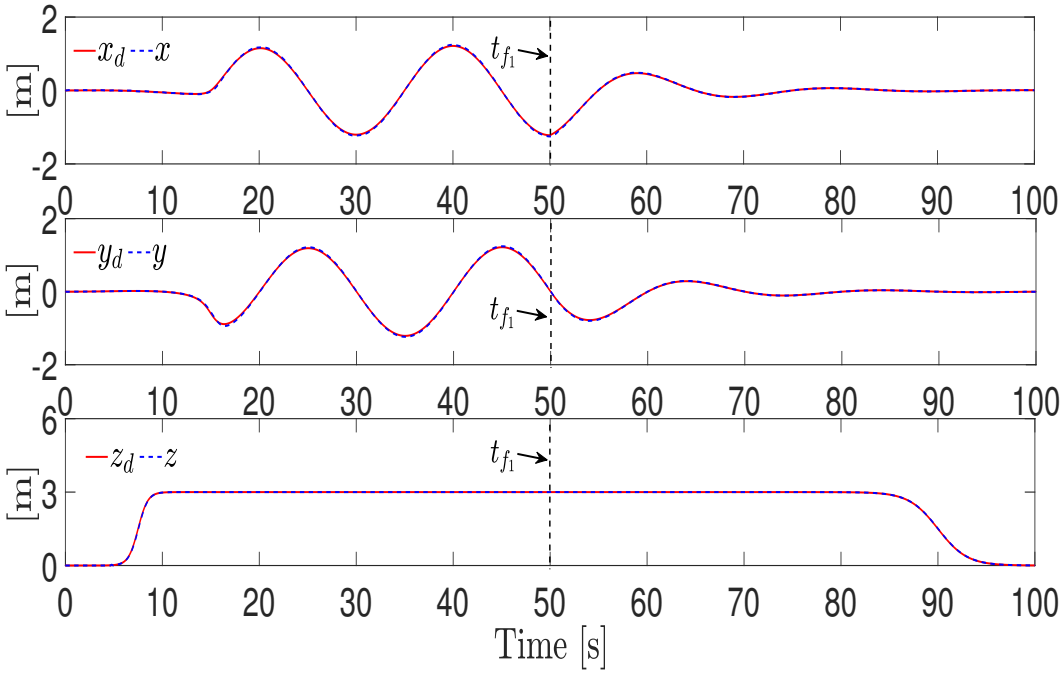

Figure 38: Trajectories of the quad–rotor. Position. Case 3

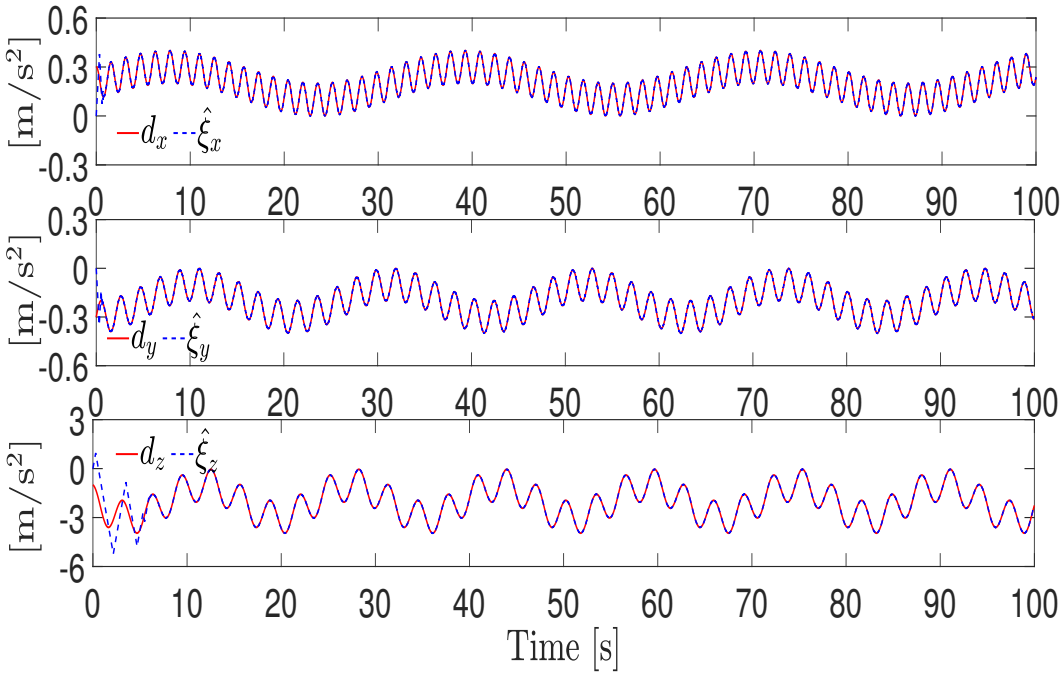

Figure 39: Disturbance identification. Position. Case 3

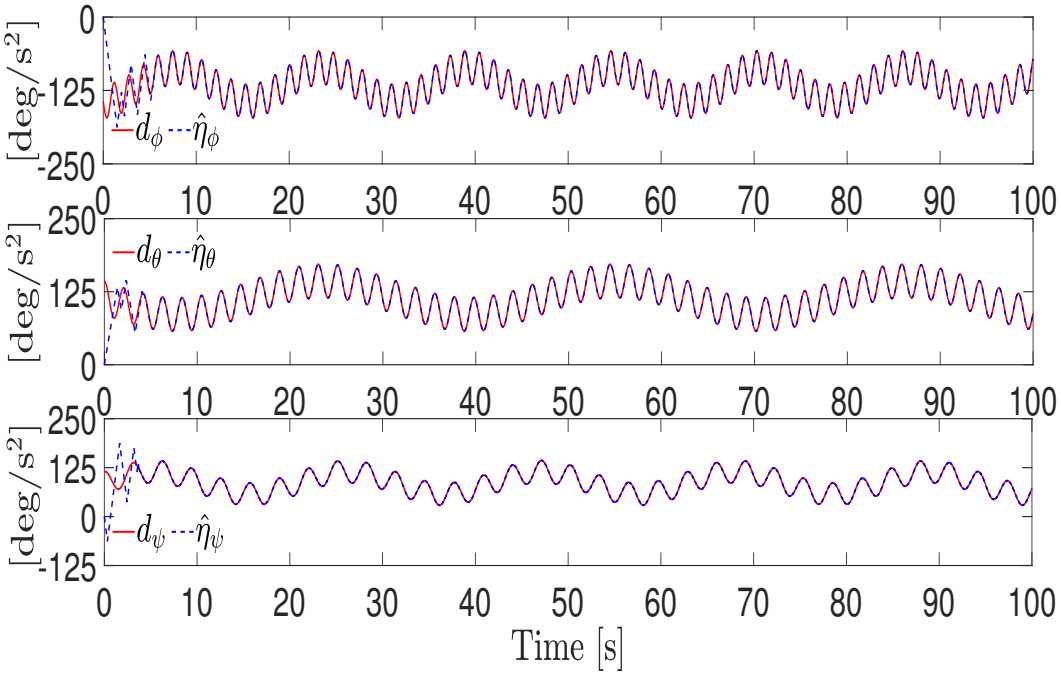

Figure 40: Disturbance identification. Orientation. Case 3

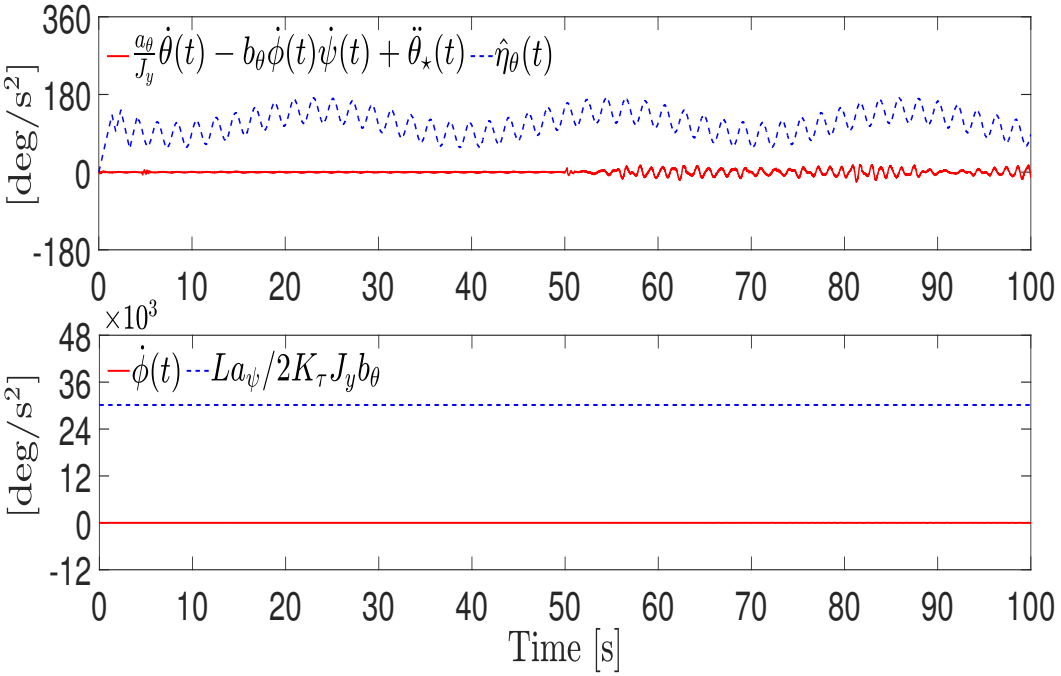

Figure 41: Disturbance and angular velocity constraints. Case 3

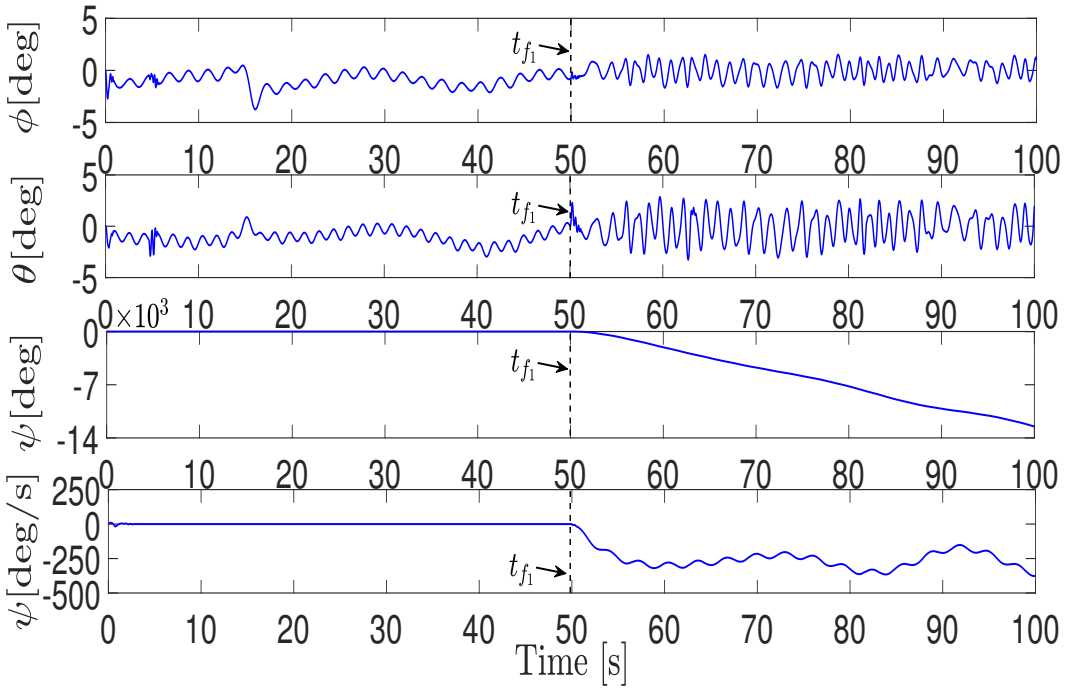

Figure 42: Trajectories of the quad–rotor. Orientation. Case 3

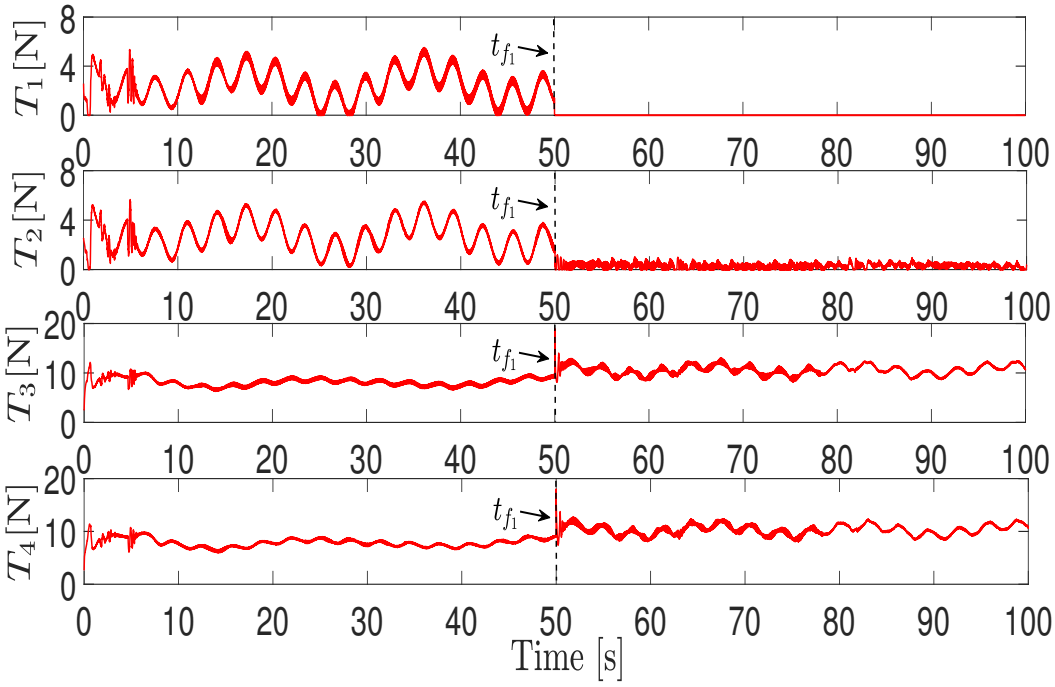

Figure 43: Rotor thrusts. Case 3

6 CONCLUSIONS

This thesis solve the following important problems:

1. Design robust control strategies to robustly track a desired trajectory despite some disturbances.
   Proposed Solution: Robust trajectory tracking control strategies, which are based on different HOSMCs and PID controllers, together with an FT–SMO, as well as an AEM–based controller, together with GSTOs, are proposed. Such strategies allow the tracking error to converge to zero exponentially. Experimental results are presented.

2. Design an FD method to detect, isolate and identify the magnitude of multiple LOEs, despite some disturbances.
   Proposed Solution: An FT–SMO is designed to estimate some state variables and provide fault information through a set of residuals. Based on these residuals, an FD strategy is proposed to achieve the detection, isolation and identification of multiple faults. Experimental results are presented.

3. Design an FTC to achieve the tracking of a desired trajectory under the influence of possible multiple LOEs and disturbances.
   Proposed Solution: An active FTC, that makes use of the proposed FD, is designed based on the actuator fault accommodation methodology. Such a strategy partially compensate the effect of possible multiple LOEs, ensuring the exponential convergence of the position tracking error dynamics to a region of the origin, and the finite–time convergence of the attitude tracking error dynamics to zero. Experimental results are presented.

4. Design an FTC to achieve the tracking of a desired trajectory under the influence of a rotor failure and disturbances.
   Proposed Solution: The rotor failure is isolated using the proposed FD. Then, a combination of an FT–SMO, PID controllers, and HOSMCs is proposed. Such a strategy allows the position tracking error tracking to converge to zero exponentially without breaking physical restrictions. Numerical simulations are presented.

It is worth mentioning that multimedia content regarding the strategies depicted in this thesis can be found in the following link:

https://www.youtube.com/channel/UCp2D3LSvBAkh4tCt_fOE20g

A

APPENDIX – PROOFS OF THE MAIN RESULTS

A.1 PROOF OF PROPOSITION 1

Due to the observer convergence properties, given in Theorem 5, from (38) it is clear that in the absence of faults, *i.e.*, $f \equiv 0$, the residual vector can be rewritten as $\hat{\chi}_3(t) = d(t)$, and it follows that $\|\hat{\chi}_3\|_\infty \leqslant \|D\|$; thus, based on (40), no faults are detected.

During the occurrence of a fault, (38) satisfies $\|\hat{\chi}_3\|_f = \|d - \zeta(\chi_1)Mf\|_f$. Therefore, if (39) holds, (40) is satisfied. This concludes the proof.

A.2 PROOF OF PROPOSITION 2

From (36) and (38) it follows that

$$\hat{\chi}_z(t) = d_z(t) - \frac{c\phi c\theta}{m}(f_1(t) + f_2(t) + f_3(t) + f_4(t)), \tag{76a}$$

$$\hat{\chi}_\theta(t) = d_\theta(t) + J_y^{-1}L(f_2(t) - f_1(t)), \tag{76b}$$

$$\hat{\chi}_\phi(t) = d_\phi(t) + J_x^{-1}L(f_4(t) - f_3(t)), \tag{76c}$$

$$\hat{\chi}_\psi(t) = d_\psi(t) + J_z^{-1}K_\tau(f_3(t) + f_4(t) - f_1(t) - f_2(t)). \tag{76d}$$

for all $t \geqslant \mathcal{T}_1$. Note that the fault in the i–th rotor satisfies $f_i(t) = T_i(t)\gamma_i(t) \geqslant 0$, for all $t \geqslant t_{f_i}$, since the thrust T_i is proportional to the square of the rotation speed Ω_i, *i.e.*, $T_i = k_i\Omega_i^2$, with k_i a positive constant; and the LOE $\gamma_i \in [0, 1)$.

In order to proof that Algorithm 1 isolates faults in rotors 1 and 2, let us suppose the occurrence of a single fault in the rotor 1. Then, (76b) can be rewritten as $\hat{\chi}_\theta(t) = d_\theta(t) - J_y^{-1}Lf_1(t)$, for all $t \geqslant t_{f_1}$. Thus, since f_1 is strongly detectable, (44a) holds; and then, $\|\hat{\chi}_\theta\|_\infty > D_5$, $\hat{\chi}_\theta(t) < 0$ is satisfied, and hence, a fault in rotor 1 is isolated (Algorithm 1 – line 1).

In the occurrence of a single fault in the rotor 2, (76b) can be rewritten as $\hat{\chi}_\theta(t) = d_\theta(t) + J_y^{-1}Lf_2(t)$, for all $t \geqslant t_{f_2}$. Hence, due to the fact that f_2 is strongly detectable, (44b) is satisfied; and then, $\|\hat{\chi}_\theta\|_\infty > D_5$, $\hat{\chi}_\theta(t) > 0$ holds, and hence, a fault in rotor 2 is isolated (Algorithm 1 – line 5).

In the case of simultaneous faults in rotors 1 and 2, consider that $\|f_1\| > \|f_2\|$; then, it follows that $\|\hat{\chi}_\theta\|_\infty > D_5$ and $\hat{\chi}_\theta(t) < 0$, for all $t \geqslant t_{f_1}$, and hence, a fault in rotor 1 is isolated (Algorithm 1 – line 1). Moreover, solving for f_2 from (76), it is given that

$$f_2(t) = \frac{d_z(t) - \hat{\chi}_z(t)}{4m^{-1}c\phi(t)c\theta(t)} + \frac{d_\psi(t) - \hat{\chi}_\psi(t)}{4J_z^{-1}K_\tau} - \frac{d_\theta(t) - \hat{\chi}_\theta(t)}{2J_y^{-1}L}.$$

Since the external perturbations d_z, d_ϕ, d_θ and d_ψ are unknown, it is not possible to provide an exact estimation for f_2. Nevertheless, due to the estimation properties of the FT–SMO, it is possible to give some upper and lower bounds for such external perturbations as in (41). In this sense, the functions given in (42) are proposed to compensate some knowledge of the external perturbations depending on the residuals behavior. In

this way, using (42) to provide an estimation of the external disturbance, one can give an estimation of the magnitude of f_2 by means of ρ_2 in (43b). Therefore, since the fault in the i–th rotor satisfies $f_i(t) \geqslant 0$, if $\rho_2(t) > 0$, for some $t \geqslant t_{f_1}$, a fault in rotor 2 is isolated (Algorithm 1 – line 2).

On the other hand, when $\|f_2\| > \|f_1\|$; then $\|\hat{\chi}_\theta\|_\infty > D_5$ and $\hat{\chi}_\theta(t) > 0$ are satisfied for all $t \geqslant t_{f_2}$, and hence, a fault in rotor 2 is isolated (Algorithm 1 – line 5). Additionally, solving for f_1 from (76), and using (42) to provide an estimation of the disturbances, an estimation of the magnitude of f_1 can be given by means of ρ_1 in (43a). Hence, since the fault in the i–th rotor satisfies $f_i(t) \geqslant 0$, if $\rho_1(t) > 0$ for all $t \geqslant t_{f_2}$, a fault in rotor 1 is isolated (Algorithm 1 – line 6).

Finally, when $\|f_1\| = \|f_2\|$; then $\|\hat{\chi}_\theta\|_\infty \leqslant D_5$ is satisfied for all $t \geqslant \max\{t_{f_1}, t_{f_2}\}$. On the other hand, solving for $f_1 + f_2$ from (76a) and (76d), it is given that

$$f_1(t) + f_2(t) = \frac{d_z(t) - \hat{\chi}_z(t)}{2m^{-1}c\phi(t)c\theta(t)} + \frac{d_\psi(t) - \hat{\chi}_\psi(t)}{2J_z^{-1}K_\tau}. \tag{77}$$

Using (42), we can obtain the estimation of $f_1 + f_2$. However, note that in (76a) and (76d) the 4 faults are involved. Then, in order to determine if there is a fault in rotors 1 and 2, the upper bounds of the disturbances, which affects rotors 1 and 2, are subtracted from (77); such a calculation is given by means of λ_1 in (43e). Hence, if $\|\hat{\chi}_\theta\|_\infty \leqslant D_5$ and $\lambda_1(t) > 0$ for all $t \geqslant 0$, a fault in rotor 1 and 2 are isolated (Algorithm 1 – line 9). Otherwise, the alarms corresponding to rotors 1 and 2 remain deactivated (Algorithm 1 – line 10).

The workability of the Algorithm 2, where faults in rotors 3 and 4 are addressed, can be proved following the same strategy. This concludes the proof.

A.3 PROOF OF PROPOSITION 3

From the identification of the total uncertainty in the system given in (38), *i.e.*, $\hat{\chi}_3(t) = d(t) - \zeta(\chi_1)Mf(t)$, for all $t \geqslant T_1$, one obtains that

$$f(t) = M^{-1}\zeta^{-1}(\chi_1)(d(t) - \Phi(t)). \tag{78}$$

Then, using (42) to estimate the disturbance d, one can provide a fault identification $\hat{f}(t)$ as in (45). Note that the isolation matrix $\mathcal{A}(t)$ prevents from providing a wrong fault identification. The fault estimation error, obtained from (45) and (78), is given as

$$\tilde{f}(t) = f(t) - \hat{f}(t) = M^{-1}\zeta^{-1}(\chi_1)\left(d(t) - \sigma(t)\right). \tag{79}$$

The minimum identification error of the fault in rotor 1 is given by the lower bound:

$$\|I_\theta M^{-1}\zeta^{-1}(\chi_1)\|_{f_1}\left[\|I_\theta D\| - \left\|\begin{pmatrix}\underline{d}_z\\ \underline{d}_\theta\\ \underline{d}_\psi\end{pmatrix}\right\|\right] \leqslant \|f_1 - \hat{f}_1\|_{f_1},$$

while the maximum identification error is determined by the upper bound as $\|f_1 - \hat{f}_1\|_{f_1} \leqslant \|I_\theta M^{-1}\zeta^{-1}(\chi_1)\|_{f_1}\|I_\theta D\|$, which is obtained when it is not possible to compensate some knowledge of the perturbations. The same procedure is followed to obtain the fault estimation error bounds (46b), (46c) and (46d). This concludes the proof.

A.4 PROOF OF THEOREM 6

The attitude tracking error dynamics is given as

$$\begin{aligned}\dot{e}_\eta &= \varepsilon_\eta,\\ \dot{\varepsilon}_\eta &= J\left(\tau - I_\eta M f(t)\right) + \Xi w_\eta(\eta_2) - \Lambda_\eta \eta_2 + d_\eta(t) - \ddot{\eta}_d.\end{aligned}$$

Let us prove that the tracking error dynamics for the roll angle ϕ is UFTS when the controller (54b) is applied. Then, the closed–loop tracking error dynamics for ϕ is given as

$$\dot{e}_\phi = \varepsilon_\phi, \tag{80a}$$

$$\dot{\varepsilon}_\phi = \bar{\nu}_\phi - k_{\phi 1}\lceil e_\phi \rfloor^{\frac{1}{3}} - k_{\phi 2}\lceil \varepsilon_\phi \rfloor^{\frac{1}{2}}, \tag{80b}$$

$$\dot{\bar{\nu}}_\phi = -k_{\phi 3}\lceil e_\phi \rfloor^{0} - k_{\phi 4}\lceil \varepsilon_\phi \rfloor^{0} + \bar{\Delta}_\phi(t), \tag{80c}$$

where $\bar{\nu}_\phi = \nu_\phi - J_x^{-1}L(\tilde{f}_3(t) - \tilde{f}_4(t)) + d_\phi(t)$ and $\bar{\Delta}_\phi(t) = -J_x^{-1}L(\dot{\tilde{f}}_3(t) - \dot{\tilde{f}}_4(t)) + \dot{d}_\phi(t)$. From (79), it is given that $\dot{\tilde{f}}(t) = M^{-1}\zeta^{-1}(\eta_1)\dot{d}(t) + M^{-1}\dot{\zeta}^{-1}(\eta_1)d(t)$, and thus

$$\begin{aligned}\dot{\tilde{f}}_1(t) &= \frac{m}{4c\phi c\theta}\dot{d}_z(t) + \frac{J_z}{4K_\tau}\dot{d}_\psi(t) + \frac{J_y}{2L}\dot{d}_\theta(t) + \rho(t),\\ \dot{\tilde{f}}_2(t) &= \frac{m}{4c\phi c\theta}\dot{d}_z(t) + \frac{J_z}{4K_\tau}\dot{d}_\psi(t) - \frac{J_y}{2L}\dot{d}_\theta(t) + \rho(t),\\ \dot{\tilde{f}}_3(t) &= \frac{m}{4c\phi c\theta}\dot{d}_z(t) - \frac{J_z}{4K_\tau}\dot{d}_\psi(t) + \frac{J_x}{2L}\dot{d}_\phi(t) + \rho(t),\\ \dot{\tilde{f}}_4(t) &= \frac{m}{4c\phi c\theta}\dot{d}_z(t) - \frac{J_z}{4K_\tau}\dot{d}_\psi(t) - \frac{J_x}{2L}\dot{d}_\phi(t) + \rho(t),\end{aligned}$$

where $\rho(t) = m(\dot{\theta}c\phi s\theta + \dot{\phi}s\phi c\theta)d_z(t)/4c^2\phi c^2\theta$. Then, based on the previous equalities, it follows that $\dot{\tilde{f}}_3(t) - \dot{\tilde{f}}_4(t) = J_x L^{-1}\dot{d}_\phi(t)$, and hence, (80c) can be rewritten as $\dot{\bar{\nu}}_\phi = -k_{\phi 3}\lceil e_\phi \rfloor^{0} - k_{\phi 4}\lceil \varepsilon_\phi \rfloor^{0}$. Hence, if the gains are selected as $k_{\phi 1} = 25\varpi^{\frac{2}{3}}$, $k_{\phi 2} = 15\varpi^{\frac{1}{2}}$, $k_{\phi 3} = 2.3\varpi$ and $k_{\phi 4} = 1.1\varpi$ with any $\varpi > 0$; then, according to [20], the finite–time convergence to zero is ensured for the tracking error dynamics (80). The same procedure can be follow to prove the finite–time convergence to zero for the tracking error dynamics of pitch and yaw angles, *i.e.*, $(e_\eta; \varepsilon_\eta) = 0$ is UFTS.

Then, the position tracking error dynamics, taking into account the virtual control (54a), is given as

$$\dot{\epsilon}_\xi = A_k \epsilon_\xi + B\left[d_\xi(t) - \frac{g_\xi(\eta_1)}{m}\sum_{i=1}^{4}\tilde{f}_i(t) + w_\xi(\eta_1, u_z, \nu)\right], \tag{81}$$

$$A = \begin{pmatrix} 0_{6\times 3} & I_6 \\ 0_3 & 0_{3\times 6}\end{pmatrix}, \qquad B = \begin{pmatrix} 0_{6\times 3} \\ I_3\end{pmatrix},$$

where $A_k := A + BK_\xi \in \mathbb{R}^{9\times 9}$, $\epsilon_\xi := (\bar{e}_\xi^T, e_\xi^T, \varepsilon_\xi^T) \in \mathbb{R}^9$ and $K_\xi = (\mathbf{1}K_{i\xi}, \mathbf{1}K_{p\xi}, \mathbf{1}K_{d\xi}) \in \mathbb{R}^{1\times 9}$, with $\mathbf{1} := (1,1,1) \in \mathbb{R}^{1\times 3}$. The nonlinear decoupling term $w_\xi = u_m g_\xi(\eta_1) - G - \nu$ is Lipschitz in η_1 and continuous in u_m, then it follows that $\|w_\xi\|_\infty \leqslant L_\eta \|e_\eta\|_\infty$, for all $\eta_1, \nu \in \mathbb{R}^3$ and $u_m \in \mathbb{R}$, for some positive $L_\eta > 0$. This implies that w_ξ vanishes when

$e_\eta = 0$. Hence, the closed–loop tracking error dynamics (81), considering $w_\xi \equiv 0$, can be rewritten as

$$\dot{\epsilon}_\xi = A_k \epsilon_\xi + B \left[d_\xi(t) - \frac{g_\xi(\eta_1)}{m} \sum_{i=1}^{4} \tilde{f}_i(t) \right]. \tag{82}$$

Let us propose a candidate Lyapunov function $V \in \mathbb{R}^9 \to \mathbb{R}$ as $V(\epsilon_\xi) = \epsilon_\xi^T P \epsilon_\xi$, with $P = P^T > 0 \in \mathbb{R}^{9\times 9}$. The time derivative of V, along the trajectories of the system (82), satisfies

$$\dot{V}(\epsilon_\xi) = \epsilon_\xi^T (PA_k + A_k^T P)\epsilon_\xi + 2\epsilon_\xi^T PB \left[d_\xi(t) - \frac{g_\xi(\eta_1)}{m} \sum_{i=1}^{4} \tilde{f}_i(t) \right].$$

Since the pair (A, B) is controllable, there always exists K_ξ such that A_k is Hurwitz; and thus, it holds that $PA_k + A_k^T P = -Q$, with $Q = Q^T > 0 \in \mathbb{R}^{9\times 9}$. Then, the time derivative of V is upper bounded as

$$\begin{aligned} &\dot{V}(\epsilon_\xi) \leqslant -(1-\mu)\lambda_{\min}\{Q\}\|\epsilon_\xi\|^2, \\ &\forall \|\epsilon_\xi\| \geqslant \frac{2\lambda_{\max}\{P\}}{\mu\lambda_{\min}\{Q\}} \left(\|d_\xi\|_\infty + \frac{1}{m} \sum_{i=1}^{4} \|\tilde{f}_i\|_\infty \right), \end{aligned}$$

for any $\mu \in (0, 1)$. Then, the position tracking error dynamics is ISS with respect to d_ξ and $\tilde{f}$.

A.5 PROOF OF LEMMA 2

The convergence to zero of the attitude tracking error dynamics, when the CTC is active (Algorithm 3 – lines 2, 5, 9 and 12), is given in [2]. Then, only the convergence to zero of the attitude tracking error dynamics, when the positive (Algorithm 3 – lines 6 and 11) and negative controllers (Algorithm 3 – lines 3 and 8) are active, will be proven.

Let us assume that the rotor 1 has failed. Then, according to Algorithm 3 – line 3, the angular moment τ_θ must be negative, and thus, it is designed as

$$\tau_\theta = \frac{J_y}{2}(\bar{\tau}_\theta + f_\theta(\eta_2, \hat{\eta}_\theta, \ddot{\theta}_\star) - |\bar{\tau}_\theta + f_\theta(\eta_2, \hat{\eta}_\theta, \ddot{\theta}_\star)|), \tag{83}$$

where $f_\theta(\eta_2, \hat{\eta}_\theta, \ddot{\theta}_\star) = -b_\theta \dot{\phi}\dot{\psi} + \frac{a_\theta}{J_y}\dot{\theta} - \hat{\eta}_\theta + \ddot{\theta}_\star$. Note that if $\bar{\tau}_\theta + f_\theta(\eta_2, \hat{\eta}_\theta, \ddot{\theta}_\star) \leqslant 0$, the angular moment τ_θ given in (83) is rewritten as $\tau_\theta = J_y(\bar{\tau}_\theta + f_\theta(\eta_2, \hat{\eta}_\theta, \ddot{\theta}_\star))$, where the CTC is active, just as in Algorithm 3 – lines 9 and 12. On the other hand, if $\bar{\tau}_\theta + f_\theta(\eta_2, \hat{\eta}_\theta, \ddot{\theta}_\star) > 0$, the control signal (83) is given by $\tau_\theta = 0$, where the control effort is null, in order to avoid negative thrusts.

The closed–loop tracking error dynamics for θ, taking into account (83), is written as

$$\begin{aligned} \dot{e}_\theta &= \varepsilon_\theta, \\ \dot{\varepsilon}_\theta &= \frac{\bar{\tau}_\theta + f_\theta(\eta_2, \hat{\eta}_\theta, \ddot{\theta}_\star) - |\bar{\tau}_\theta + f_\theta(\eta_2, \hat{\eta}_\theta, \ddot{\theta}_\star)|}{2} - f_\theta(\eta_2, \hat{\eta}_\theta, \ddot{\theta}_\star). \end{aligned}$$

Such a dynamics can be viewed as a state–dependent switched system where the switching surface is given by $\mathcal{S} := \{(\bar{\tau}_\theta, \eta_2, \hat{\eta}_\theta, \ddot{\theta}_\star) \in \mathbb{R} \times \mathbb{R}^2 \times \mathbb{R} \times \mathbb{R}^2 : \bar{\tau}_\theta + f_\theta(\eta_2, \hat{\eta}_\theta, \ddot{\theta}_\star) = 0\}$, *i.e.*,

$$\dot{e}_\theta = \varepsilon_\theta, \tag{84a}$$
$$\dot{\varepsilon}_\theta = g_{\sigma(t)}(\bar{\tau}_\theta, \eta_2, \hat{\eta}_\theta, \ddot{\theta}_\star), \tag{84b}$$
$$\sigma(t) = \begin{cases} 1, & \text{if } f_\theta(\eta_2, \hat{\eta}_\theta, \ddot{\theta}_\star) \leqslant -\bar{\tau}_\theta, \\ 2, & \text{if } f_\theta(\eta_2, \hat{\eta}_\theta, \ddot{\theta}_\star) > -\bar{\tau}_\theta, \end{cases} \tag{84c}$$

where $g_1(\bar{\tau}_\theta, \eta_2, \hat{\eta}_\theta, \ddot{\theta}_\star) = \bar{\tau}_\theta$ and $g_2(\bar{\tau}_\theta, \eta_2, \hat{\eta}_\theta, \ddot{\theta}_\star) = b_\theta \dot{\phi}\dot{\psi} - \frac{a_\theta}{J_y}\dot{\theta} + \hat{\eta}_\theta - \ddot{\theta}_\star$. In order to provide the convergence properties of the tracking error dynamics (84), the analysis is carried out for each operating mode, *i.e.*, for $\sigma = 1, 2$.

1) Case $\sigma = 1$: In this case it holds that $f_\theta(\eta_2, \hat{\eta}_\theta, \ddot{\theta}_\star) \leqslant -\bar{\tau}_\theta$, implying that $g_1(\bar{\tau}_\theta, \eta_2, \hat{\eta}_\theta, \ddot{\theta}_\star) = \bar{\tau}_\theta$, and the tracking error dynamics (84) is rewritten as

$$\dot{e}_\theta = \varepsilon_\theta, \tag{85a}$$
$$\dot{\varepsilon}_\theta = \nu_\theta - k_{\theta 0} \lceil e_\theta \rfloor^{\frac{1}{3}} - k_{\theta 1} \lceil \varepsilon_\theta \rfloor^{\frac{1}{2}}, \tag{85b}$$
$$\dot{\nu}_\theta = -k_{\theta 2} \lceil e_\theta \rfloor^{0} - k_{\theta 3} \lceil \varepsilon_\theta \rfloor^{0}. \tag{85c}$$

Then, at steady state $(e_\theta, \varepsilon_\theta, \nu_\theta) = 0$, according to [20], the system (85) is UFTS. Thus, it follows that $\bar{\tau}_\theta(t) = \nu_\theta - k_{\theta 0} \lceil e_\theta \rfloor^{\frac{1}{3}} - k_{\theta 1} \lceil \varepsilon_\theta \rfloor^{\frac{1}{2}} = 0$, for all $t \geqslant T_\theta$; and hence, the switching condition turns into $f_\theta(\eta_2, \hat{\eta}_\theta, \ddot{\theta}_\star) \leqslant 0$, implying that (83) is rewritten as

$$\tau_\theta = J_y f_\theta(\eta_2, \hat{\eta}_\theta, \ddot{\theta}_\star) = J_y(-b_\theta \dot{\phi}\dot{\psi} + \frac{a_\theta}{J_y}\dot{\theta} - \hat{\eta}_\theta + \ddot{\theta}_\star). \tag{86}$$

Since $f_\theta(\eta_2, \hat{\eta}_\theta, \ddot{\theta}_\star) \leqslant 0$, then the control law (86) is negative. Recalling that $\hat{\eta}_\theta(t) = d_\theta(t)$, for all $t \geqslant \mathcal{T}$ with $\mathcal{T} < t_{f1}$, if $\hat{\eta}_\theta(t) = d_\theta(t) \geqslant \frac{a_\theta}{J_y}\dot{\theta}(t) - b_\theta \dot{\phi}(t)\dot{\psi}(t) + \ddot{\theta}_\star(t)$ holds for all $t \geqslant t_{f1}$, *i.e.*, the constraint (69a), then $f_\theta(\eta_2(t), \hat{\eta}_\theta(t), \ddot{\theta}_\star(t)) \leqslant 0$, for all $t \geqslant t_{f1}$; and hence, system (85) never switches to the case $\sigma = 2$, and hence, $(e_\theta, \varepsilon_\theta, \nu_\theta) = 0$ is UFTS.

2) Case $\sigma = 2$: In this case it holds that $f_\theta(\eta_2, \hat{\eta}_\theta, \ddot{\theta}_\star) > -\bar{\tau}_\theta$, implying that $g_2(\bar{\tau}_\theta, \eta_2, \hat{\eta}_\theta, \ddot{\theta}_\star) = b_\theta \dot{\phi}\dot{\psi} - \frac{a_\theta}{J_y}\dot{\theta} + \hat{\eta}_\theta - \ddot{\theta}_\star$, and the tracking error dynamics (84) is rewritten as

$$\dot{e}_\theta = \varepsilon_\theta, \tag{87a}$$
$$\dot{\varepsilon}_\theta = b_\theta \dot{\phi}\dot{\psi} - \frac{a_\theta}{J_y}\dot{\theta} + d_\theta - \ddot{\theta}_\star. \tag{87b}$$

If constraint (69a), *i.e.*, $\hat{\eta}_\theta(t) = d_\theta(t) \geqslant \frac{a_\theta}{J_y}\dot{\theta}(t) - b_\theta \dot{\phi}(t)\dot{\psi}(t) + \ddot{\theta}_\star(t)$, holds for all $t \geqslant t_{f1}$, then it follows that $f_\theta(\eta_2(t), \hat{\eta}_\theta(t), \ddot{\theta}_\star(t)) \leqslant 0$, for all $t \geqslant t_{f1}$. Taking into account that $\varepsilon_\theta = \dot{\theta} - \dot{\theta}_\star$, (87b) can be written as follows

$$\dot{\varepsilon}_\theta = b_\theta \dot{\phi}\dot{\psi} - \frac{a_\theta}{J_y}\dot{\theta}_\star - \frac{a_\theta}{J_y}\varepsilon_\theta + d_\theta.$$

The solution of the previous differential equation is given by

$$\varepsilon_\theta(t) = \varepsilon_\theta(t_{f1}) e^{-\frac{a_\theta}{J_y}(t-t_{f1})} + \int_{t_{f1}}^{t} e^{-\frac{a_\theta}{J_y}(t-\tau)} (b_\theta \dot{\phi}(\tau)\dot{\psi}(\tau) - \frac{a_\theta}{J_y}\dot{\theta}_\star(\tau) + d_\theta(\tau) - \ddot{\theta}_\star(\tau))d\tau.$$

Then, due to the convergence properties of the CTC, the roll angular velocity $\dot{\phi}$ converges to a bounded reference $\dot{\phi}_\star$; the yaw angular velocity $\dot{\psi}$ is bounded, as it will be shown by Lemma 3, and due to Assumption 2, the disturbance d_θ is also bounded. Thus, ε_θ is bounded, and it follows that $\dot{\theta}$ and $\ddot{\theta}_\star$ are bounded, consequently $f_\theta(\eta_2, \hat{\eta}_\theta, \ddot{\theta}_\star) = -b_\theta \dot{\phi}\dot{\psi} + \frac{a_\theta}{J_y}\dot{\theta} - d_\theta(t) + \ddot{\theta}_\star$ is bounded and $f_\theta(\eta_2(t), \hat{\eta}_\theta(t), \ddot{\theta}_\star(t)) \leqslant 0$, for all $t \geqslant t_{f1}$.

Taking into account the previous analysis, and considering the solution of the differential equation given in (87a), *i.e.*,

$$e_\theta = e_\theta(t_{f1}) + \int_{t_{f1}}^{t} \varepsilon_\theta(\tau)d\tau,$$

it is clear that

$$\lim_{t\to\infty} \varepsilon_\theta(t) \geqslant 0 \Rightarrow \lim_{t\to\infty} e_\theta(t) = \infty.$$

Therefore, the previous statements imply that

$$\lim_{t\to\infty} \nu_\theta(t) < 0,$$

and thus

$$\lim_{t\to\infty} \bar{\tau}_\theta(t) = \lim_{t\to\infty} (\nu_\theta - k_{\theta 0} \lceil e_\theta \rfloor^{\frac{1}{3}} - k_{\theta 1} \lceil \varepsilon_\theta \rfloor^{\frac{1}{2}}) = -\infty.$$

Therefore, since $f_\theta(\eta_2(t), \hat{\eta}_\theta(t), \ddot{\theta}_\star(t)) \leqslant 0$ is bounded, and $\bar{\tau}_\theta \to -\infty$, for all $t \geqslant t_{f1}$, there always exists a finite time $t_{\sigma 1}$ such that $f_\theta(\eta_2(t), \hat{\eta}_\theta(t), \ddot{\theta}_\star(t)) \leqslant -\bar{\tau}_\theta(t)$, and hence, system (85) always switches to the case $\sigma = 1$, for which, $(e_\theta, \varepsilon_\theta, \nu_\theta) = 0$ is UFTS.

The previous analysis, together with the fact that $(e_\phi, \varepsilon_\phi) = 0$ is UFTS, implies that, at steady state $(\bar{e}_\eta, \bar{\varepsilon}_\eta) = 0$, the attitude tracking error dynamics is UFTS. The same procedure can be followed to analyze the convergence properties of the Algorithm 3 when other rotors have failed. This concludes the proof.

A.6 PROOF OF LEMMA 3

In this proof, the yaw dynamics is analyzed in the occurrence of a rotor failure. With this aim, the results given by Theorem 7 and Lemmas 1 and 2 are considered; then, it is demonstrated that the yaw angular acceleration can be bounded at steady state. Next, the conditions to ensure the boundedness of the yaw angular velocity are obtained by means of the acceleration upper bound.

Consider the loss of the rotor 1. Then, using (61), the yaw dynamics (70) can be rewritten as

$$\ddot{\psi} = -\frac{K_\tau}{J_z}(u_z + 2\frac{\tau_\theta}{L}) + b_\psi \dot{\phi}\dot{\theta} - \frac{a_\psi}{J_z}\dot{\psi} + d_\psi, \tag{88}$$

and by substituting u_z, given in (67a), one obtains

$$\ddot{\psi} = -\frac{K_\tau}{J_z}(m\sqrt{\nu_x^2 + \nu_y^2 + (\nu_z + g)^2} + 2\frac{\tau_\theta}{L}) + b_\psi \dot{\phi}\dot{\theta} - \frac{a_\psi}{J_z}\dot{\psi} + d_\psi. \tag{89}$$

As it was shown by Lemma 2, at steady state, $\tau_\theta = J_y(-b_\theta\dot{\phi}\dot{\psi} + \frac{a_\theta}{J_y}\dot{\theta} - \hat{\eta}_\theta + \ddot{\theta}_\star)$ as in (86). Then, at steady state, (89) satisfies

$$\ddot{\psi} = -\frac{mK_\tau}{J_z}\sqrt{\nu_x^2 + \nu_y^2 + (\nu_z + g)^2} + b_\psi\dot{\phi}\dot{\theta} - \frac{a_\psi}{J_z}\dot{\psi} + d_\psi - \frac{2K_\tau J_y}{LJ_z}\left(\frac{a_\theta}{J_y}\dot{\theta} - b_\theta\dot{\phi}\dot{\psi} - \hat{\eta}_\theta + \ddot{\theta}_\star\right). \quad (90)$$

Taking into account that the angular velocities and the disturbances are bounded the previous solution satisfies

$$\|\ddot{\psi}\|_{f_1} \leqslant L_{\psi_1} + \left(\frac{2K_\tau J_y b_\theta \delta_\phi}{LJ_z} - \frac{a_\psi}{J_z}\right)\|\dot{\psi}\|, \quad (91)$$

with $L_{\psi_1} = b_\psi\delta_\phi\delta_\theta + D_\psi + \frac{mK_\tau}{J_z}L_\nu + \frac{2K_\tau}{LJ_z}(a_\theta\delta_\theta + J_y(D_\theta + \delta_{\theta\star}))$. Subsequently, the solution satisfies

$$\|\dot{\psi}\|_{f_1} \leqslant \|\dot{\psi}(t_{f_1})\|_{f_1} e^{\left(\frac{2K_\tau J_y}{LJ_z} b_\theta \delta_\phi - \frac{a_\psi}{J_z}\right)(t - t_{f_1})} + L_{\psi 1}\left(1 - e^{\left(\frac{2K_\tau J_y}{LJ_z} b_\theta \delta_\phi - \frac{a_\psi}{J_z}\right)(t - t_{f_1})}\right),$$

for all $t \geqslant t_{f_1}$. Therefore, if (71) holds, *i.e.*, $\|\delta_\phi\|_\infty \leqslant \frac{LJ_z a_\psi}{2K_\tau J_y J_z b_\theta}$, for all $t \geqslant t_{f_1}$, then it is clear that

$$\lim_{t\to\infty} \|\dot{\psi}\|_{f_1} \leqslant L_{\psi 1}.$$

The same result is obtained if the rotor 2 fails and similar conclusions can be obtained considering a failure in the other rotors. This concludes the proof.

B

APPENDIX – EXPERIMENTAL PLATFORM

The QBall2 is a quad–rotor propelled by four brushless motors fitted with 10–inch propellers, it is enclosed within a protective carbon fiber cage. In order to measure on–board sensors and to drive the motors, the QBall2 utilizes an on–board avionics data acquisition card (DAQ) and a wireless Gumstix DuoVero embedded computer, both given by Quanser. This research experimental platform uses a ground control station with the real–time control software QUARC, that generates real–time code directly from MATLAB/Simulink to the on-board computer via WiFi, allowing to configure the system parameters and to observe sensor measurements in real–time (for more details, please see [92]). The QBall2 position and attitude are tracked and accurately measured using an OptiTrack camera system with six synchronized infrared cameras connected to the ground control station. Additionally, the experimental platform is composed of an industrial fan allowing to generate wind gusts (see Fig. 44).

The parameters of the model (1), given by Quanser, are: $m = 1.79[kg]$, $J_x = J_y = 0.03[Ns^2/rad]$, $J_z = 0.04[Ns^2/rad]$, $a_x = a_y = a_z = 0.021[Ns/kgm]$, $a_\phi = a_\theta = 0.009[Ns/rad]$, $a_\psi = 0.012[Ns/rad]$, $L = 0.2$ [m] and $K_\tau = 0.0057$ [Ns/rad^2].

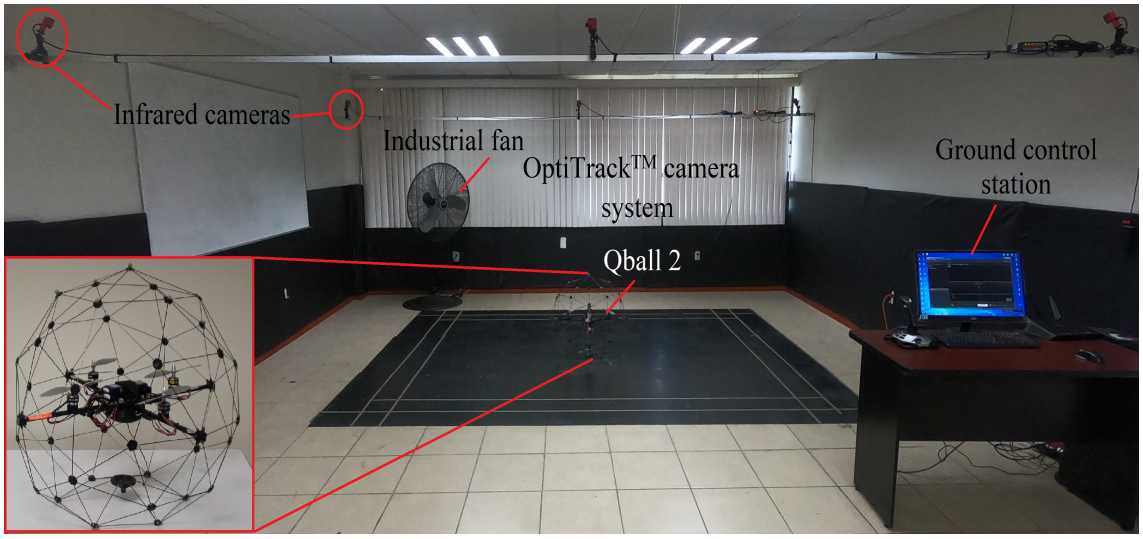

Figure 44: Experimental platform

C

APPENDIX – PUBLICATIONS

INTERNATIONAL JOURNALS

1. H. Ríos, R. Falcón, O. A. González and A. Dzul. "Continuous Sliding–Modes Control Strategies for Quad–Rotor Robust Tracking: Real–Time Application". IEEE Transactions on Industrial Electronics 66 (2019), pp. 1264-1272. [2]

2. R. Falcón, H. Ríos and A. Dzul. "Comparative Analysis of Continuous Sliding–Modes Control Strategies for Quad–Rotor Robust Tracking". Control Engineering Practice 90, 2019, pp. 241-256.[44]

3. R. Falcón, H. Ríos, M. Mera and A. Dzul. "An Attractive Ellipsoid–based Robust Control for Quad–Rotor Tracking". IEEE Transactions on Industrial Electronics 67(9), 2020, pp. 7851-7860. [3]

4. R. Falcón, H. Ríos and A. Dzul. "A Robust Fault Diagnosis for Quad–Rotors: A Sliding–Mode Observer Approach". IEEE/ASME Transactions on Mechatronics, DOI: 10.1109/TMECH.2022.3156854, 2022. [77]

5. R. Falcón, H. Ríos and A. Dzul. "Active Sliding–Mode Fault–Tolerant Control for Robust Tracking in Quad–Rotors under a Rotor Failure". International Journal of Robust and Nonlinear Control, DOI: 10.1002/rnc.6288, 2022. [82]

INTERNATIONAL CONFERENCES

1. R. Falcón, O.A. González, H. Ríos and A. Dzul. "Quad–Rotor Robust Tracking: A Continuous Sliding–Mode Control Strategy". In the 15th International Workshop on Variable Structure Systems and Sliding Mode Control, Austria, 2018, pp. 390-395. [72]

2. R. Falcón, H. Ríos and A. Dzul. "An Actuator Fault Accommodation Sliding–Mode Control Approach for Trajectory Tracking in Quad–Rotors". In the 60th IEEE Conference on Decision and Control, Austin, Texas, USA, 2021, pp. 7100–7105. [79]

NATIONAL CONFERENCES

1. R. Falcón, H. Ríos, M. Mera and A. Dzul. "Output–based Robust Control for Quad–Rotor Tracking: An Attractive Ellipsoid Approach". In the XX Congreso Mexicano de Robótica, 2018, pp. 116-121. [73]

2. H. Castañeda, R. Falcón, A. Dzul and J. L. Gordillo. "Control de Vuelo de un Quad–Rotor Utilizando un Control por Modos Deslizantes Adaptable". In Congreso Nacional de Control Automático 2019, Puebla, México, pp. 85-90 [74]

3. R. Falcón, H. Ríos y A. Dzul. "Diagnóstico de Fallas basado en Observadores por Modos Deslizantes para un Quad–Rotor". In Congreso Nacional de Control Automático 2019, Puebla, México, pp. 495-500. [76]

4. R. Falcón, H. Ríos and A. Dzul. "Control Tolerante a Fallas Activo para un Quad–Rotor ante la Pérdida de un Actuador". In the 27° Congreso Argentino de Control Automático AADECA'20 Virtual, pp. 93-98. [80]

5. R. Falcón, H. Ríos and A. Dzul. "Fault Accommodation Sliding–Mode Control for Quad-–Rotor Tracking Trajectory". In the 2021 Congreso Nacional de Control Automático, Guanajuato, México, pp. 267–272. [78]

6. R. Falcón, H. Ríos and A. Dzul. "Active Fault Tolerant Control for a Quad–Rotor in case of a Rotor Failure". In the XXIII Robotics Mexican Congress, Tijuana, Baja California, México, 2021, pp. 75–80. [81]

7. R. Falcón, H. Ríos and A. Dzul. "A Robust Control Strategy for Target Tracking using a Quad–Rotor". Accepted in the 2022 Congreso Nacional de Control Automático, Chiapas, México. [75]

BIBLIOGRAPHY

[1] I. Palunko, P. Cruz, and R Fierro. "Agile load transportation." In: *IEEE Robotics & Automation Magazine* 19.3 (2012), pp. 69–79.

[2] H. Ríos, R. Falcón, O.A. González, and A. Dzul. "Continuous Sliding-Modes Control Strategies for Quad-Rotor Robust Tracking: Real-Time Application." In: *IEEE Transactions on Industrial Electronics* 66 (2019), pp. 1264–1272.

[3] R. Falcón, H. Ríos, M. Mera, and A Dzul. "Attractive Ellipsoid-Based Robust Control for Quadrotor Tracking." In: *IEEE Transactions on Industrial Electronics* 67.9 (2020), pp. 7851–7860.

[4] Z. T. Dydek, A. M. Annaswamy, and E. Lavretsky. "Adaptive Control of Quadrotor UAVs: A Design Trade Study With Flight Evaluations." In: *IEEE Transactions on Control Systems Technology* 21.4 (2013), pp. 1400–1406. ISSN: 1063-6536.

[5] T.-T. Tran, S. Sam Ge, and W. He. "Adaptive control of a quadrotor aerial vehicle with input constraints and uncertain parameters." In: *International Journal of Control* 91.5 (2018), pp. 1140–1160.

[6] M. A. Mohd Basri, A. R. Husain, and K. A. Danapalasingam. "Enhanced Backstepping Controller Design with Application to Autonomous Quadrotor Unmanned Aerial Vehicle." In: *Journal of Intelligent & Robotic Systems* 79.2 (2014), pp. 295–321.

[7] F. Chen, W. Lei, K. Zhang, G. Tao, and B. Jiang. "A novel nonlinear resilient control for a quadrotor UAV via backstepping control and nonlinear disturbance observer." In: *Nonlinear Dynamics* 85.2 (Apr. 2016), pp. 1281–1295.

[8] P. Castillo, A. Dzul, and R. Lozano. "Real-time stabilization and tracking of a four-rotor mini rotorcraft." In: *IEEE Transactions on Control Systems Technology* 12.4 (2004), pp. 510–516. ISSN: 1063-6536.

[9] M. Chen and M. Huzmezan. "A combined mbpc/2 dof h infinity controller for a quad rotor UAV." In: *AIAA Guidance, Navigation, and Control Conference and Exhibit*. 2003, p. 5520.

[10] B. Zhao, B. Xian, Y. Zhang, and X Zhang. "Nonlinear Robust Adaptive Tracking Control of a Quadrotor UAV Via Immersion and Invariance Methodology." In: *IEEE Transactions on Industrial Electronics* 62.5 (2015), pp. 2891–2902.

[11] Z. Zuo. "Trajectory tracking control design with command-filtered compensation for a quadrotor." In: *IET Control Theory & Applications* 4.11 (2010), pp. 2343 –2355.

[12] E. Altug, J. P. Ostrowski, and R. Mahony. "Control of a quadrotor helicopter using visual feedback." In: *Proceedings 2002 IEEE International Conference on Robotics and Automation*. Vol. 1. 2002, pp. 72–77.

[13] D. Lee, H.J. Kim, and S. Sastry. "Feedback Linearization vs. Adaptive Sliding Mode Control for a Quadrotor Helicopter." In: *International Journal of Control, Automation and Systems* 7.3 (2009), pp. 419–428.

[14] V. Utkin, J. Guldner, and J. Shi. *Sliding Modes in Electromechanical Systems*. London: Taylor and Francis, 1999.

[15] C. Edwards and S. K. Spurgeon. *Sliding mode control: theory and applications*. Vol. 7. CRC Press, 1998.

[16] L. Fridman. "Singularly perturbed analysis of chattering in relay control systems." In: *IEEE Transactions on Automatic Control* 47.12 (2002), pp. 2079–2084.

[17] V. I. Utkin. *Sliding modes in control and optimization*. Vol. 116. Springer-Verlag Berlin, 1992.

[18] A. Levant. "High-order sliding modes: differentiation and output-feedback control." In: *International Journal of Control* 76.9-10 (2003), pp. 924–941.

[19] A. Levant. "Sliding order and sliding accuracy in sliding mode control." In: *International Journal of Control* 58.6 (1993), pp. 1247–1263.

[20] V. Torres-González, T. Sanchez, L. M. Fridman, and J. A. Moreno. "Design of Continuous Twisting Algorithm." In: *Automatica* 80 (2017), pp. 119–126.

[21] L. Fridman, J. A. Moreno, B. Bandyopadhyay, S. Kamal, and A. Chalanga. "Continuous Nested Algorithms: The Fifth Generation of Sliding Mode Controllers." In: *Recent Advances in Sliding Modes: From Control to Intelligent Mechatronics*. Ed. by X. Yu and M. Ö. Efe. Springer International Publishing, 2016. Chap. 2, pp. 5–35.

[22] S. Kamal, J. A. Moreno, A. Chalanga, B. Bandyopadhyay, and L. Fridman. "Continuous terminal sliding-mode controller." In: *Automatica* 69 (2016), pp. 308–314.

[23] L. R. García-Carrillo, A.E. Dzul-López, R. Lozano, and C. Pégard. *Quad Rotorcraft Control*. Advances in Indutrial Control. London: Springer-Verlag London Heidelberg New York Dordrecht, 2013.

[24] R. C. Avram, X. Zhang, and J. Muse. "Quadrotor Actuator Fault Diagnosis and Accommodation Using Nonlinear Adaptive Estimators." In: *IEEE Transactions on Control Systems Technology* 25.6 (2017), pp. 2219–2226.

[25] Y. Zhong, Y. Zhang, W. Zhang, J. Zuo, and H. Zhan. "Robust Actuator Fault Detection and Diagnosis for a Quadrotor UAV With External Disturbances." In: *IEEE Access* 6 (2018), pp. 48169–48180.

[26] Z. Cen, H. Noura, T. B. Susilo, and Y. Al Younes. "Robust fault diagnosis for Quadrotor UAVs using adaptive Thau observer." In: *Journal of Intelligent & Robotic Systems* 73.1-4 (2014), pp. 573–588.

[27] H. Liu, W. Zhao, Z. Zuo, and Y. Zhong. "Robust Control for Quadrotors with Multiple Time-Varying Uncertainties and Delays." In: *IEEE Transactions on Industrial Electronics* (2017). DOI:10.1109/TIE.2016.2612618.

[28] S. Bertrand, N. Guénard, T. Hamel, H. Piet-Lahanier, and L. Eck. "A hierarchical controller for miniature VTOL UAVs: design and stability analysis using singular perturbation theory." In: *Control Engineering Practice* 19.10 (2011), pp. 1099–1108.

[29] X. Wang and B. Shirinzadeh. "Nonlinear augmented observer design and application to quadrotor aircraft." In: *Nonlinear Dynamics* 80.3 (2015), pp. 1463–1481.

[30] P. Martin and E. Salaün. "Design and implementation of a low-cost observer-based attitude and heading reference system." In: *Control Engineering Practice* 18.7 (2010), pp. 712–722.

[31] D. Lee, T. C. Burg, B. Xian, and D. M. Dawson. "Output feedback tracking control of an underactuated quad-rotor UAV." In: *American Control Conference, 2007. ACC'07*. IEEE. 2007, pp. 1775–1780.

[32] Z. Lendek, A. Berna, J. Guzmán-Giménez, A. Sala, and P. García. "Application of Takagi-Sugeno observers for state estimation in a quadrotor." In: *Decision and Control and European Control Conference (CDC-ECC), 2011 50th IEEE Conference on*. IEEE. 2011, pp. 7530–7535.

[33] F. Oliva-Palomo, A. Sanchez-Orta, P. Castillo, and H. Alazki. "Nonlinear ellipsoid based attitude control for aggressive trajectories in a quadrotor: Closed-loop multi-flips implementation." In: *Control Engineering Practice* 77 (2018), pp. 150–161.

[34] L. Derafa, A. Benallegue, and L. Fridman. "Super twisting control algorithm for the attitude tracking of a four rotors UAV." In: *Journal of the Franklin Institute* 349.2 (2012), pp. 685–699.

[35] H. Wang, X. Ye, Y. Tian, G. Zheng, and N. Christov. "Model-Free-Based Terminal SMC of Quadrotor Attitude and Position." In: *IEEE Transactions on Aerospace and Electronic Systems* 52.5 (2016), pp. 2519–2528.

[36] L. Luque-Vega, B. Castillo-Toledo, and A.G. Loukianov. "Robust block second order sliding mode conrol for a quadrotor." In: *Journal of Franklin Institute* 349.1 (2012), pp. 719–739.

[37] E.-H. Zheng, J.-J. Xiong, and J.-L. Luo. "Second order sliding mode control for a quadrotor UAV." In: *ISA Transactions* 53.4 (2014), pp. 1350–1356.

[38] I. González, S. Salazar, and R. Lozano. "Chattering-Free Sliding Mode Altitude Control for a Quad-Rotor Aircraft: Real-Time Application." In: *Journal of Intelligent & Robotic Systems* 73.1 (2014), pp. 137–155.

[39] Z. Jia, J. Yu, Y. Mei, Y. Chen, Y. Shen, and X. Ai. "Integral Backstepping Sliding Mode Control for Quadrotor Helicopter under External Uncertain Disturbances." In: *Aerospace Science and Technology* (2017). DOI: 10.1016/j.ast.2017.05.022.

[40] C. Mnasri and M. Gasmi. "LMI-based adaptive fuzzy integral sliding mode control of mismatched uncertain systems." In: *International Journal of Applied Mathematics and Computer Science* 21.4 (2011), 605–615.

[41] L. Besnard, Y. B. Shtessel, and B. Landrum. "Quadrotor vehicle control via sliding mode controller driven by sliding mode disturbance observer." In: *Journal of the Franklin Institute* 349 (2012), pp. 658–684.

[42] A. Benallegue, A. Mokhtari, and L. Fridman. "High-order sliding-mode observer for a quadrotor UAV." In: *International Journal of Robust and Nonlinear Control* 18.4-5 (2008), pp. 427–440.

[43] A. Mokhtari, A. Benallegue, and Y. Orlov. "Exact linearization and sliding mode observer for a quadrotor unmanned aerial vehicle." In: *International Journal of Robotics & Automation* 21.1 (Jan. 2006), pp. 39 –49.

[44] R. Falcón, H. Ríos, and A Dzul. "Comparative analysis of continuous sliding-modes control strategies for quad-rotor robust tracking." In: *Control Engineering Practice* 90 (2019), pp. 241–256.

[45] M. Blanke, M. Kinnaert, J. Lunze, and M. Staroswiecki. *Diagnosis and fault tolerant control*. New York: Springer, 2003.

[46] Y. Song, L. He, D. Zhang, J. Qian, and J. Fu. "Neuroadaptive Fault-Tolerant Control of Quadrotor UAVs: A More Affordable Solution." In: *IEEE Transactions on Neural Networks and Learning Systems* 30.7 (2019), pp. 1975–1983. ISSN: 2162-237X.

[47] A.-R. Merheb, H. Noura, and F. Bateman. "Design of passive fault-tolerant controllers of a quadrotor based on sliding mode theory." In: *International Journal of Applied Mathematics and Computer Science* 25.3 (2015), pp. 561–576.

[48] B. Xiao, Q. Hu, and Y. Zhang. "Adaptive Sliding Mode Fault Tolerant Attitude Tracking Control for Flexible Spacecraft Under Actuator Saturation." In: *IEEE Transactions on Control Systems Technology* 20.6 (2012), pp. 1605–1612. ISSN: 1063-6536.

[49] B. Wang and Y Zhang. "An Adaptive Fault-Tolerant Sliding Mode Control Allocation Scheme for Multirotor Helicopter Subject to Simultaneous Actuator Faults." In: *IEEE Transactions on Industrial Electronics* 65.5 (2018), pp. 4227–4236.

[50] P. Tang, D. Lin, D. Zheng, S. Fan, and J Ye. "Observer based finite-time fault tolerant quadrotor attitude control with actuator faults." In: *Aerospace Science and Technology* 105968 (2020).

[51] X. Nian, W. Chen, X. Chu, and Z Xu. "Robust adaptive fault estimation and fault tolerant control for quadrotor attitude systems." In: *International Journal of Control* 93.3 (2020), pp. 725–737.

[52] B. Wang, Y. Shen, and Y. Zhang. "Active fault-tolerant control for a quadrotor helicopter against actuator faults and model uncertainties." In: *Aerospace Science and Technology* 99 (2020), p. 105745.

[53] P. Lyu, S. Liu, J. Lai, and J. Liu. "An analytical fault diagnosis method for yaw estimation of quadrotors." In: *Control Engineering Practice* 86 (2019), pp. 118–128. ISSN: 0967-0661.

[54] J. Chang, J. Cieslak, J. Dávila, J. Zhou, A. Zolghadri, and Z. Guo. "A Two-Step Approach for an Enhanced Quadrotor Attitude Estimation via IMU Data." In: *IEEE Transactions on Control Systems Technology* 26.3 (2018), pp. 1140–1148.

[55] H. Aguilar-Sierra, G. Flores, S. Salazar, and R. Lozano. "Fault Estimation for a Quad-Rotor MAV Using a Polynomial Observer." In: *Journal of Intelligent & Robotic Systems* 73 (2013), pp. 455–468.

[56] A. Freddi, S. Longhi, and A. Monteriù. "A Diagnostic Thau Observer for a Class of Unmanned Vehicles." In: *Journal of Intelligent & Robotic Systems* 67.1 (2012), pp. 61–73.

[57] W. Han, Z. Wang, and Y. Shen. "Fault estimation for a Quadrotor unmanned aerial vehicle by integrating the parity space approach with recursive least squares." In: *Proceedings of the Institution of Mechanical Engineers, Part G: Journal of Aerospace Engineering* 232.4 (2018), pp. 783–796.

[58] M. H. Amoozgar, A. Chamseddine, and Y. Zhang. "Experimental test of a two-stage Kalman filter for actuator fault detection and diagnosis of an unmanned quadrotor helicopter." In: *Journal of Intelligent & Robotic Systems* 70.1-4 (2013), pp. 107–117.

[59] F. Chen, R. Jiang, K. Zhang, B. Jiang, and G. Tao. "Robust backstepping Sliding-Mode Control and observer-based fault estimation for a Quadrotor UAV." In: *IEEE Transactions on Industrial Electronics* 63.8 (2016), pp. 5044–5056.

[60] K. P. B. Chandra, H. Alwi, and C. Edwards. "Fault Reconstruction for a Quadrotor Using an LPV Sliding Mode Observer." In: *IFAC-PapersOnLine* 48.21 (2015), pp. 374–379.

[61] E. Capello, E. Punta, and L. Fridman. "Strategies for control, fault detection and isolation via sliding mode techniques for a 3-DOF helicopter." In: *The 55th Conference on Decision and Control*. 2016, pp. 6464–6469.

[62] J. Liu, B. Jiang, and Y. Zhang. "Sliding mode observer-based fault detection and isolation in flight control systems." In: *The IEEE International Conference on Control Applications*. 2007, pp. 1049–1054.

[63] X. Wang, S. Sun, E.-J. van Kampen, and Q. Chu. "Quadrotor Fault Tolerant Incremental Sliding Mode Control driven by Sliding Mode Disturbance Observers." In: *Aerospace Science and Technology* 87 (2019), pp. 417–430. ISSN: 1270-9638.

[64] A.-R. Merheb, H. Noura, and F. Bateman. "Emergency control of AR drone quadrotor UAV suffering a total loss of one rotor." In: *IEEE/ASME Transactions on Mechatronics* 22.2 (2017), pp. 961–971.

[65] V. Lippiello, F. Ruggiero, and D. Serra. "Emergency landing for a quadrotor in case of a propeller failure: A backstepping approach." In: *2014 IEEE/RSJ International Conference on Intelligent Robots and Systems* 4782-4788 (2014).

[66] M. W. Mueller and R D'Andrea. "Stability and control of a quadrocopter despite the complete loss of one, two, or three propellers." In: *2014 IEEE International Conference on Robotics and Automation* 45-52 (2014).

[67] A. Lanzon, A. Freddi, and S Longhi. "Flight Control of a Quadrotor Vehicle Subsequent to a Rotor Failure." In: *Journal of Guidance Control and Dynamics* 37 (2014), pp. 580–591.

[68] S. Sun, L. Sijbers, X. Wang, and C De Visser. "High-Speed Flight of Quadrotor Despite Loss of Single Rotor." In: *IEEE Robotics and Automation Letters* 3 (2018), pp. 3201–3207.

[69] Z. Hou, P. Lu, and Z Tu. "Nonsingular terminal sliding mode control for a quadrotor UAV with a total rotor failure." In: *Aerospace Science and Technology* 98 105716 (2020), pp. 1–18.

[70] A. Poznyak, A. Polyakov, and V. Azhmyakov. *Attractive Ellipsoids in Robust Control*. Systems & Control: Foundations & Applications. Birkhäuser, 2014.

[71] J. Moreno. "Lyapunov Approach for Analysis and Design of Second Order Sliding Mode Algorithms." In: *Sliding Modes after the First Decade of the 21st Century*. Ed. by L. Fridman, J. Moreno, and R. Iriarte. Vol. 412. Lecture Notes in Control and Information Science. Berlin Heidelberg: Springer Verlag, 2012. Chap. 4, pp. 113–149.

[72] R. Falcón, O.A. González, H. Ríos, and A. Dzul. "Quad-Rotor Robust Tracking: A Continuous Sliding-Mode Control Strategy." In: *2018 15th International Workshop on Variable Structure Systems (VSS)*. 2018, pp. 390–395.

[73] R. Falcón, H. Ríos, M. Mera, and A. Dzul. "Output-based Robust Control for Quad-Rotor Tracking: An Attractive Ellipsoid Approach." In: *2018 XX Congreso Mexicano de Robótica (COMRob)*. 2018, pp. 1–6.

[74] H. Castañeda, R. Falcón, A. Dzul, and J. L. Gordillo. "Control de Vuelo de un Quad-Rotor Utilizando un Control por Modos Deslizantes Adaptable." In: *2019 Congreso Nacional de Control Automático (CNCA)*. 2019, pp. 85–90.

[75] R. Falcón, H. Ríos, and A. Dzul. "A Robust Control Strategy for Target Tracking using a Quad–Rotor." In: *2021 Congreso Nacional de Control Automático (CNCA)*. 2022, Accepted.

[76] R. Falcón, H. Ríos, and A. Dzul. "Diagnóstico de Fallas basado en Observadores por Modos Deslizantes para un Quad-Rotor." In: *2019 Congreso Nacional de Control Automático (CNCA)*. 2019, pp. 495–500.

[77] R. Falcón, H. Ríos, and A. Dzul. "A Robust Fault Diagnosis for Quad-Rotors: A Sliding-Mode Observer Approach." In: *IEEE/ASME Transactions on Mechatronics* (2022). DOI: 10.1109/TMECH.2022.3156854.

[78] R. Falcón, H. Ríos, and A. Dzul. "Fault Accommodation Sliding-Mode Control for Quad-Rotor Tracking Trajectory." In: *2021 Congreso Nacional de Control Automático (CNCA)*. 2021, pp. 267–272.

[79] R. Falcón, H. Ríos, and A. Dzul. "An Actuator Fault Accommodation Sliding-Mode Control Approach for Trajectory Tracking in Quad-Rotors." In: *2021 60th IEEE Conference on Decision and Control (CDC)*. 2021, pp. 7100–7105.

[80] R. Falcón, H. Ríos, and A. Dzul. "Control Tolerante a Fallas Activo para un Quad-Rotor ante la Pérdida de un Actuador." In: *27° Congreso Argentino de Control Automático (AADECA'20) Virtual,* 2020, pp. 93–98.

[81] R. Falcón, H. Ríos, and A. Dzul. "Active Fault Tolerant Control for a Quad-Rotor in case of a Rotor Failure." In: *2021 XXIII Robotics Mexican Congress (ComRob)*. 2021, pp. 75–80.

[82] R. Falcón, H. Ríos, and A. Dzul. "Active Sliding–Mode Fault–Tolerant Control for Robust Tracking in Quad– Rotors under a Rotor Failure." In: *International Journal of Robust and Nonlinear Control* (2022). DOI: 10.1002/rnc.6288.

[83] H. Khalil. *Nonlinear Systems*. New Jersey, U.S.A.: Prentice Hall, 2002.

[84] A. Polyakov. "Nonlinear feedback design for fixed-time stabilization of linear control systems." In: *IEEE Transactions on Automatic Control* 57.8 (2012), pp. 2106–2110.

[85] E. D. Sontag. "On the Input-to-State Stability Property." In: *European Journal of Control* 1.1 (1995), pp. 24–36.

[86] W. Khan and M. Nahon. "A propeller model for general forward flight conditions." In: *International Journal of Intelligent Unmanned Systems* 3.2/3 (2015), pp. 72–92.

[87] H. Ríos, J. González-Sierra, and A. Dzul. "Robust Tracking Output-Control for a Quad-Rotor: A Continuous Sliding-Mode Approach." In: *Journal of the Franklin Institute* 354 (2017), pp. 6672–6691.

[88] R. Seeber and M. Horn. "Stability proof for a well-established super-twisting parameter setting." In: *Automatica* 84 (2017), pp. 241–243.

[89] J. Cieslak, D. Efimov, A. Zolghadri, D. Henry, and P. Goupil. "Design of a non-homogeneous differentiator for actuator oscillatory failure case reconstruction in noisy environment." In: *Proceedings of the Institution of Mechanical Engineers, Part I: Journal of Systems and Control Engineering* 229.3 (2015), pp. 266–275.

[90] Á. Mercado-Uribe and J. A. Moreno. "Discontinuous integral action for arbitrary relative degree in sliding-mode control." In: *Automatica* 118 (2020), p. 109018.

[91] E. Cruz-Zavala and J. A. Moreno. "Higher Order Sliding Mode Control Using Discontinuous Integral Action." In: *IEEE Transactions on Automatic Control* 65.10 (2019), pp. 4316–4323.

[92] Quanser Consulting Inc. "Quanser QBall2 Datasheet v1.2." [Online]: Available: https://www.quanser.com/wp-content/uploads/2017/03/ QBall-2-Datasheet-v1 .2.pdf. 2017.